ARMY RESEARCH LABORATORY
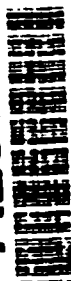
ARL

Evaluation of Simple Spherical Spreading Model for Near Vertical Acoustical Propagation

By John M. Noble
Battlefield Environment Directorate

ARL-TR-532

August 1994

DTIC
ELECTE
NOV. 21 199
S B D

DTIC QUALITY INSPECTED 8

94 11 18 042

NOTICES

Disclaimers

The findings in this report are not to be construed as an official Department of the Army position, unless so designated by other authorized documents.

The citation of trade names and names of manufacturers in this report is not to be construed as official Government indorsement or approval of commercial products or services referenced herein.

Destruction Notice

When this document is no longer needed, destroy it by any method that will prevent disclosure of its contents or reconstruction of the document.

PAGES _____ ARE MISSING IN ORIGINAL DOCUMENT

REPORT DOCUMENTATION PAGE

Public reporting burden for this collection of information is estimated to average 1 hour per response, including the time for reviewing instructions, searching existing data sources, gathering and maintaining the data needed, and completing and reviewing the collection of information. Send comments regarding this burden estimate or any other aspect of this collection of information, including suggestions for reducing this burden, to Washington Headquarters Services, Directorate for Information Operations and Reports, 1215 Jefferson Davis Highway, Suite 1204, Arlington, VA 22202-4302, and to the Office of Management and Budget, Paperwork Reduction Project (0704-0188), Washington, DC 20503.

1. AGENCY USE ONLY (Leave blank)	2. REPORT DATE	3. REPORT TYPE AND DATES COVERED
	August 1994	Final

4. TITLE AND SUBTITLE

Evaluation of Simple Spherical Spreading Model for Near Vertical Acoustic Propagation

5. FUNDING NUMBERS

6. AUTHOR(S)

John M. Noble

7. PERFORMING ORGANIZATION NAME(S) AND ADDRESS(ES)

U.S. Army Research Laboratory
Battlefield Environment Directorate
ATTN: AMSRL-BE-W
White Sands Missile Range, NM 88002-5501

8. PERFORMING ORGANIZATION REPORT NUMBER

ARL-TR-532

9. SPONSORING / MONITORING AGENCY NAME(S) AND ADDRESS(ES)

U.S. Army Research Laboratory
2800 Powder Mill Road
Adelphi, MD 20783-1145

10. SPONSORING / MONITORING AGENCY REPORT NUMBER

ARL-TR-532

11. SUPPLEMENTARY NOTES

12a. DISTRIBUTION / AVAILABILITY STATEMENT

Approved for public release; distribution is unlimited.

12b. DISTRIBUTION CODE

A

13. ABSTRACT (Maximum 200 words)

A comparison study was performed to evaluate the performance of a simple spherical spreading plus molecular absorption model to a more complex acoustic propagation model for near vertical propagation. The problem of near vertical propagation is important since several acoustic detection systems are being developed for the Army. The operational use of a simple acoustic propagation model in the battlefield will allow for fast computation time providing rapid evaluation of the advantage or disadvantage of using the acoustic detection system. However, simple propagation models can have several limitations. To evaluate the limitations and determine the operational reliability of the simple acoustic propagation model, more complex models must be used that incorporate many effects of the ground and atmosphere on the propagation of sound. This comparison will determine the limitations.

14. SUBJECT TERMS

acoustics, propagation, spherical spreading

15. NUMBER OF PAGES

101

16. PRICE CODE

17. SECURITY CLASSIFICATION OF REPORT	18. SECURITY CLASSIFICATION OF THIS PAGE	19. SECURITY CLASSIFICATION OF ABSTRACT	20. LIMITATION OF ABSTRACT
Unclassified	Unclassified	Unclassified	SAR

1

Contents

Figures

Appendix Figures

Figures (continued)

4

Figures (continued)

1. Introduction

This report describes the work to compare a simple spherical spreading model (referred to as the candidate model) with an acoustic propagation model that incorporates geometrical spreading, refraction, complex ground interactions, molecular absorption, and some degree of diffraction for near vertical propagation. Systems that involve the case of near vertical propagation are now under consideration by the Army. This report shows how the candidate model compares to more advanced models under conditions similar to certain acoustic detection systems being developed for the Army. The comparison shows how much of an impact each of these effects have in relation to realistic types of nonturbulent atmospheric conditions on the candidate model. The source level used in the comparison is 115 dB (20 μPa) as measured 1 m from the source. For problems related to Army needs, the range of interest is less than 5 km with a slant path from the source to the receiver greater than 25° from horizontal. In the comparison, the effects studied only have a significant impact if the effect occurs within the area of interest.

2. Models Used

2.1 Candidate Model

The candidate model incorporates the two basic effects on acoustic propagation: spherical spreading and molecular absorption. The mathematical expression for the model is

$$dB = dBAmp - 20\log_{10}(R_s) - ATTN \cdot (R_s - 1) \qquad (1)$$

where

dB $\quad$ = the sound pressure level at the receiver

dBAmp = the sound pressure level of the target in decibels

$R_s \quad$ = the slant path distance from the target to the receiver in meters

ATTN $\;$ = the attenuation coefficient caused by the molecular absorption in decibels per meter.

The attenuation coefficients used in the comparison are calculated using the ANSI Standard S1.26-1978. [1] The slant range is subtracted by one because the reference level of the target is relative to 1 m. Although the model is basic, it will be shown that it works well for most cases because of the geometries involved.

2.2 Fast Field Program

The Fast Field Program (FFP) is an acoustic propagation model based on a solution of the acoustic wave equation. The FFP was developed for use in atmospheric acoustics around 1985. [2,3] The FFP allows researchers the opportunity to incorporate the effects mentioned earlier. The derivation of the FFP is beyond the scope of this report; however, there are several good references on the details of the derivation. [4,5] The FFP incorporates the

effects of refraction and ground impedance on the sound field as it propagates through the atmosphere, which allows for modeling the effects that refractive shadow zones and ducting have on atmospheric acoustics. Acoustic ducting is an atmospheric phenomena in which the temperature and vector wind speed gradients combine to give a condition in which sound is trapped near the ground. The condition allows for excellent propagation conditions for ground-based sensors; however, it could cause the opposite propagation conditions for an elevated receiver. [6]

2.3 Spherical Model

The spherical model is very similar to the candidate model except it incorporates the effects of the complex ground impedance. [7] When sound is reflected from the ground, the wave undergoes a change in the amplitude and phase. The reflected wave can propagate from the ground and interfere with another part of the wave causing constructive or destructive interference. The effect of the ground on acoustic propagation depends on the frequency of the sound wave. At low frequencies (less than 100 Hz), the ground is acoustically hard resulting in near perfect reflection. Because of the ground being acoustically hard, the sound field from a target is not very dependent on the ground characteristics for low frequencies. As the frequency increases, the sound field from a target looks similar to the electric field from a dipole radiator. The location and number of constructive and destructive interference lobes depends on the characteristics of the ground and the acoustic frequency. The discussion on the effects of the ground continues in section 4.2.

2.4 Ray Trace Model

A ray trace model [8] is very useful to visually determine how the sound is propagating through the atmosphere. This allows visualization of the effect of refraction and its influence on the sound as it propagates through the atmosphere. Section 3 presents some results from tracing rays through the atmosphere and discusses how to calculate the angular spread of sound propagating out of an acoustic duct, based solely on refraction.

10

3. Parameters Used In Comparison

3.1 Atmospheric Profiles

The atmospheric profiles determine the sound speed profiles that influence how sound propagates through the atmosphere. The atmospheric profiles can vary dramatically from day to day. However, the sound speed profiles calculated from the atmospheric profiles usually fall into a limited number of acoustic propagation characteristics. Five typical types of sound speed profiles (Cases 2-6) were chosen for this study, a sixth type was chosen as a basic benchmark (Case 1). Because the main concern is the shape of the sound speed profile, the temperature profile is used to calculate the sound speed profile, and the wind speed profile is ignored. Because the propagation characteristics of each type of profile are most important, the exact slope of the sound speed profile is not important. Inclusion of the wind speed profile does not change the types of sound speed profiles used in the comparison, but slightly alters the slopes. The propagation characteristics of the idealized profiles are consistent with real profiles collected from measurements (appendix D). The breakdown of the profiles follow:

> Case 1: Homogeneous - This is a simple type of atmosphere generally used in the comparison between acoustic models. In this case, there is no refraction due to the absence of a sound speed gradient. The propagation effects involved are geometrical spreading, molecular absorption, and complex ground impedance. The sound speed in the atmosphere was calculated based on a surface temperature of 30 °C (figure D-1).

> Case 2: Mild Upward Refraction - This type of profile corresponds to conditions in the atmosphere when the temperature profile follows a mild negative lapse rate ($0 > dT/dz > -10$ °C/km) with light winds present. The condition occurs during the early morning after the nocturnal inversion has broken; a cloudy day; or the night before the nocturnal inversion begins to build. The condition results in upward refraction causing the

11

formation of a refractive shadow zone. A refractive shadow zone is a region in which sound cannot reach the receiver from a direct or reflected path. The sound speed profile was calculated using a temperature gradient of −7 °C/km with a surface temperature of 20 °C, (figure D-2). The surface temperature is lower than for Case 3.

Case 3: Strong Upward Refraction - This type of profile corresponds to conditions in the atmosphere when the temperature profile is a super adiabatic lapse rate (dT/dz < −10 °C/km) with light winds present. This condition occurs during the day when the ground is being heated by incoming solar radiation. As in Case 2, this condition also results in upward refraction but the degree of upward refraction is greater. The distance to the refractive shadow zone from the source is less than for Case 2 because of the greater degree of upward refraction. The sound speed profile was calculated using a temperature gradient of −12 °C/km with a surface temperature of 30 °C, (figure D-3).

Case 4: Downward Refraction - This type of profile does not strictly correspond to a specific type of atmospheric condition; however, similar sound speed profiles can be formed from upper air wind shears (600 - 2000 m). This condition results in sound waves being refracted back down to the ground. The sound speed profile was calculated using a temperature gradient of +7 °C/km with a surface temperature of 20 °C, (figure D-4).

Case 5: Shallow Inversion - This type of profile occurs at night when the nocturnal inversion has built up. The temperature inversion forms an acoustic duct that causes sound to be trapped near the ground. Not all of the sound emitted by a target will be trapped within the acoustic duct. Section 3.2 discusses how to calculate the angular distribution of sound that is trapped within the acoustic duct from a source. This case is called shallow because it is relevant to nocturnal inversions with thicknesses from near surface to 200 m. The sound speed profile was

12

calculated using a temperature gradient of +20 °C/km from the surface to 150 m and −8 °C/km above that with a surface temperature of 20 °C (figure D-5).

Case 6: Deep Inversion - This type of profile occurs during the day or at night because of a wind shear present in the atmosphere or a very high temperature inversion. This type of profile is typically referred to as an inversion because the shape of the sound speed profile is very much like the sound speed profile from a nocturnal inversion. This case is called deep because the thickness of the acoustic duct is greater than 200 m. As mentioned in Case 5, a certain angular distribution of the sound is trapped within the duct (section 3.2). The sound speed profile was calculated using a temperature gradient of +15 °C/km from the surface to 300 m and a temperature gradient of −8 °C/km above that with a surface temperature of 20 °C (figure D-6).

3.2 Geometries Used

Two types of geometries were used in the comparison. In the first type of geometry, constant receiver height, the receiver remains at a height constant with range. Constant receiver height geometry is not realistic for known types of devices; however, it does illustrate refractive shadow zone effects. Heights of 500 and 1000 m were used for the constant receiver height geometry. The heights were chosen to try to minimize the effects of acoustic ducting, refractive shadow zones, and ground impedance. The second type of geometry, slant path, approximates an idealized slant flight path an acoustic receiver might take. The calculations were made for slant paths with 30°, 45°, and 60°, measured from horizontal drop paths over a 4- by 4-km grid. In each case, the height of the source is assumed to be 1 m.

13

3.3 Molecular Absorption Parameters

The value of ATTN and the numerical propagation models used the ANSI standard S1.26-1978 to obtain the molecular absorption coefficients. The molecular absorption coefficients were based on the acoustic frequencies used (50 to 450 Hz at 100 Hz intervals), temperature (30 °C for Cases 1 and 3 and 20 °C for Cases 2, 4, 5, and 6), atmospheric pressure (980 mb), and relative humidity (20 percent). The values used for molecular absorption are shown in Table 1.

Table 1. Attenuation coefficients used in comparison

Frequency (Hz)	Attenuation Coefficient (dB/m)	
	20 °C	30 °C
50	0.000171	0.000136
150	0.000866	0.000954
250	0.001383	0.001858
350	0.001828	0.002572
450	0.002307	0.003139

4. Results of Comparison

The results of the model comparison will be discussed in this section of the report. Appendices A, B, and C contain the graphs of the scenarios used. The result of every scenario is not discussed due to the massive number of results computed. The results are divided into much smaller groups according to the dominating effect. Also, the results are grouped into the two types of geometries used: constant receiver height and slant path.

4.1 Constant Receiver Height (Appendices A and B)

The constant receiver height comparison shows very good agreement in most cases between the candidate model and the FFP (dashed line = candidate model and solid line = FFP). Within 2 km, the differences between the two models are attributed to the effect of the ground impedance causing destructive interference between the direct and reflected acoustic wave paths. More on the effects of ground impedance is discussed in section 4.2.

Cases 2 and 3 (mild upward refraction and strong upward refraction) show the effects of a refractive shadow zone beginning to affect the acoustic propagation at ranges of 9 km for Case 2 (figures A-6 through A-10) and 7 km for Case 3 (figures A-11 through A-15) with a receiver height of 500 m. Using ray theory, the receiver at 500 m is in the shadow zone at a range of 9,300 m for Case 2, which is consistent with results. Because the sound speed gradient is larger in Case 3, the shadow zone occurs at a distance of 7 km. For the scenarios in which the receiver is located 1 km above the ground, the distance from the source to where the shadow zone occurs is much greater due to the increased height of the receiver. Using ray theory, the distance to the shadow zone occurs beyond 10 km. The effect of the shadow zone is not seen in the graphs for Cases 2 and 3 in appendix B because the comparison was only carried out to 10 km. In Case 3, the distance to the shadow zone is just beyond 10 km; therfore, the decreasing of the sound pressure levels near the shadow zone can just be seen near 10 km.

Cases 4, 5, and 6 (downward refraction, shallow inversion, and deep inversion) show the effects of acoustic ducting. For an elevated receiver, an acoustic duct causes a refractive shadow zone to form in the atmosphere above the ducting region beyond a certain vertical propagation angle. In Case 4, this effect is due more to the fact that a very small angular cross section of sound is reaching the receiver instead of the formation of a refractive shadow zone. The observed result looks very similar to the results from Cases 5 and 6 where a shadow zone is formed. Using ray trace theory, the vertical propagation angle, measured from horizontal, for a linear sound speed gradient is estimated by

$$\theta_s = \cos^{-1}\left|\frac{c_s}{(z_i - z_s)g + c_s}\right| \qquad .2)$$

where

c_s = the sound speed at the source
z_i = the height of the duct
z_s = the source height
g = the linear sound speed gradient.

Using this equation, the propagation angles for Cases 5 and 6 are 6° and 7°, respectively; therefore, any sound propagating greater than this angle is not trapped in the acoustic duct. The effect is shown in the comparison plots for Cases 5 and 6 and the location in which the effect begins agrees with the 6° and 7° angles. The agreement between the equation and the plots is not exact because ray theory does not accurately represent sound waves at the lower frequencies. For cases in which a logarithmic sound speed gradient is present, the vertical propagation angle will be larger due to the more intense sound speed gradients near the ground. However, the propagation angle for a logarithmic gradient is still less than 25°; therefore, because of the unique nature of the near vertical propagation, acoustic ducts are not a problem because the receiver approaches the source at an angle much greater than 25°.

4.2 Slant Path (Appendix C)

In most cases, the slant path comparisons showed very good agreement in most cases between the candidate model and the FFP. The main discrepancy in the comparisons is due to the effect of ground impedance on the sound field from the source. Figures 1 through 3 show the effects on the sound field because of ground impedance for 50, 100, and 200 Hz in a homogeneous atmosphere. Figures 1 through 3 are constant sound pressure level contours with the slant paths for 30°, 45°, and 60° overlayed. Reflections from the ground can cause amplitude and phase changes that can result in an interference pattern. Figures 2 and 3 show the interference pattern. In the field, the large decrease in sound level is not measured for two reasons: 1) The comparison was made for a single source. In the battlefield, tanks appear in a column several tens-of-meters long giving a sound field pattern that is a superposition of the sound field offset by the spacing between the tanks. The comparison helps fill in some of the destructive interference regions. 2) Scattering from atmospheric turbulence fills in the regions of destructive interference. [9] The two effects minimize the negative effect of the ground reflections on the sound field.
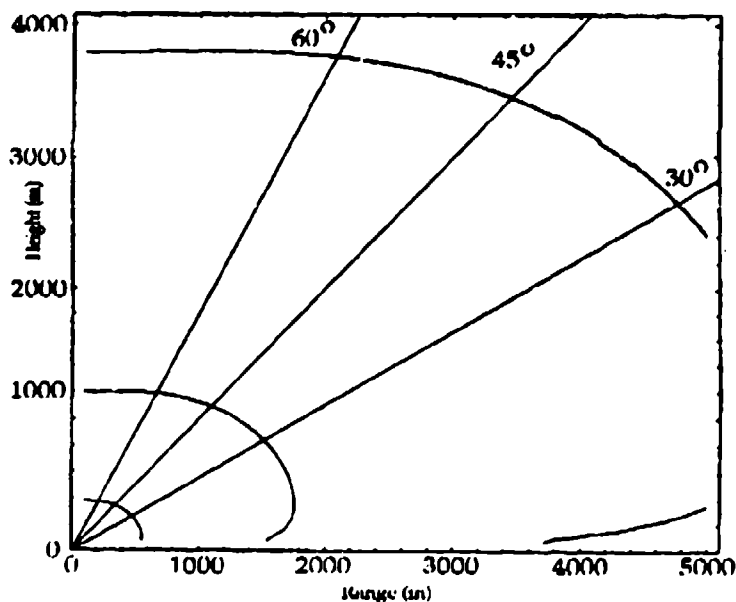
Figure 1. Constant sound pressure level contours for 50 Hz.
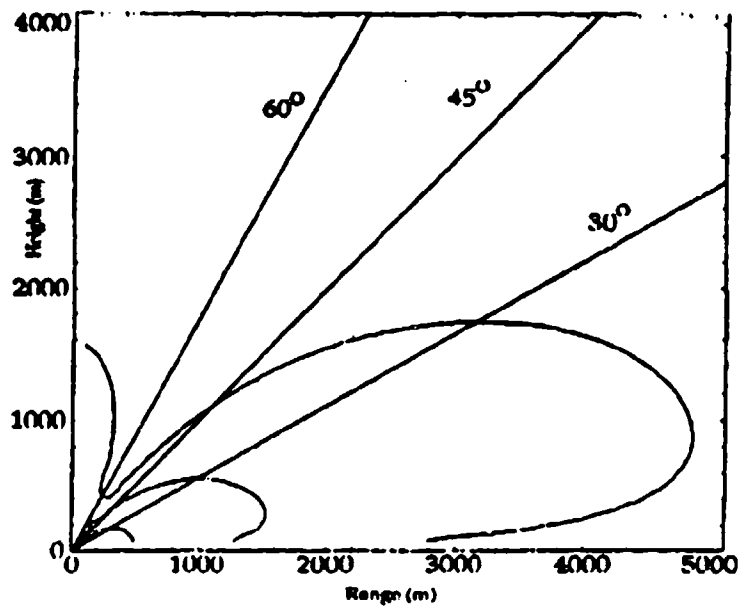
Figure 2. Constant sound pressure level contours for 100 Hz.
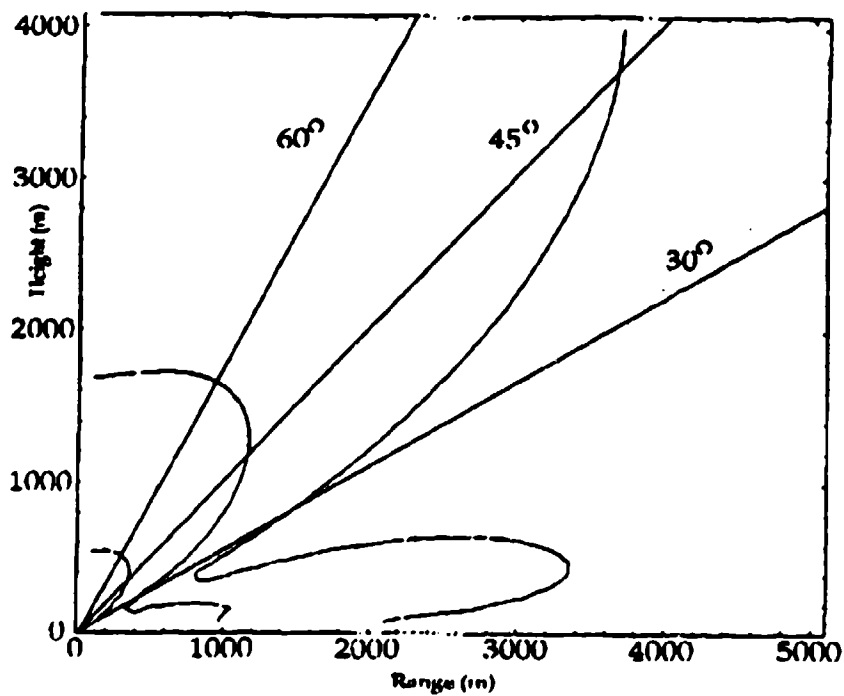
Figure 3. Constant sound pressure level contours for 200 Hz.

18

5. Conclusions

5.1 Constant Receiver Height

The comparison between the candidate model and the FFP was good for the different atmospheric cases used. Effects from refractive shadow zones and ducting were seen in the comparison, but the effects occurred at ranges greater than the range of interest for current Army needs. At close ranges, the interference caused by the ground could be seen. The effects of the ground will be reduced from superposition of the sources in the tank column and scattering from atmospheric turbulence.

5.2 Slant Path

The comparison between the candidate model and the FFP for the slant path cases showed good agreement. The slant path cases were not largely affected by the type of atmosphere being used, which is unique to the near vertical propagation. Surface-to-surface propagation shows significant differences under the different atmospheric cases. The only issue that occurred was with the interference from ground reflections. As mentioned, the interference will be minimized by superposition of the sources and scattering from atmospheric turbulence. The net effect of the ground reflections is a few decibel reduction in the predicted sound levels along certain slant paths aligned with the destructive interference lines.

5.3 General

The overall conclusion from this comparison is, for near vertical acoustic propagation, the use of a simple acoustic propagation model that only incorporates spherical spreading and molecular absorption performs as good as a more complex propagation model with the exception of the effect caused by ground reflections. Ground based sensors will be heavily impacted by the various states of the atmosphere considered in this comparison. The only potential issue is the degree of the effect from the ground reflections on the

19

sound field at the location of the receiver. Although the scope of this comparison did not address it, the degree of the ground effect will be minimized due to the superposition of the sources (because tanks typically move in columns) and scattering of the acoustic wave by atmospheric turbulence.

References

1. ANSI, Method for the Calculation of the Absorption of Sound by the Atmosphere, published by the American Institute of Physics, ANSI S1.26-1978.

2. Raspet, R., S. W. Lee, E. Kuester, D. C. Chang, W. F. Richards, R. Gilbert, and N. Bong, "Fast-field Program for a Layered Medium Bounded by Complex Impedance Surfaces," *J. Acoust. Soc. Am.* 77, 1985, pp. 345-352.

3. Lee, S. W., N. Bong, W. F. Richards, and R. Raspet, "Impedance Formulation of the Fast Field Program for Acoustic Wave Propagation in the Atmosphere," *J. Acoust. Soc. Am.* 79, 1986, pp. 628-634.

4. Swenson, G. W. Jr. and S. J. Franke, "A Brief Tutorial on the Fast Field Program (FFP) as Applied to Sound Propagation in the Air," *Applied Acoustics* 27, 1989, pp. 203-215.

5. West, M., R. A. Sack, and F. Walkden, "The Fast Field Program. A Second Tutorial: Application to Long Range Sound Propagation in the Atmosphere," *Applied Acoustics* 33, 1991, pp. 199-228.

6. Noble, John M., "The Importance of Ducting in Atmospheric Acoustics," In *Proceedings of the 1992 Battlefield Atmospherics Conference*, Ft. Bliss, TX, 1-3 Dec 1992.

7. Attenborough, K., S. I. Hayek, and J. M. Lawther, "Propagation of Sound Above a Porous Half-Space," *J. Acoust. Soc. Am.* 68, 1980, pp. 1493-1501.

8. Foreman, Terry Lee, "Acoustic Ray Models Based On Eigenrays," ARL Rep. No. ARL-TR-1, Applied Research Laboratories, The University of Texas, Austin, TX, 1977.

9.   Daigle, G. A., J. I. Piercy, and T. F. W. Embleton, "Effects of Atmospheric Turbulence on the Interface of Sound Waves Near a Hard Boundary," *J. Acoust. Soc. Am.* 64, 1978, pp. 622-630.

Appendix A

Constant Receiver Height of 500 m
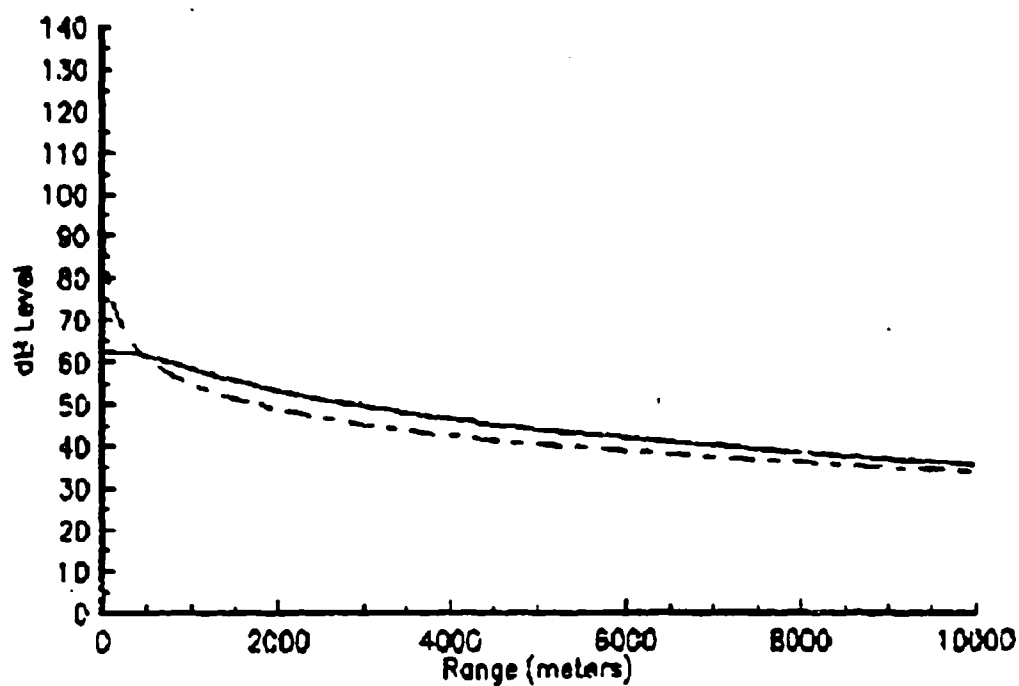
Figure A-1. 50 Hz for homogeneous profile.
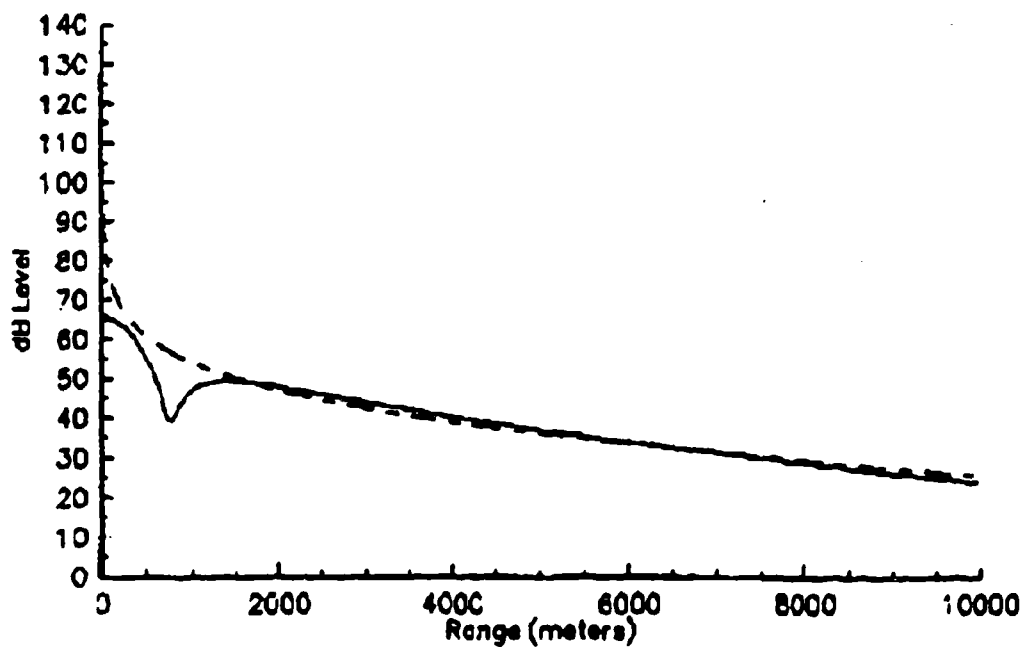
Figure A-2. 150 Hz for homogeneous profile.

24
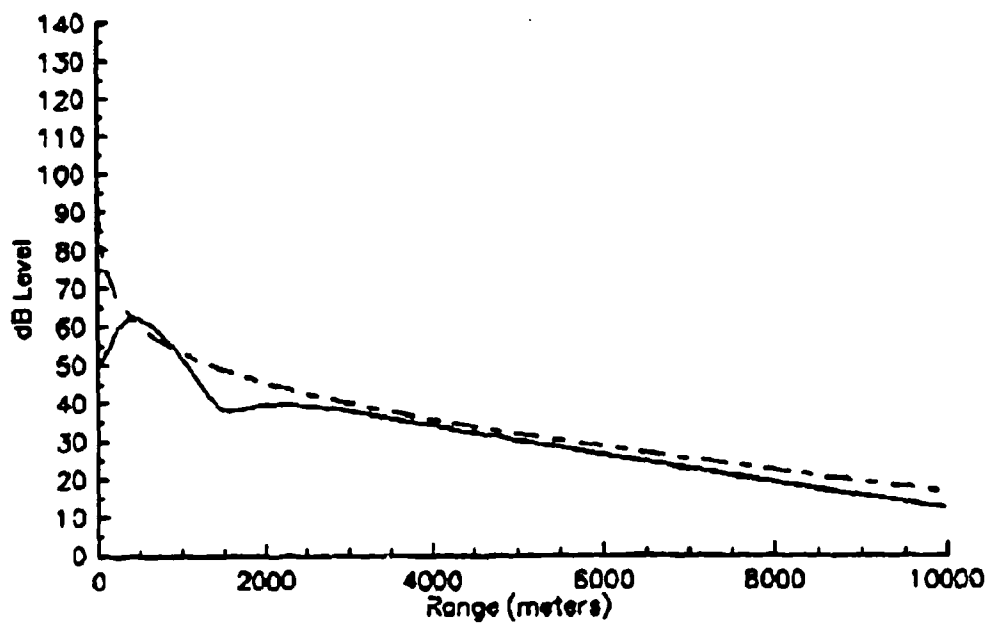
Figure A-3. 250 Hz for homogeneous profile.
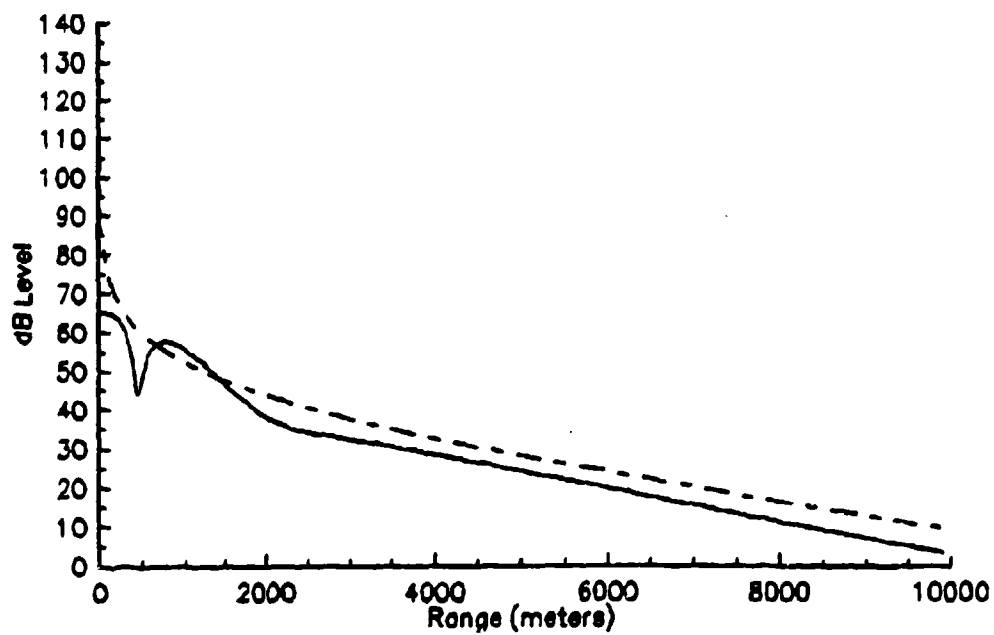
Figure A-4. 350 Hz for homogeneous profile.

25
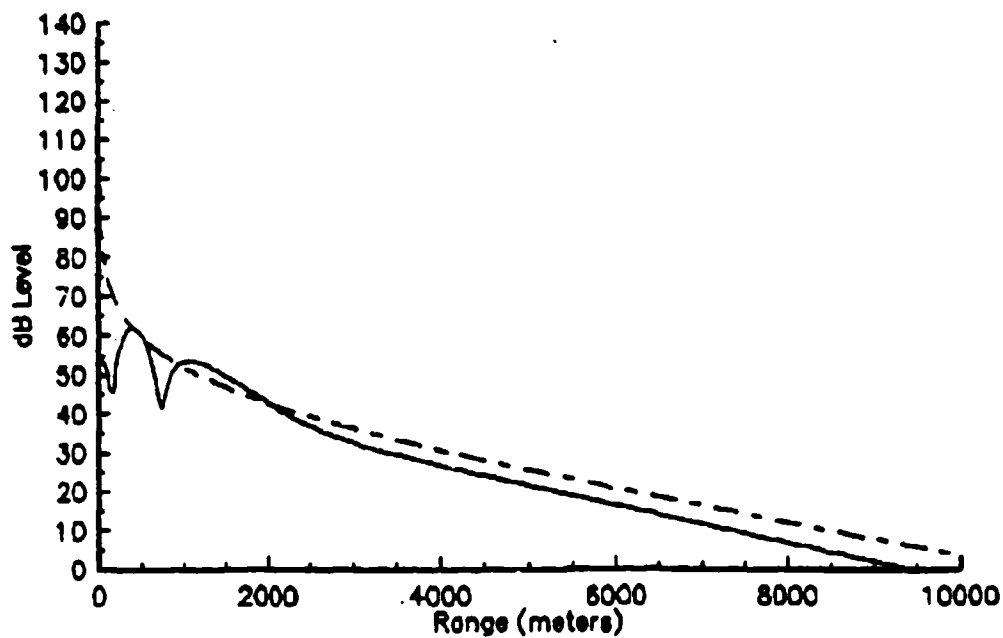
Figure A-5. 450 Hz for homogeneous profile.
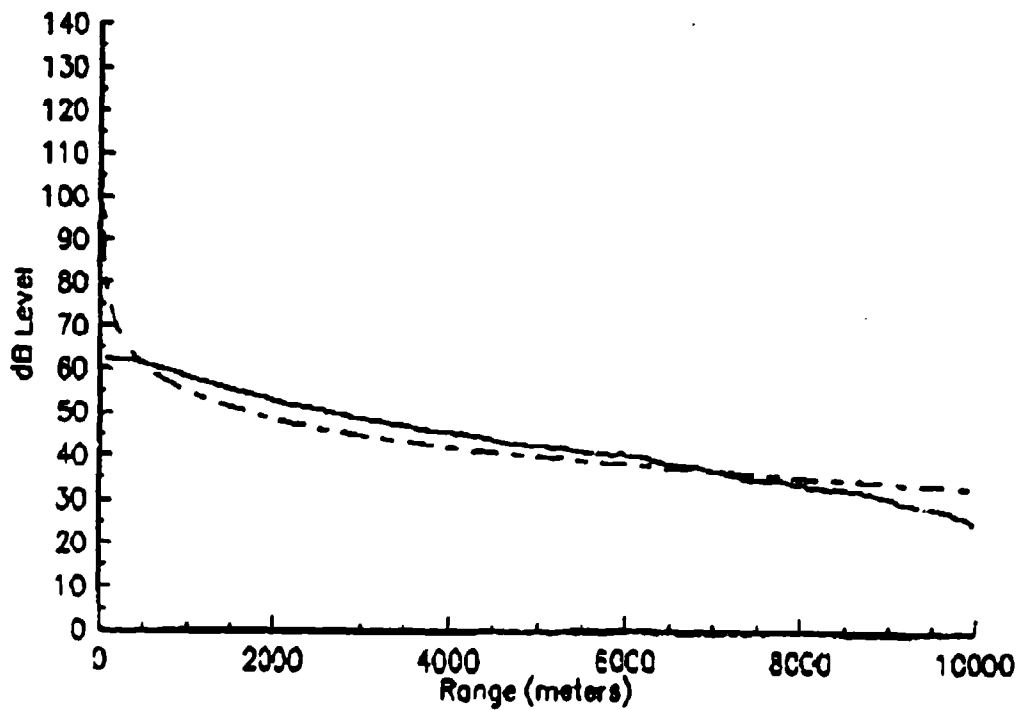
Figure A-6. 50 Hz for mild upward refraction profile.

26
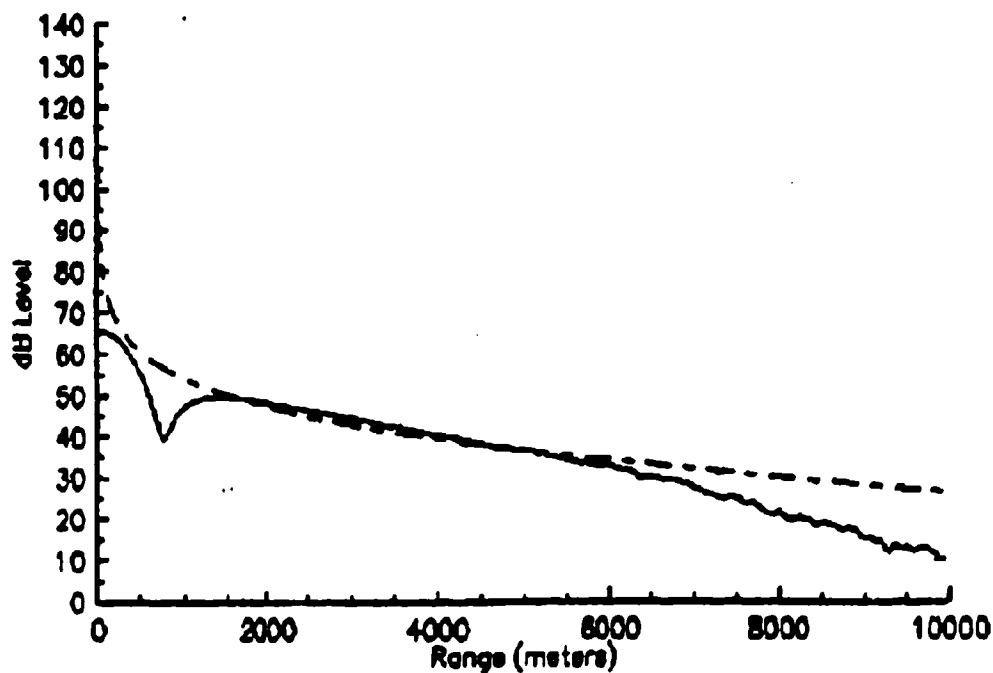
Figure A-7. 150 Hz for mild upward refraction profile.
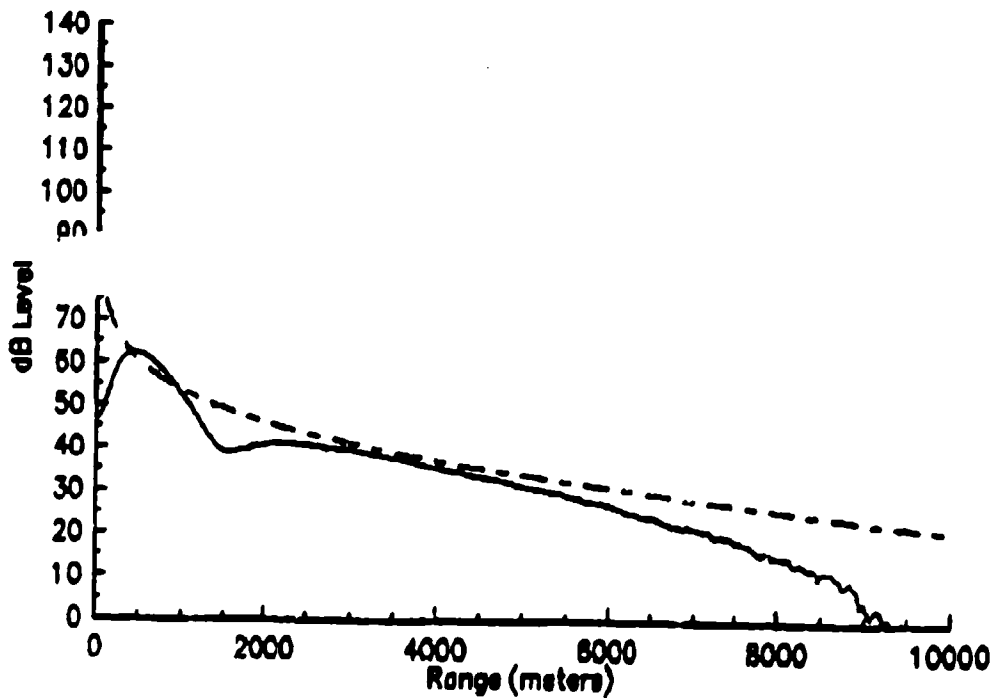
Figure A-8. 250 Hz for mild upward refraction profile.

27
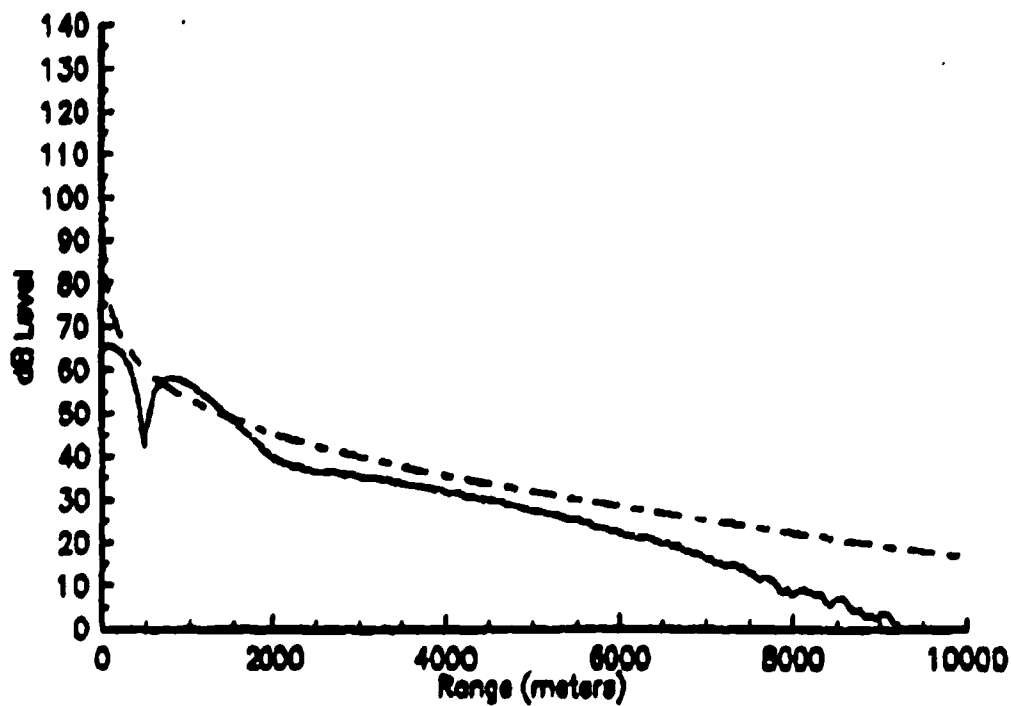
Figure A-9. 350 Hz for mild upward refraction profile.
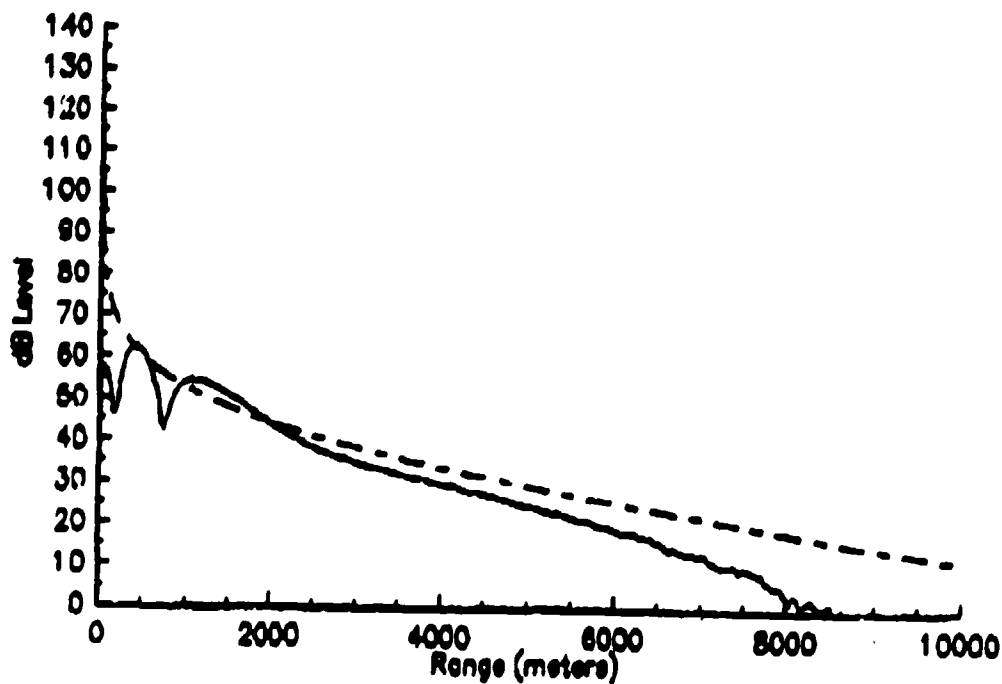
Figure A-10. 450 Hz for mild upward refraction profile.

28
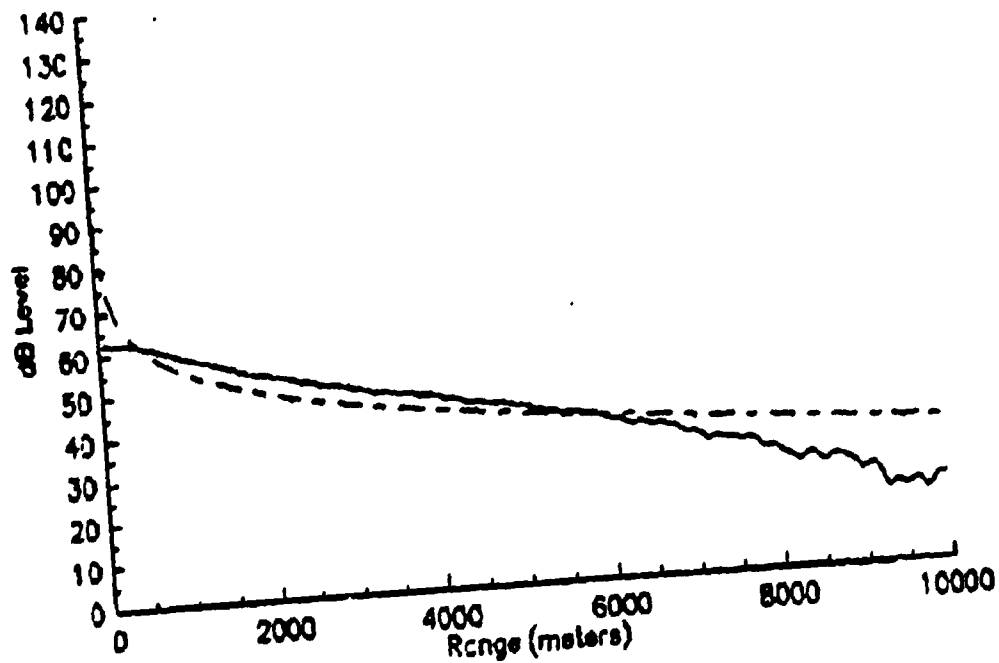
Figure A-11. 50 Hz for strong upward refraction profile.
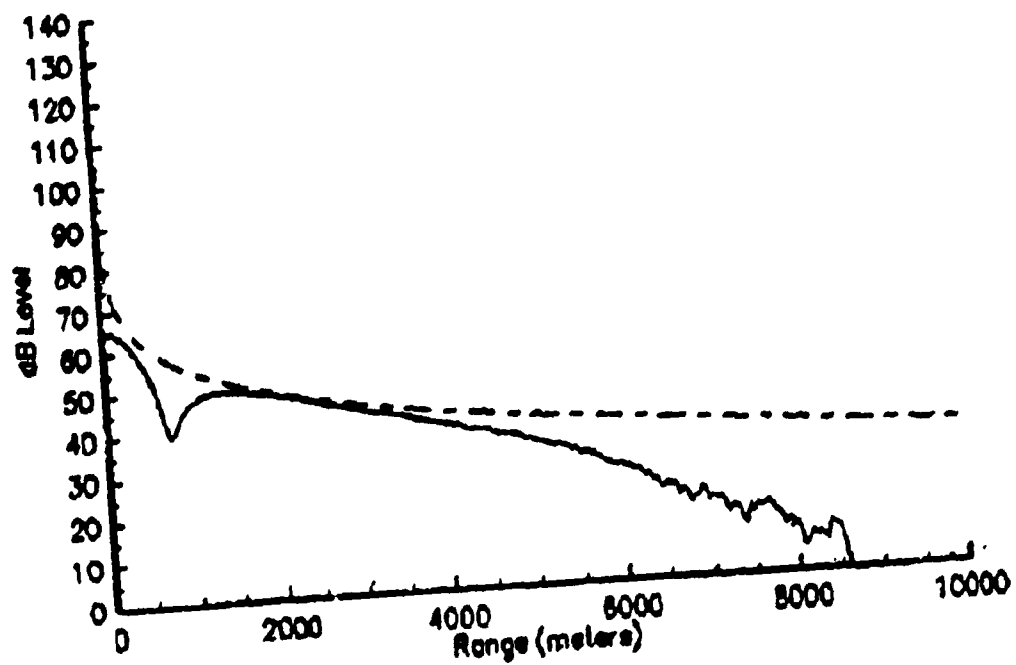
Figure A-12. 150 Hz for strong upward refraction profile.

29
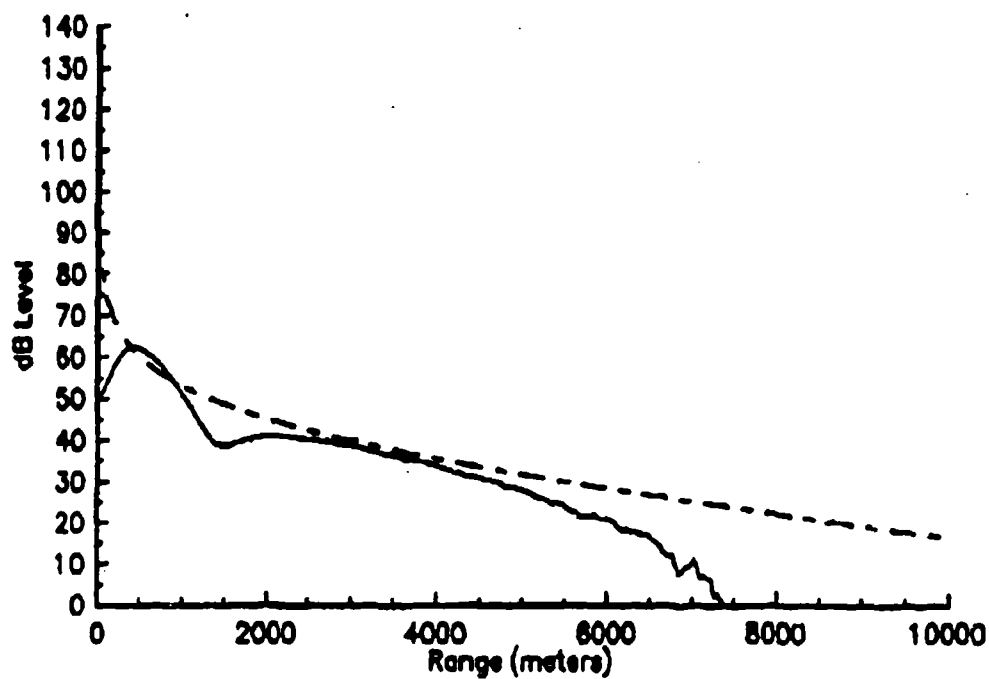
Figure A-13. 250 Hz for strong upward refraction profile.
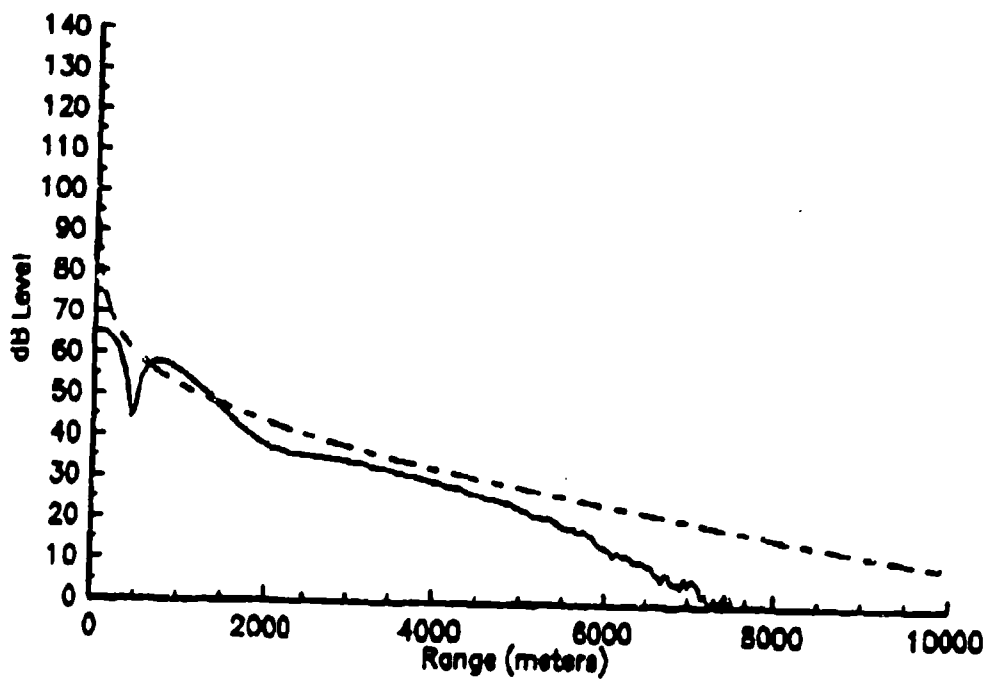
Figure A-14. 350 Hz for strong upward refraction profile.

30
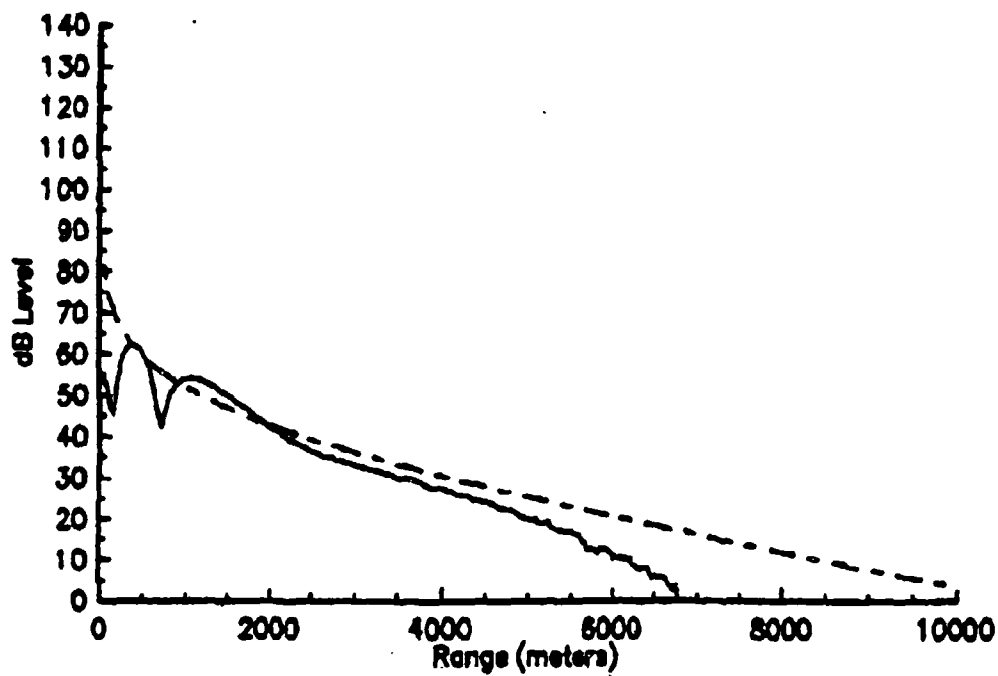
Figure A-15. 450 Hz for strong upward refraction profile.
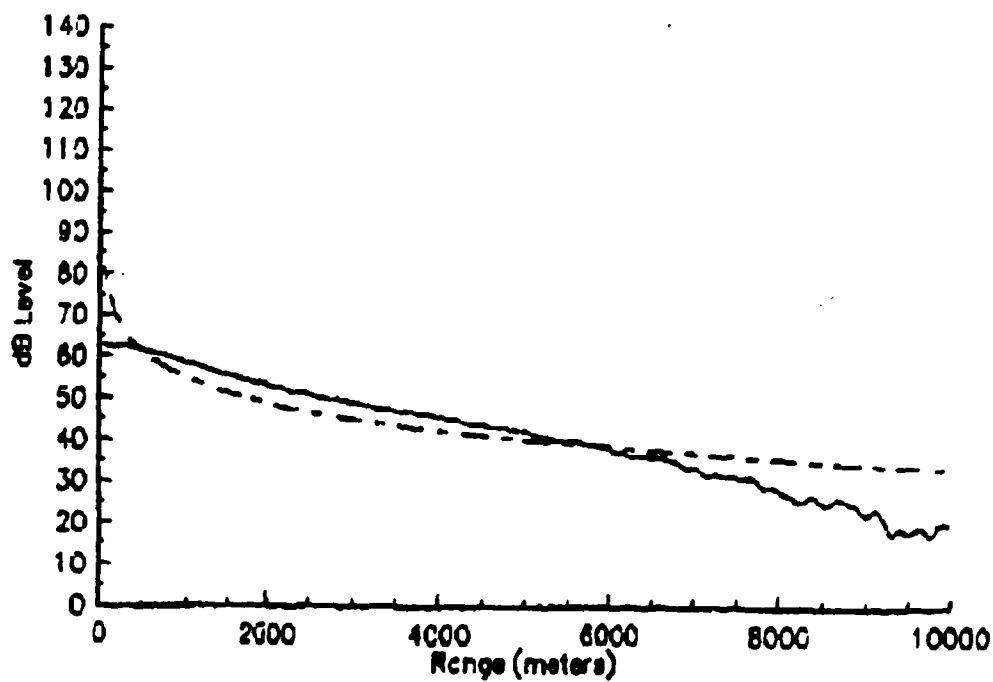
Figure A-16. 50 Hz for downward refraction profile.

31
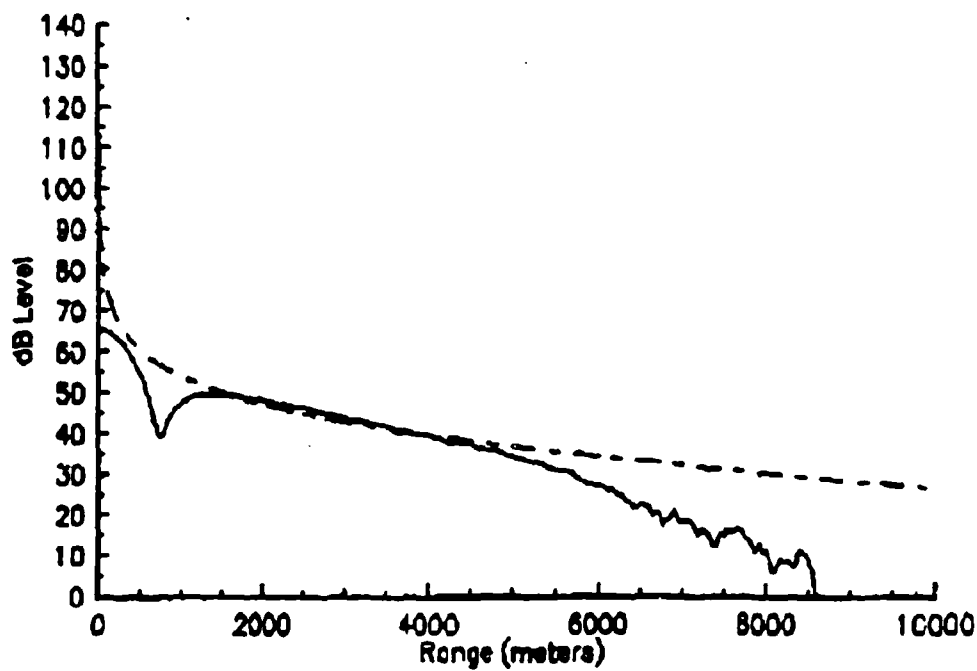
Figure A-17. 150 Hz for downward refraction profile.
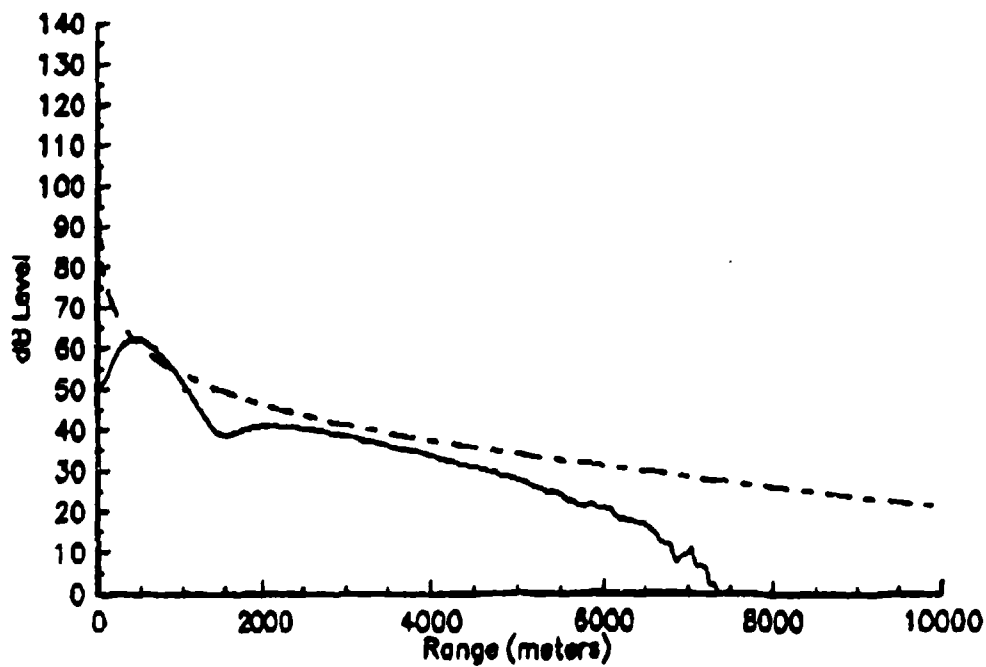
Figure A-18. 250 Hz for downward refraction profile.

32
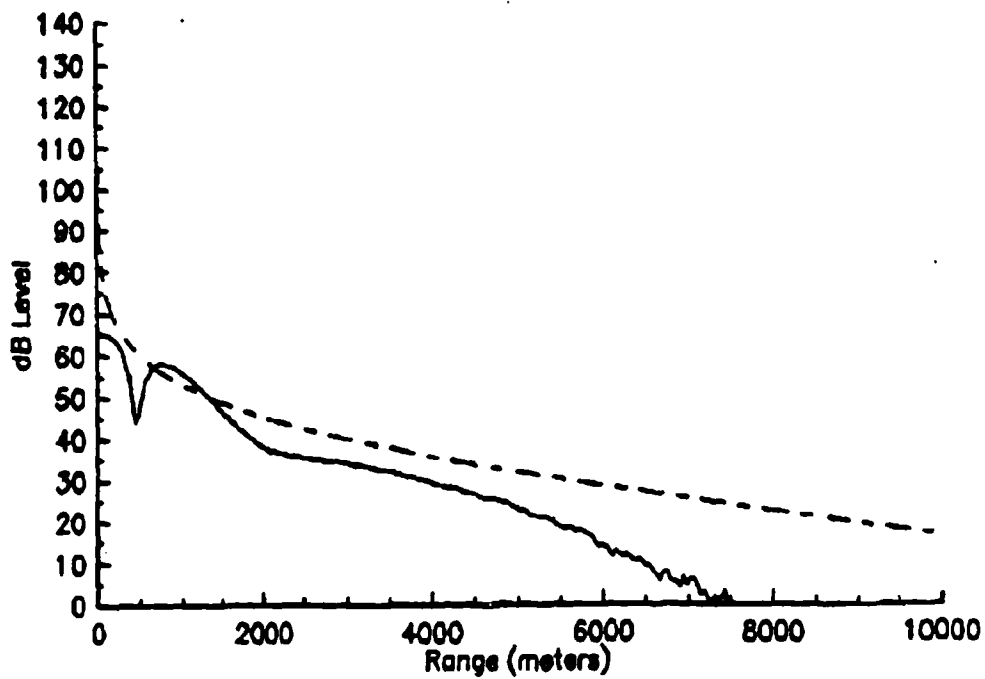
Figure A-19. 350 Hz for downward refraction profile.
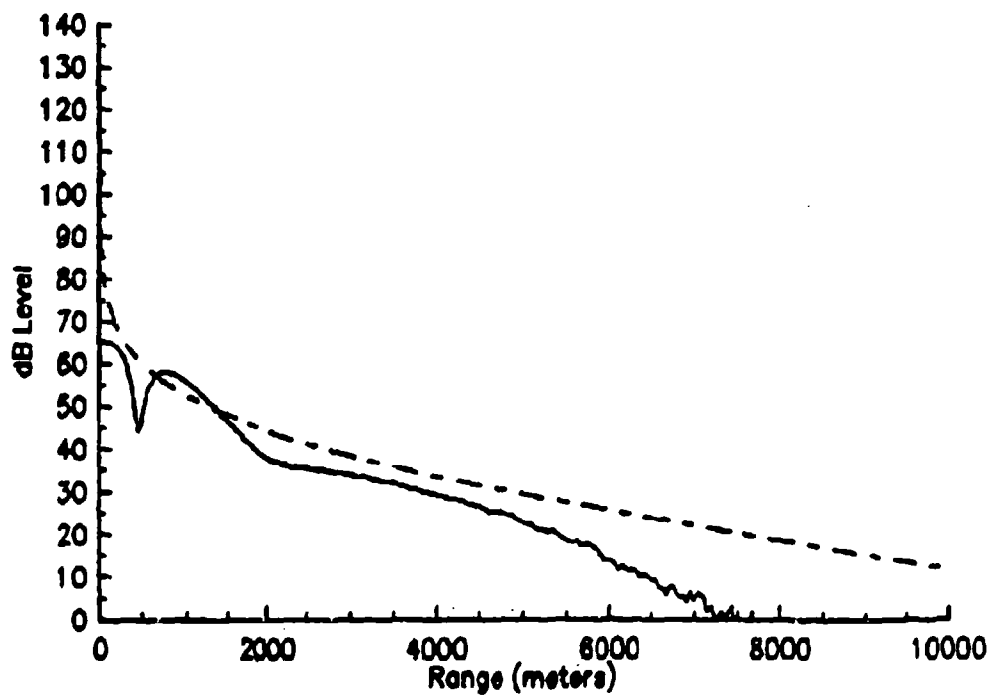
Figure A-20. 450 Hz for downward refraction profile.

33
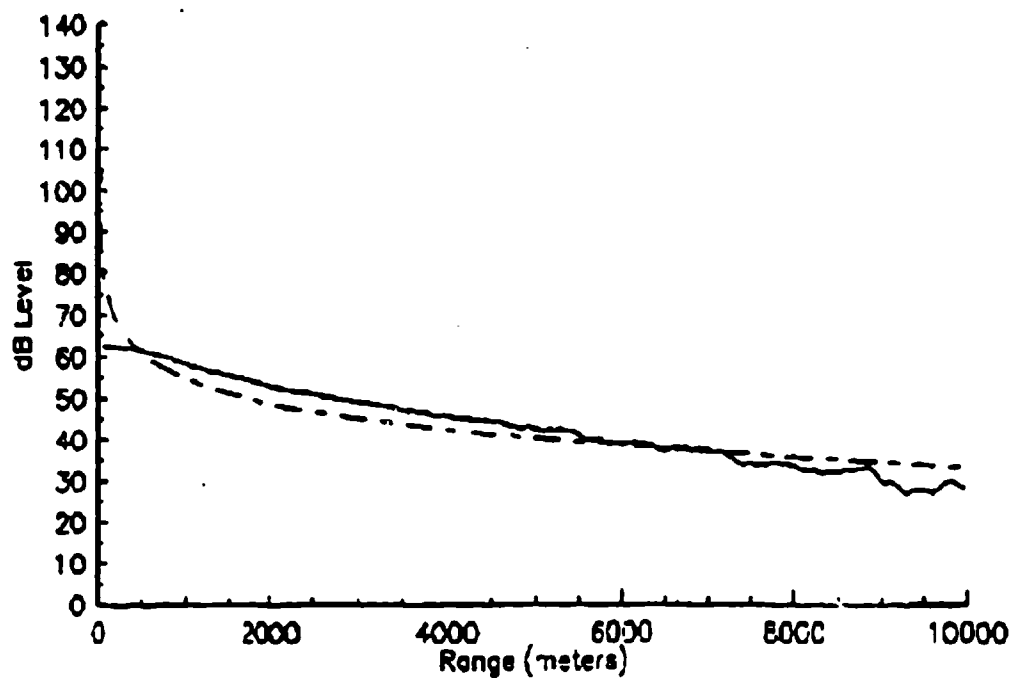
Figure A-21. 50 Hz for shallow inversion profile.
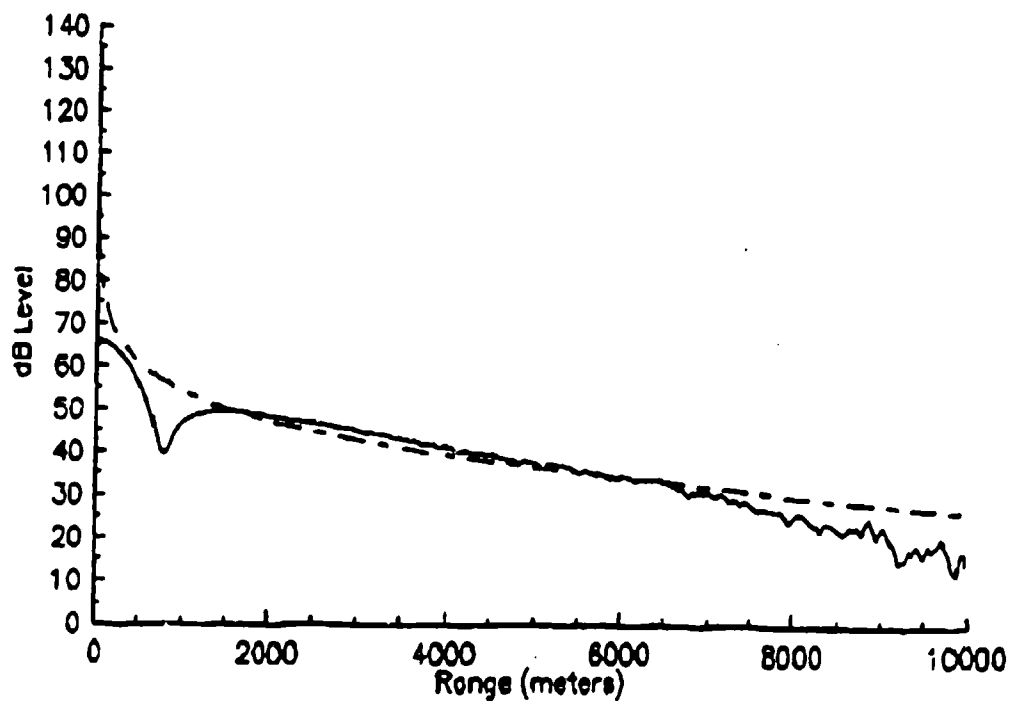
Figure A-22. 150 Hz for shallow inversion profile.

34
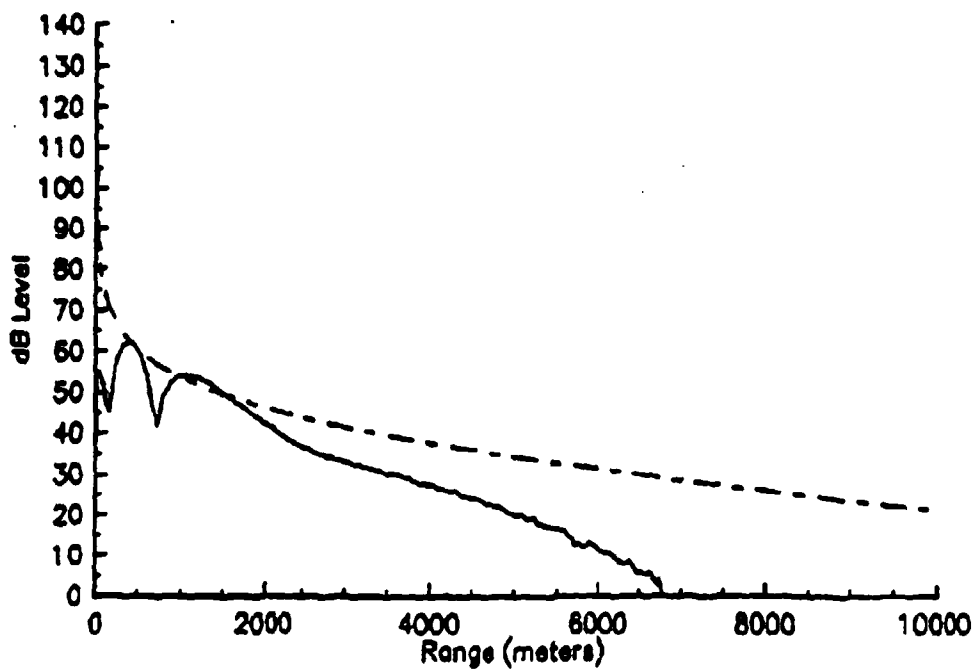
Figure A-23. 250 Hz for shallow inversion profile.
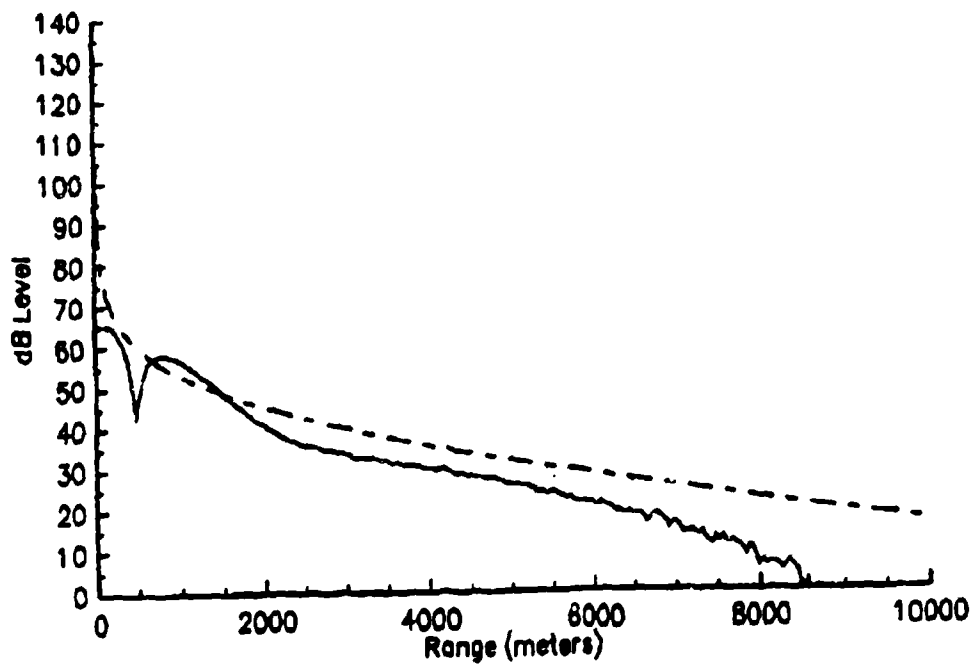
Figure A-24. 350 Hz for shallow inversion profile.

35
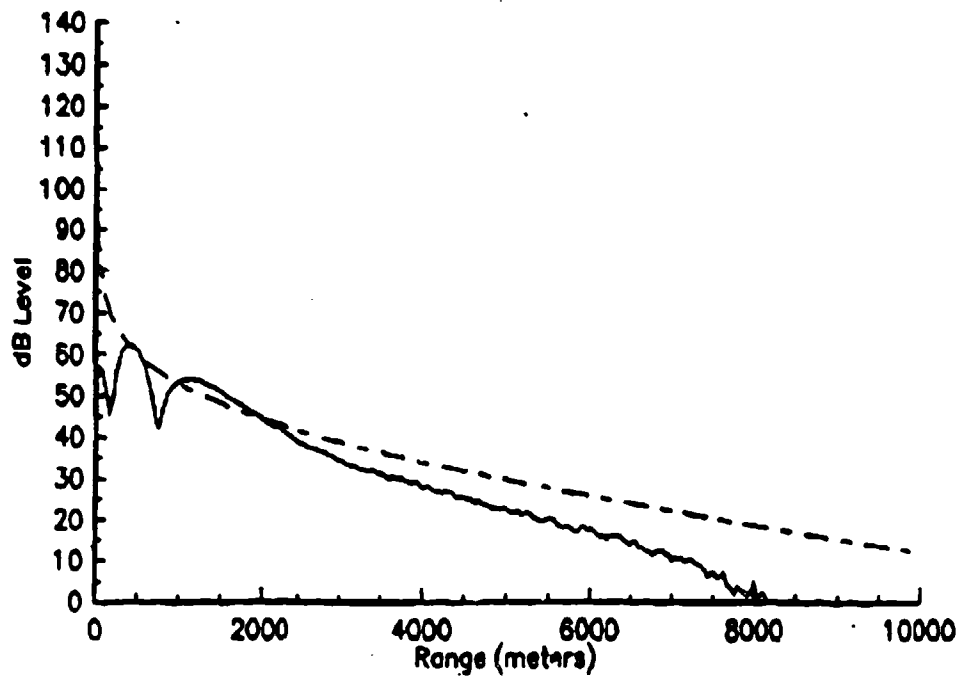
Figure A-25. 450 Hz for shallow inversion profile.
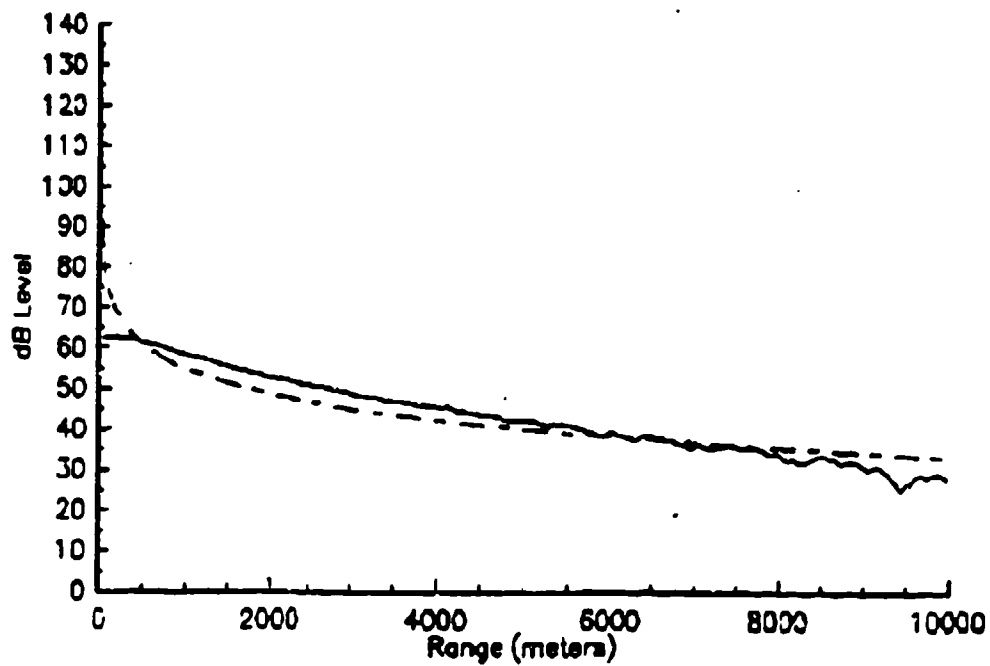
Figure A-26. 50 Hz for deep inversion profile.

36
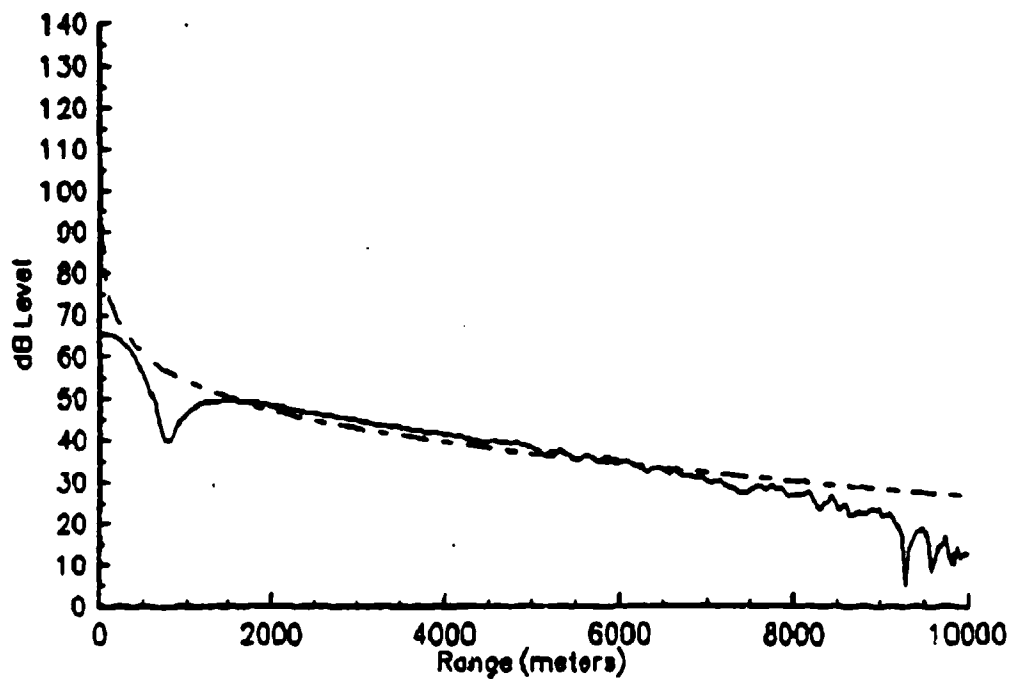
Figure A-27. 150 Hz for deep inversion profile.
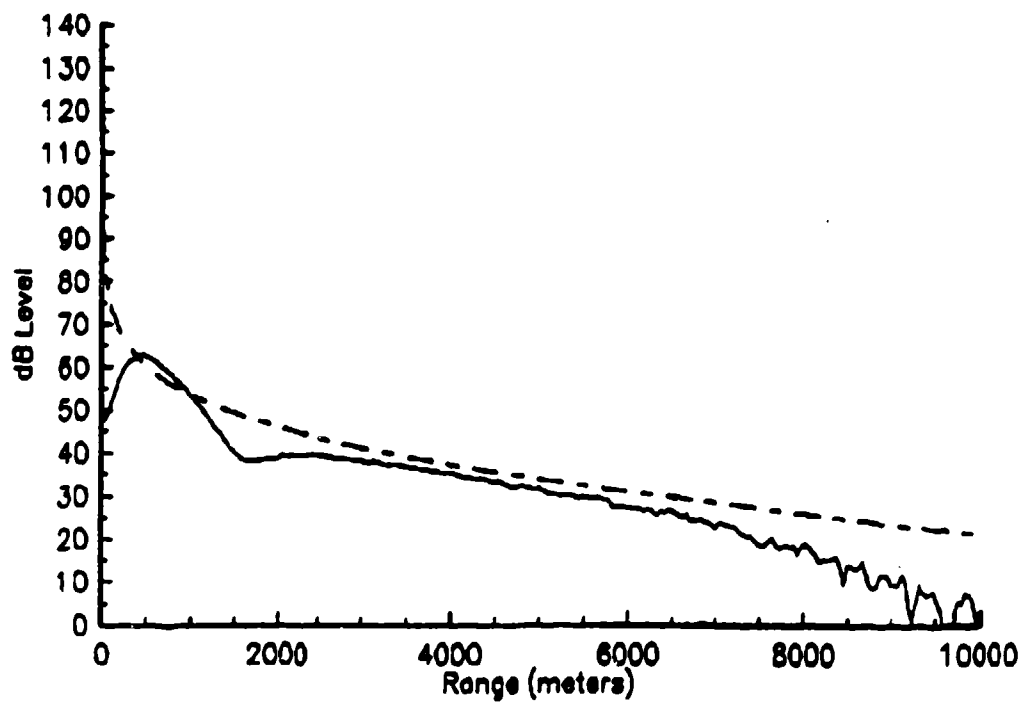
Figure A-28. 250 Hz for deep inversion profile.

37
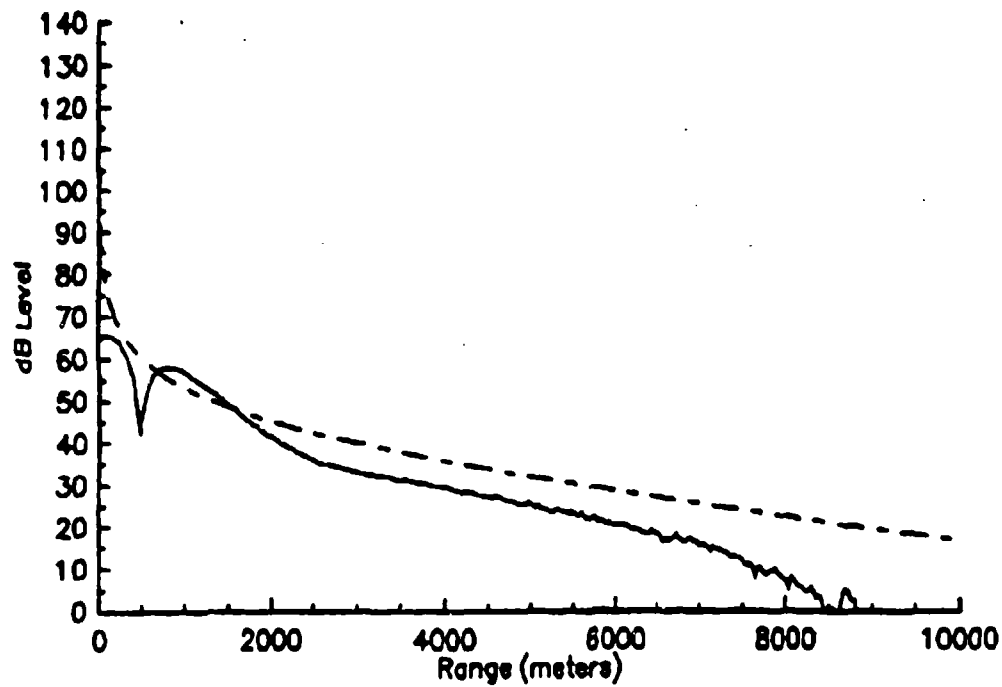
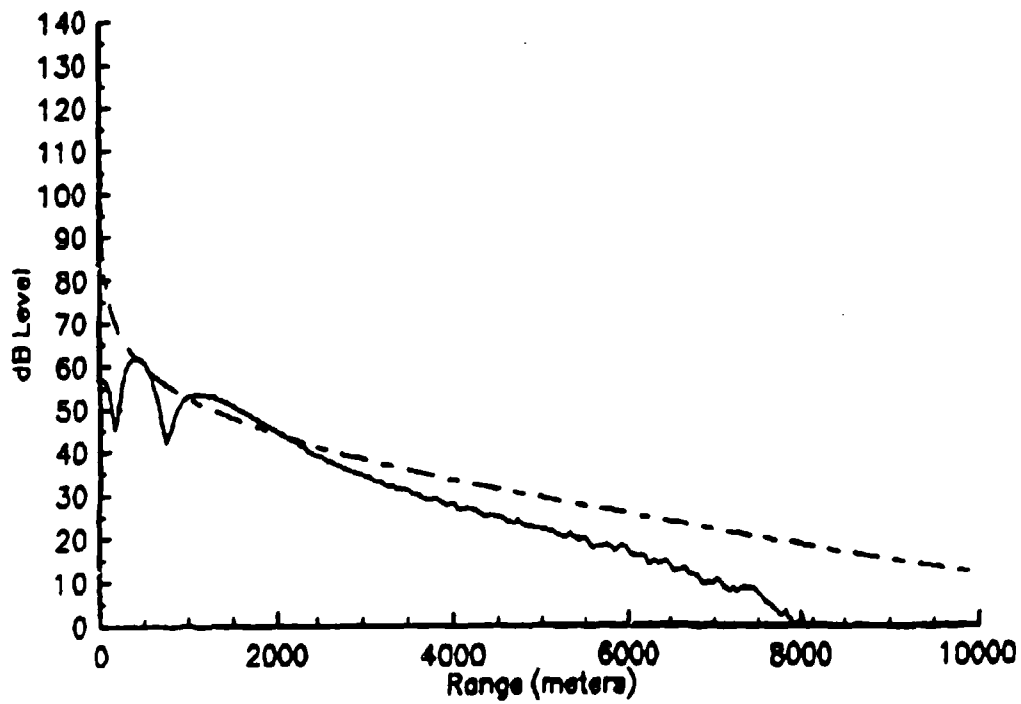Figure A-29. 350 Hz for deep inversion profile.

Figure A-30. 450 Hz for deep inversion profile.

38

Appendix B

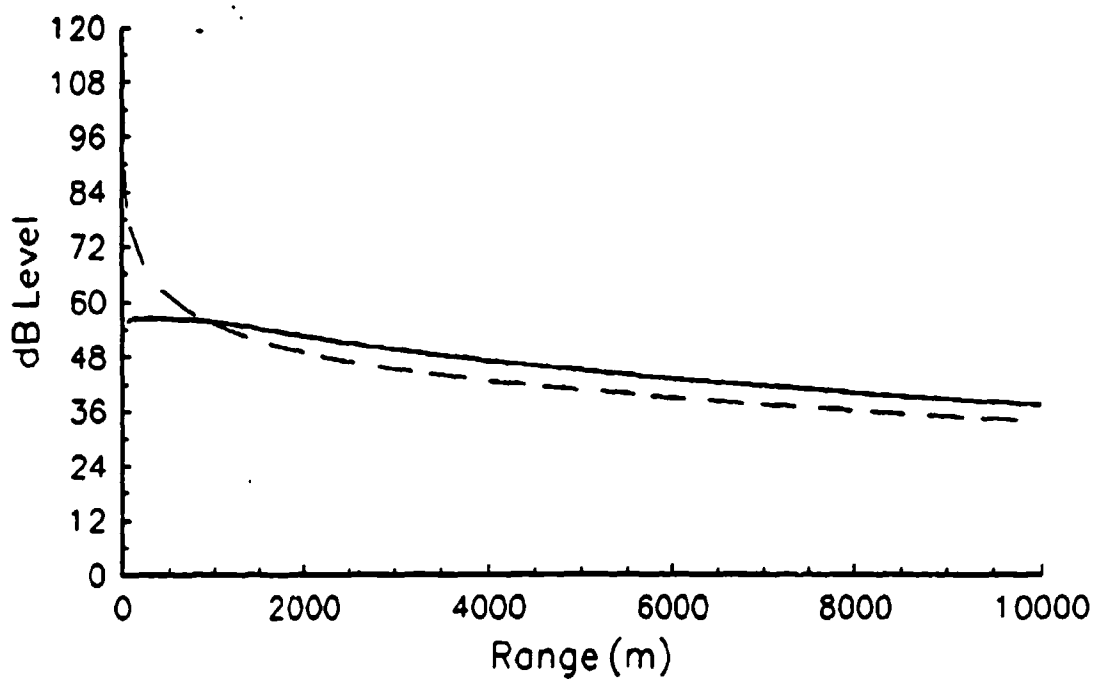## Constant Receiver Height of 1000 m
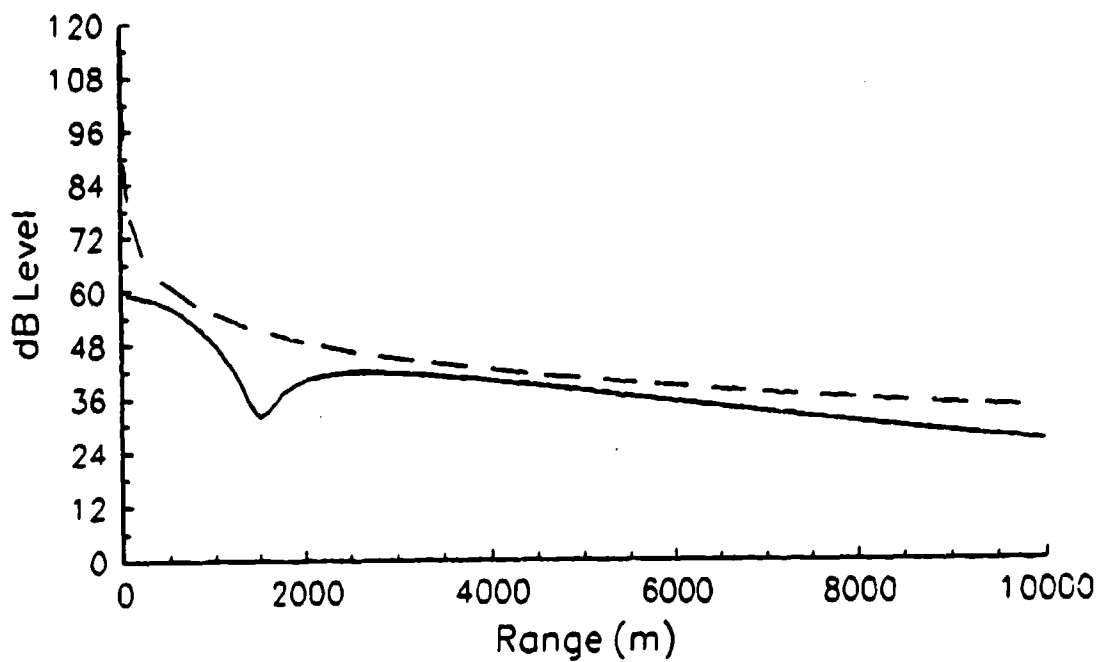
Figure B-1. 50 Hz for homogeneous profile.
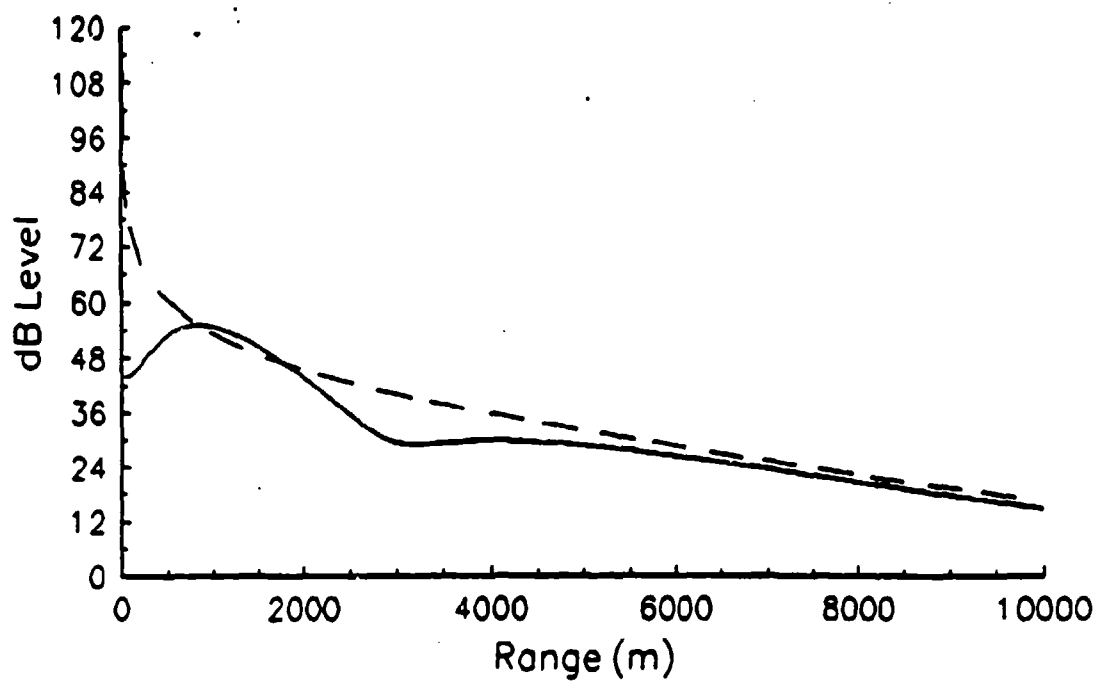

Figure B-2. 150 Hz for homogeneous profile.

40

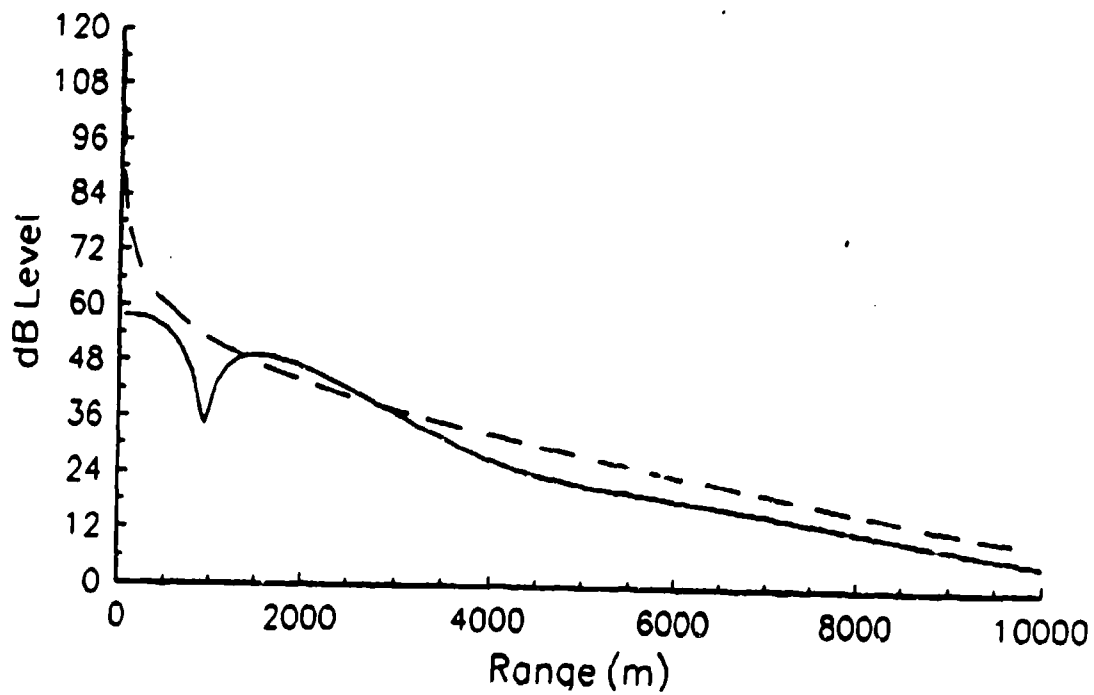**Figure B-3. 250 Hz for homogeneous profile.**

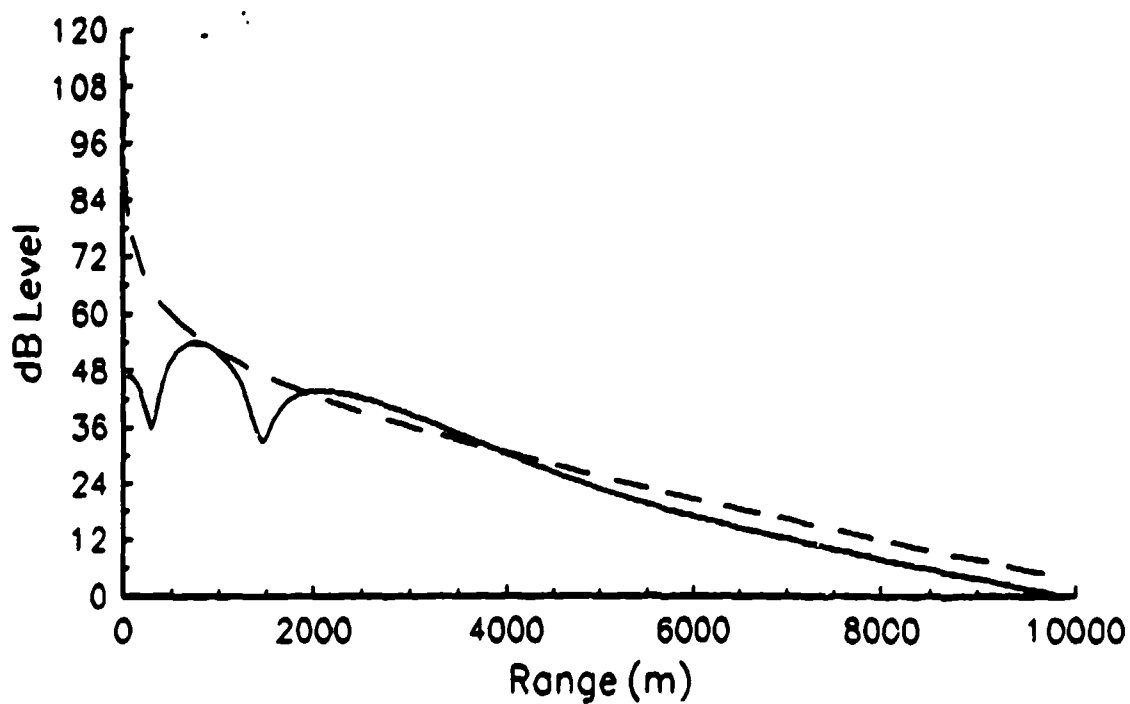**Figure B-4. 350 Hz for homogeneous profile.**

41

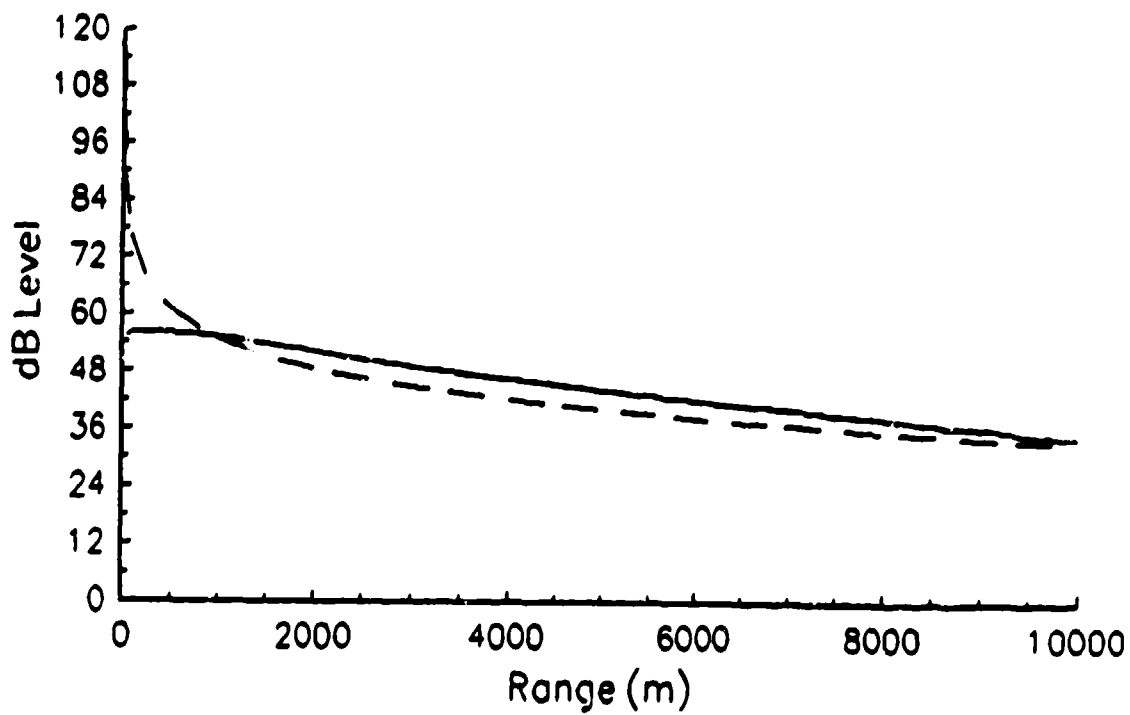**Figure B-5.** 450 Hz for homogeneous profile.

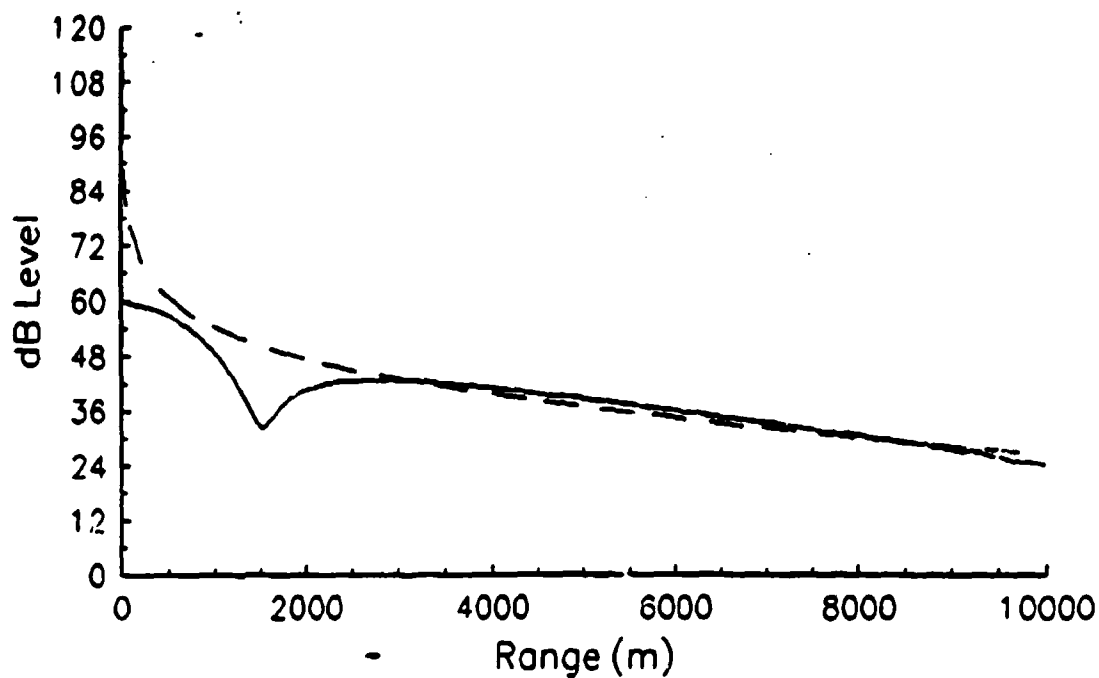**Figure B-6.** 50 Hz for mild upward refraction profile.

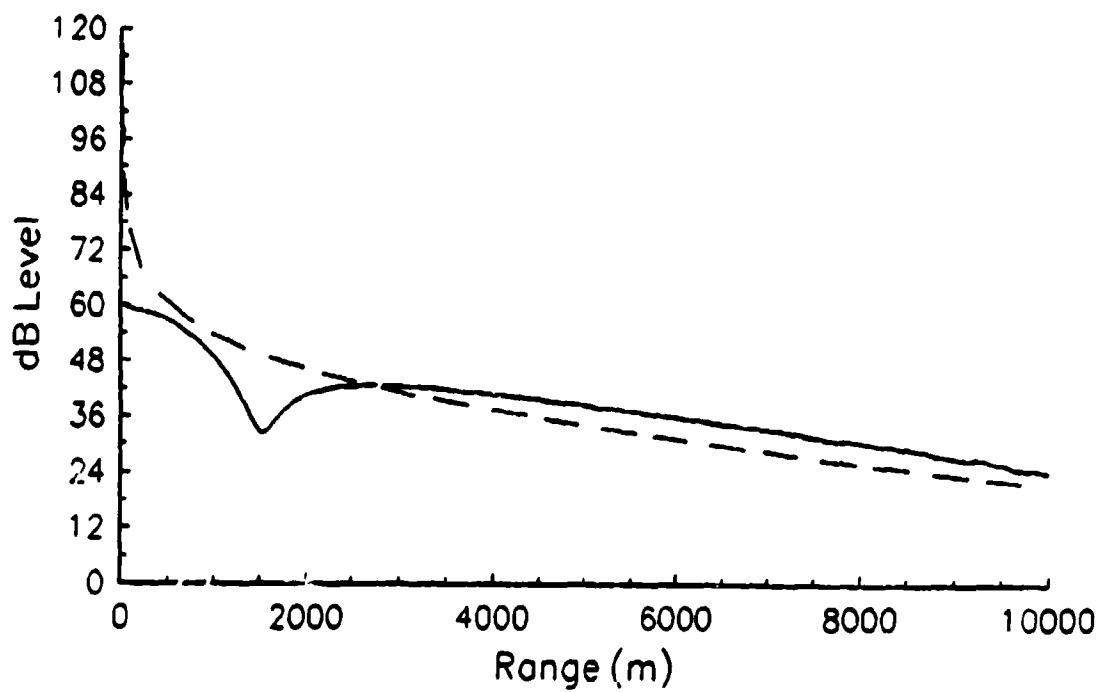42

Figure B-7. 150 Hz for mild upward refraction profile.

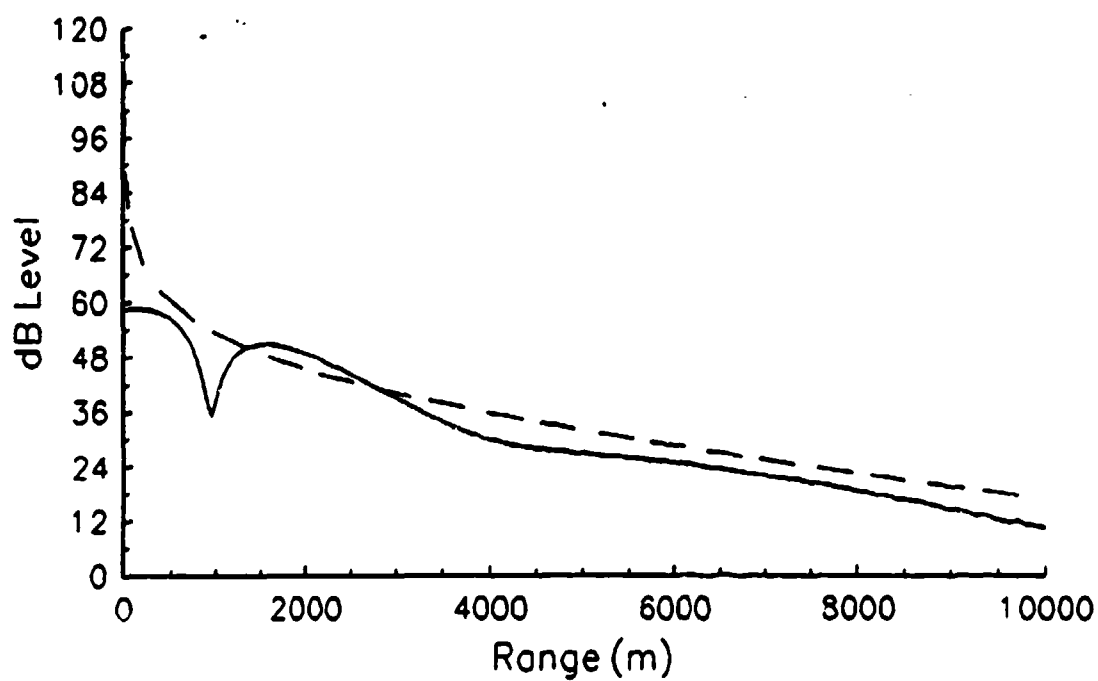**Figure B-8. 250 Hz for mild upward refraction profile.**

43

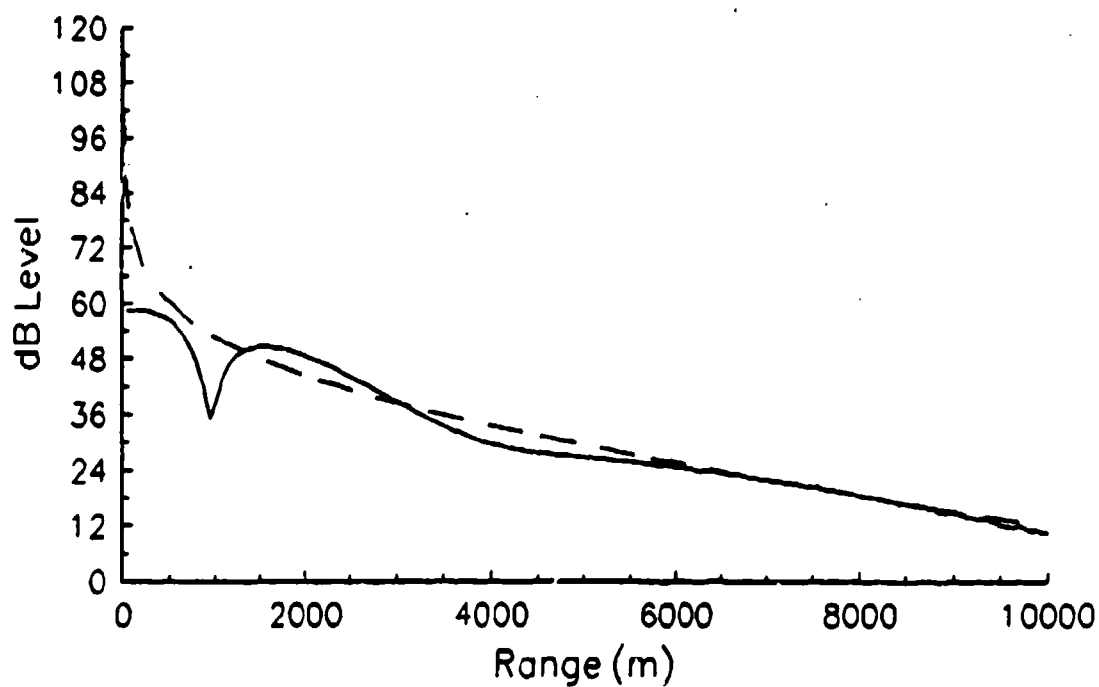**Figure B-9. 350 Hz for mild upward refraction profile.**

Figure B-10. 450 Hz for mild upward refraction profile.
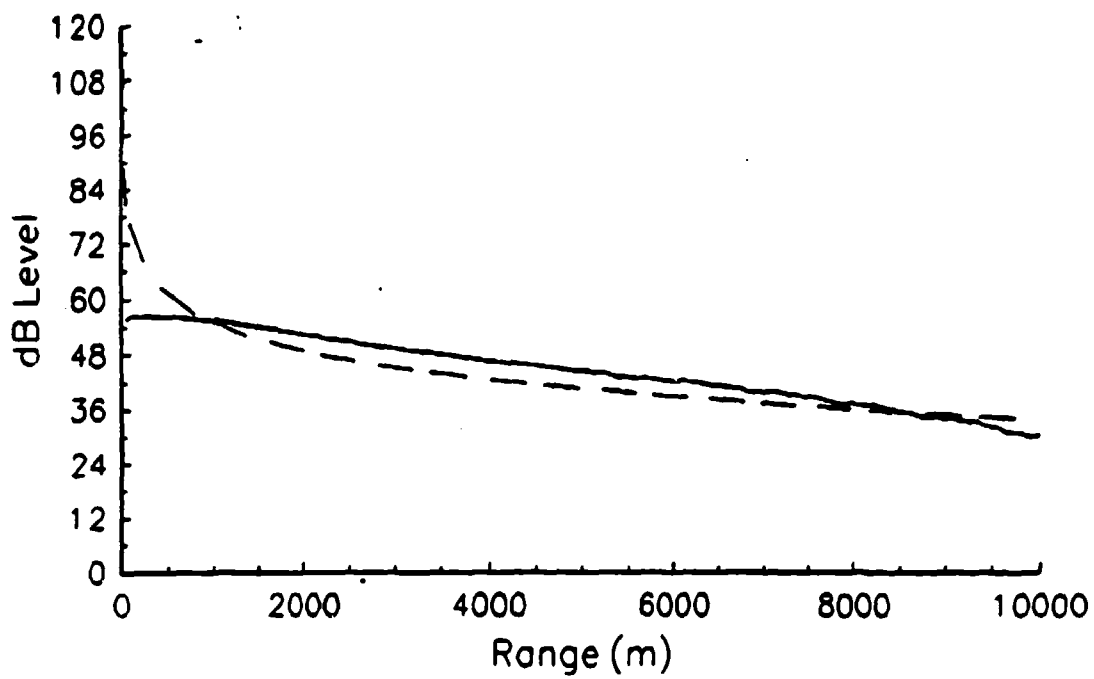
44

Figure B-11. 50 Hz for strong upward refraction profile.

Figure B-12. 150 Hz for strong upward refraction profile.
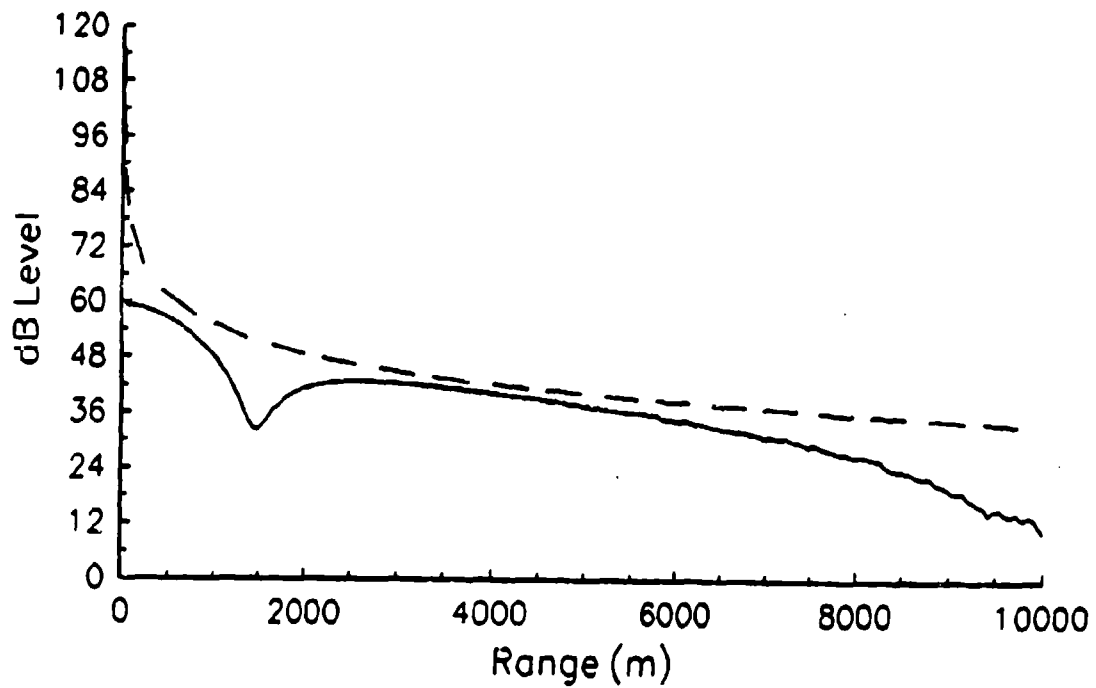
45

Figure B-13. 250 Hz for strong upward refraction profile.
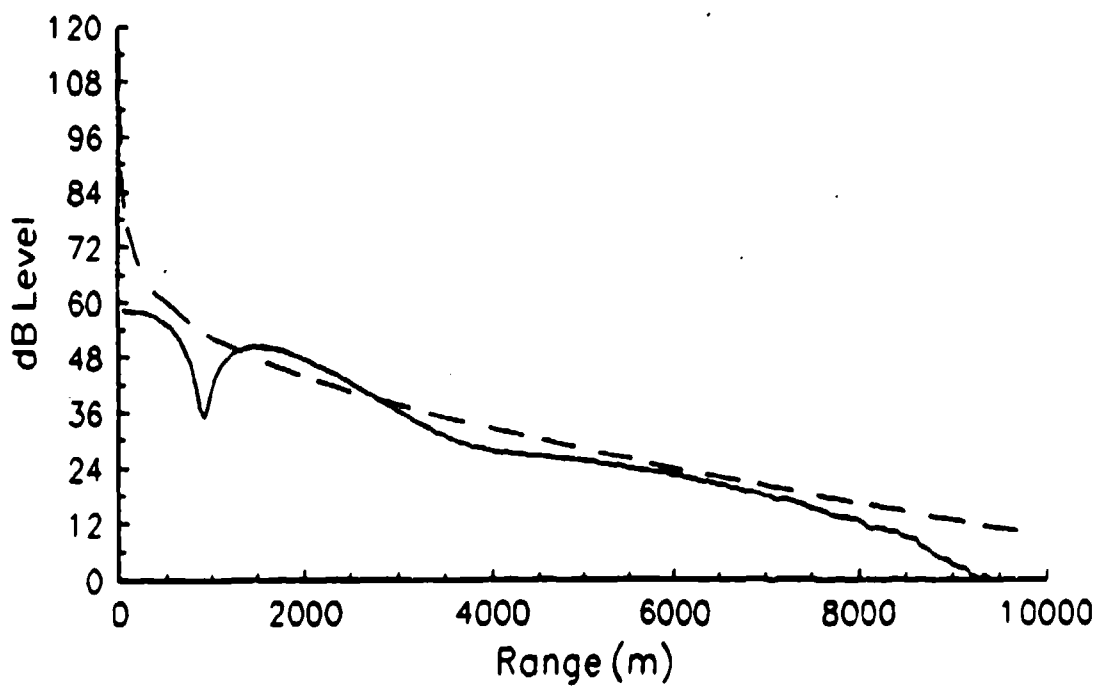
Figure B-14. 350 Hz for strong upward refraction profile.

46
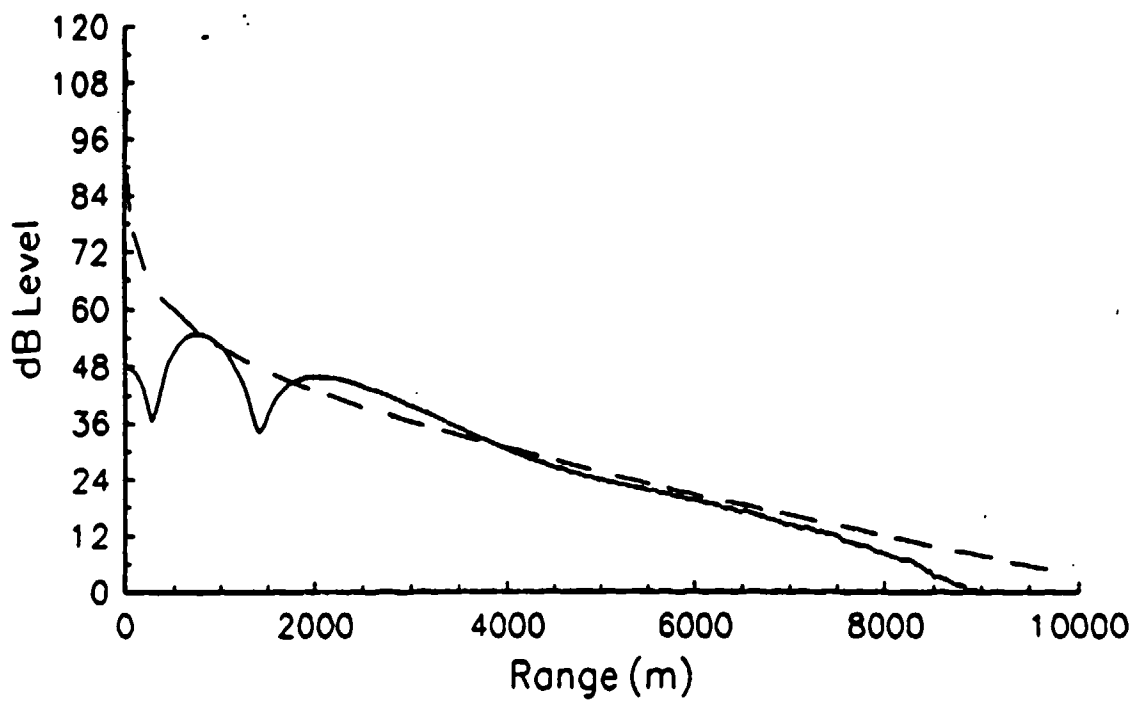
Figure B-15. 450 Hz for strong upward refraction profile.
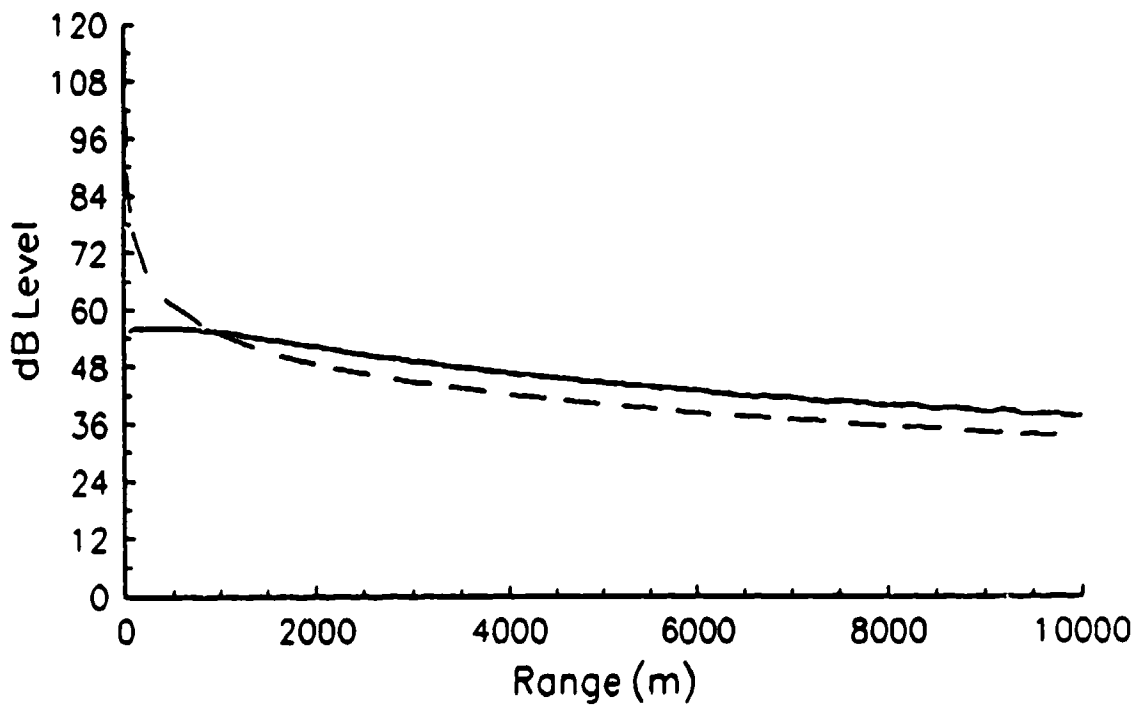
Figure B-16. 50 Hz for downward refraction profile.

47
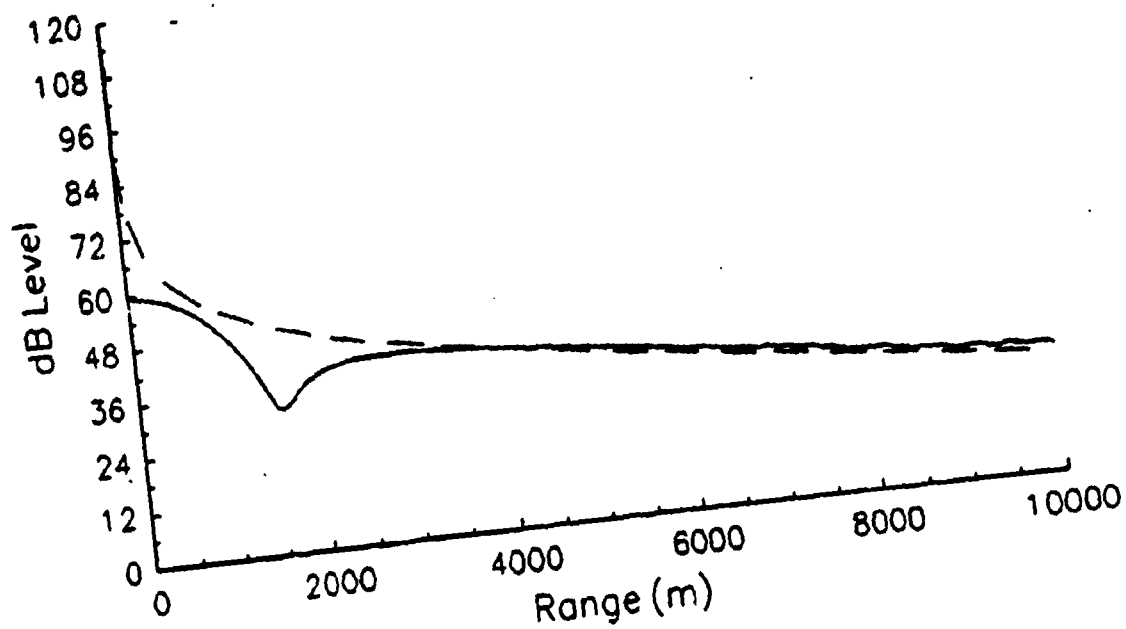
Figure B-17. 150 Hz for downward refraction profile.
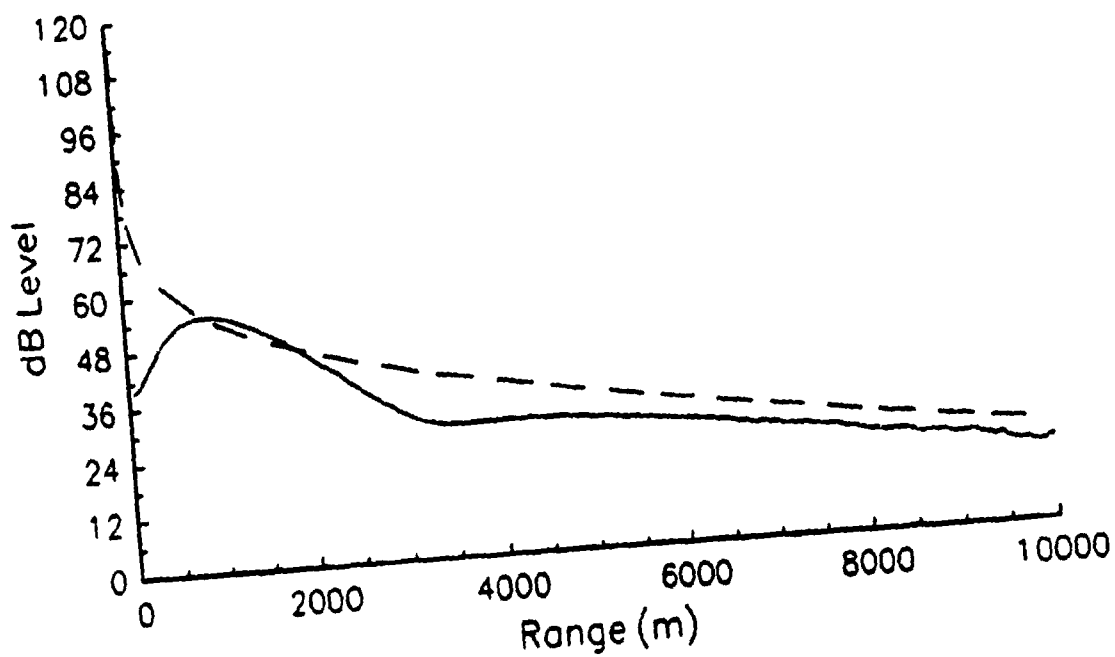
Figure B-18. 250 Hz for downward refraction profile.

48
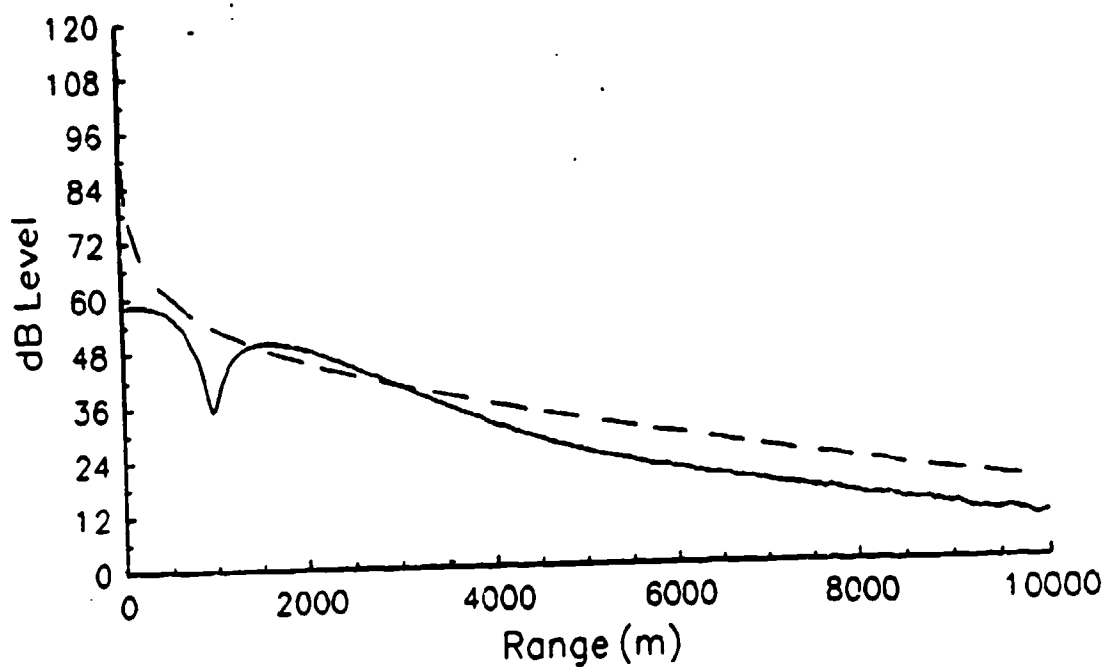
Figure B-19. 350 Hz for downward refraction profile.
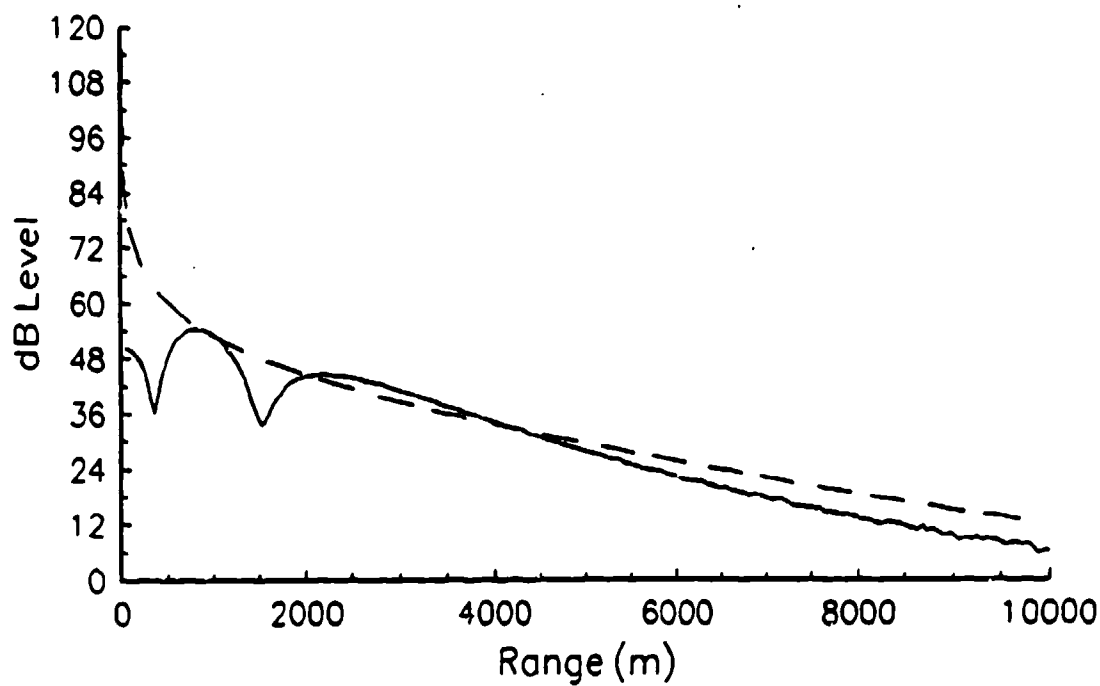
Figure B-20. 450 Hz for downward refraction profile.
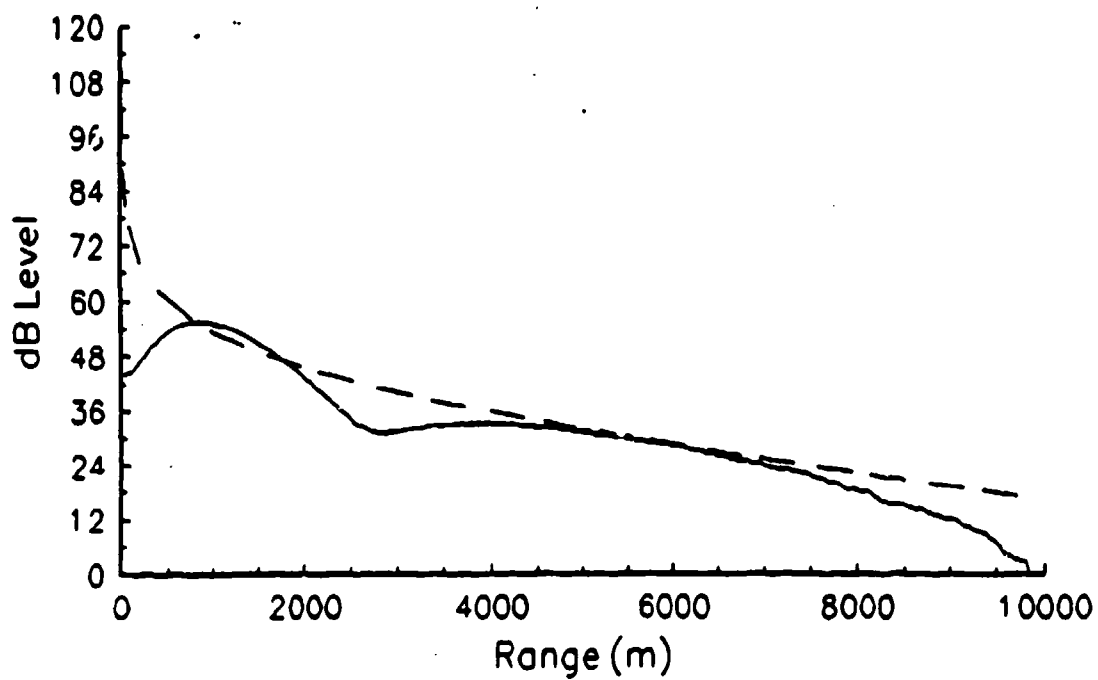
49
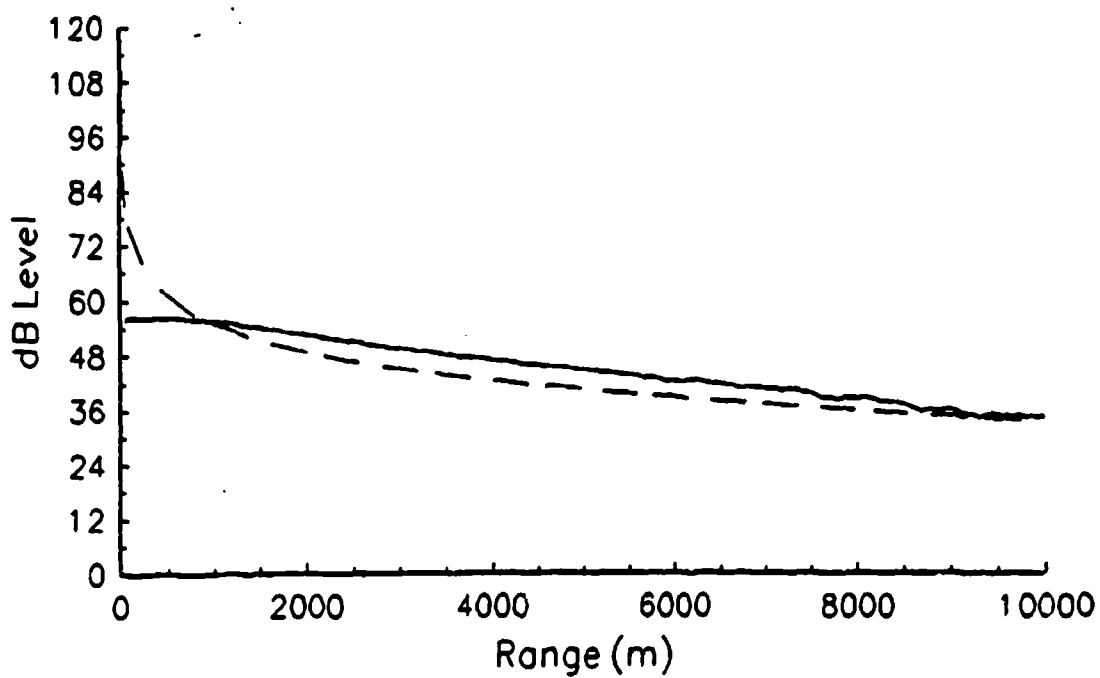
Figure B-21. 50 Hz for shallow inversion profile.
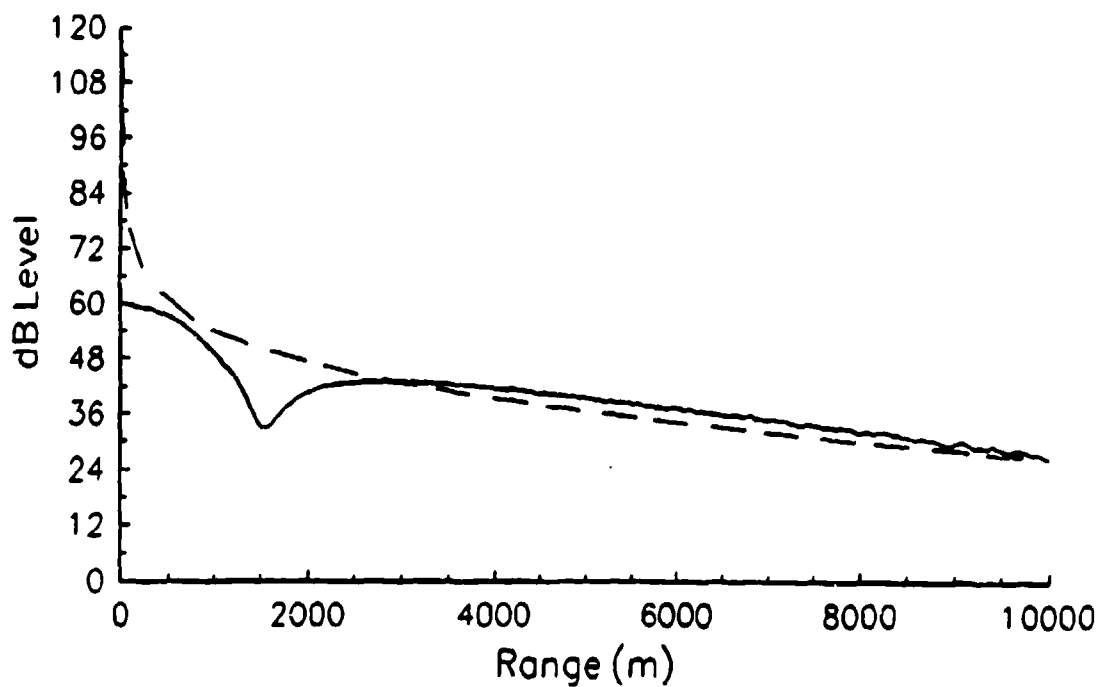
Figure B-22. 150 Hz for shallow inversion profile.

50

Figure B-23. 250 Hz for shallow inversion profile.

Figure B-24. 350 Hz for shallow inversion profile.

51

Figure B-25. 450 Hz for shallow inversion profile.

Figure B-26. 50 Hz for deep inversion profile.

52

Figure B-27. 150 Hz for deep inversion profile.

Figure B-28. 250 Hz for deep inversion profile.

Figure B-29. 350 Hz for deep inversion profile.

Figure B-30. 450 Hz for deep inversion profile.

54

Appendix C

Slant Path
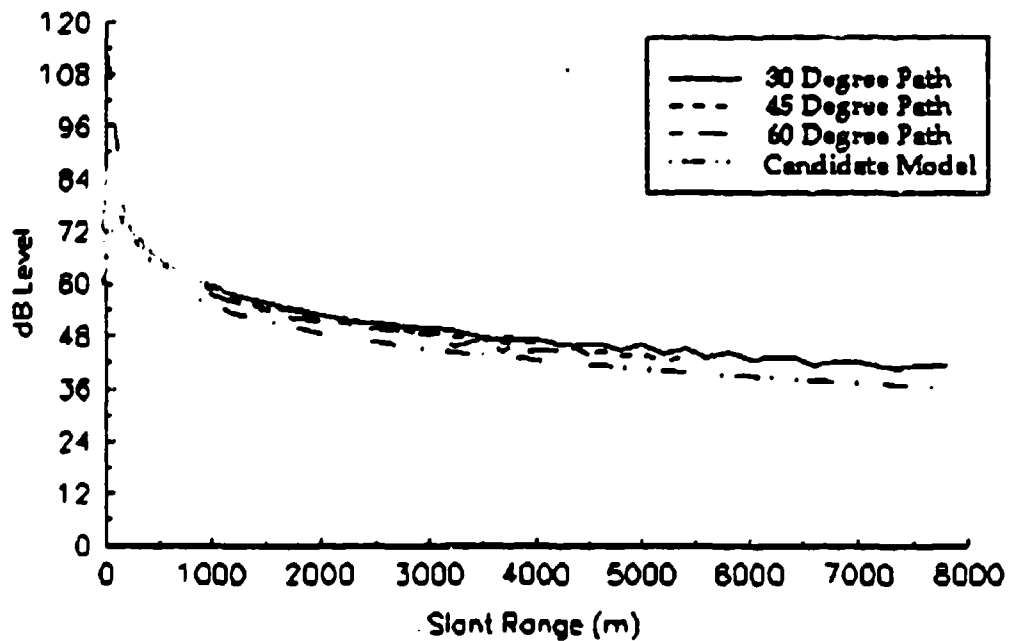
Figure C-1. 50 Hz for homogeneous profile.
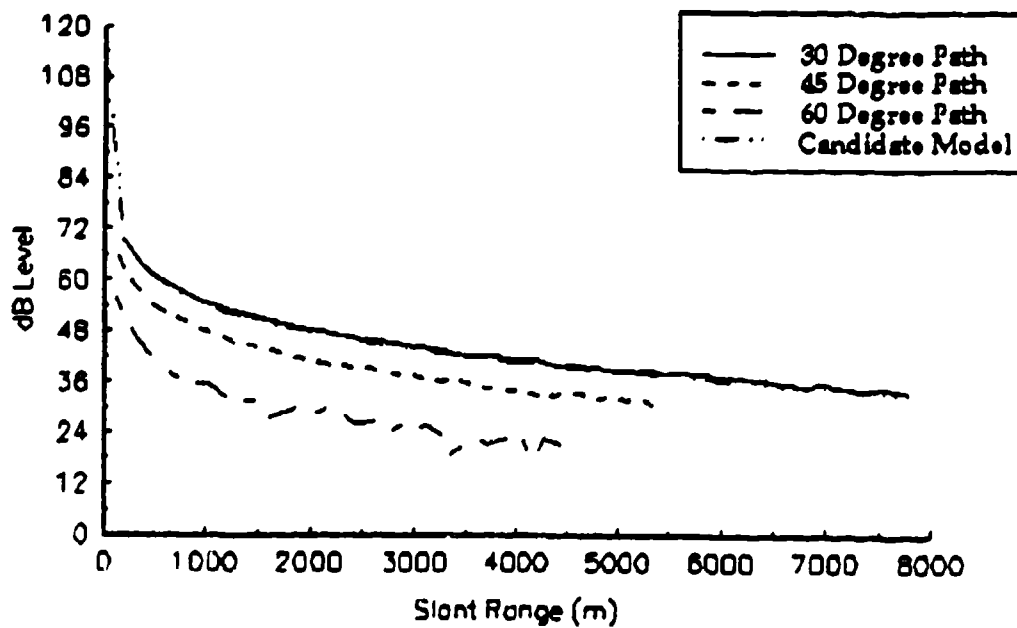
Figure C-2. 100 Hz for homogeneous profile.

56
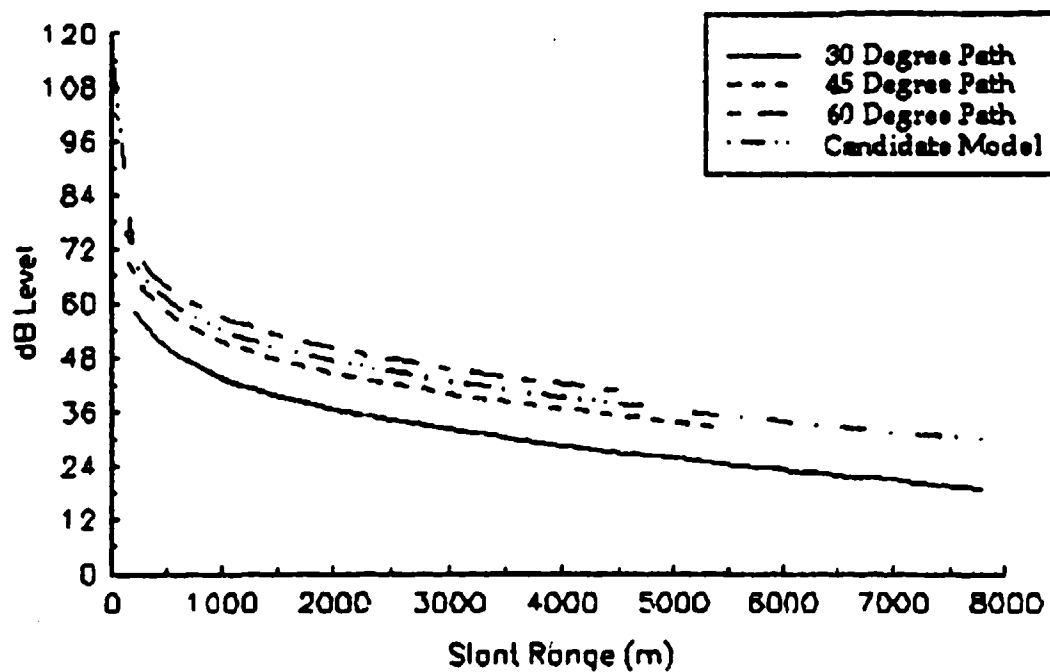
Figure C-3. 150 Hz for homogeneous profile.
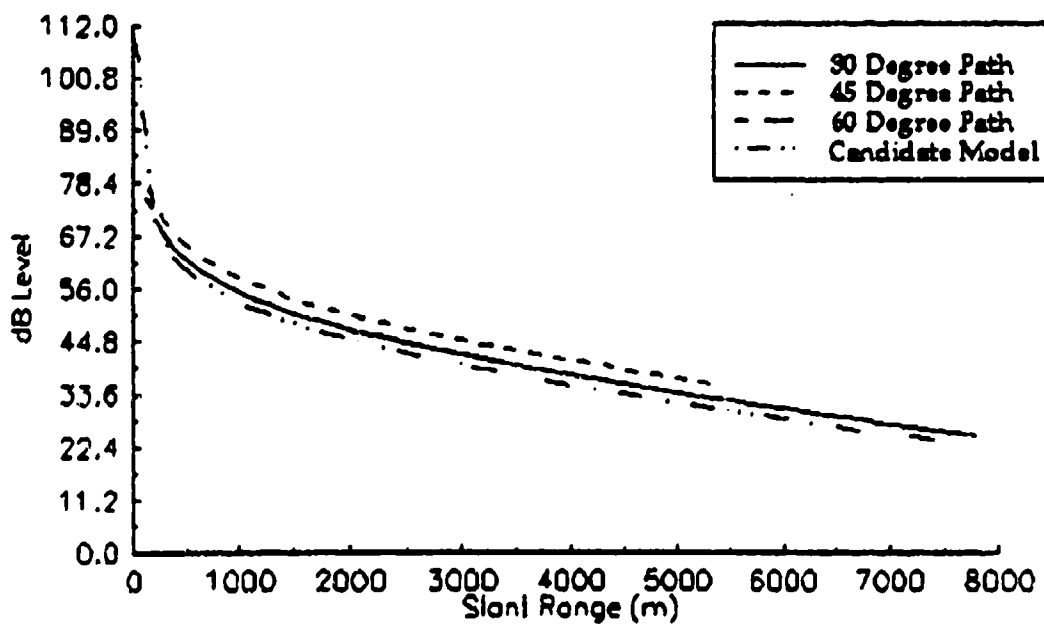
Figure C-4. 250 Hz for homogeneous profile.
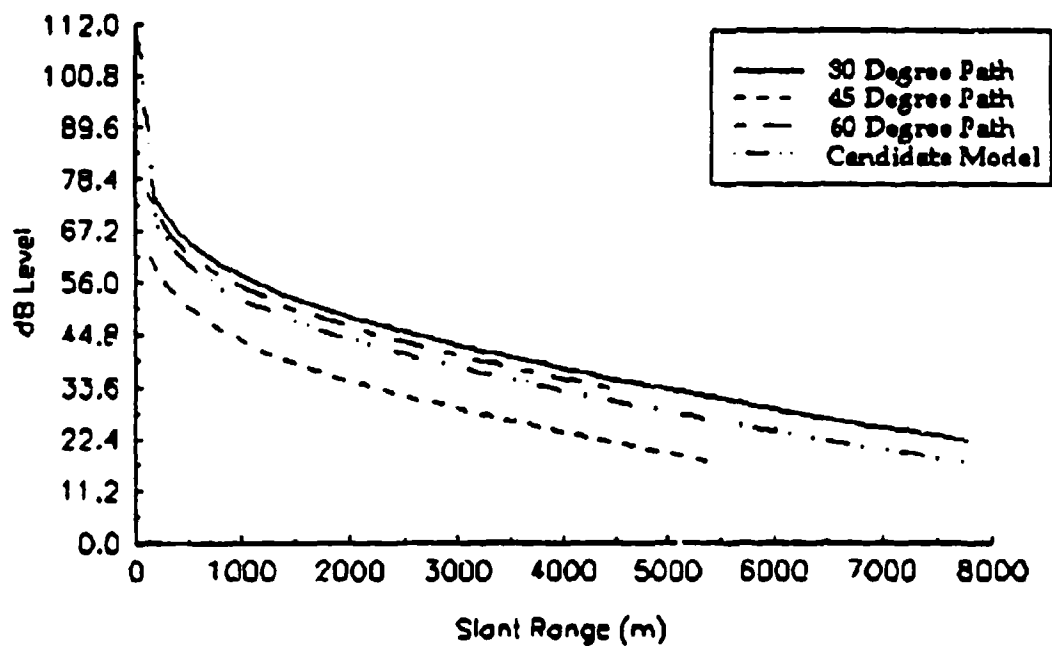
Figure C-5. 350 Hz for homogeneous profile.
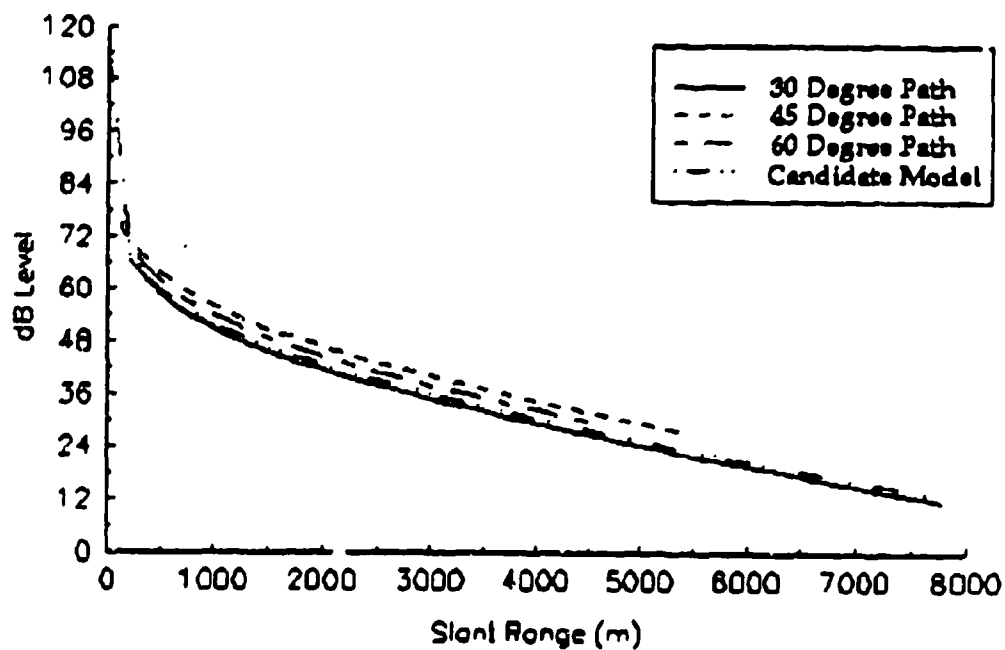
Figure C-6. 450 Hz for homogeneous profile.

58
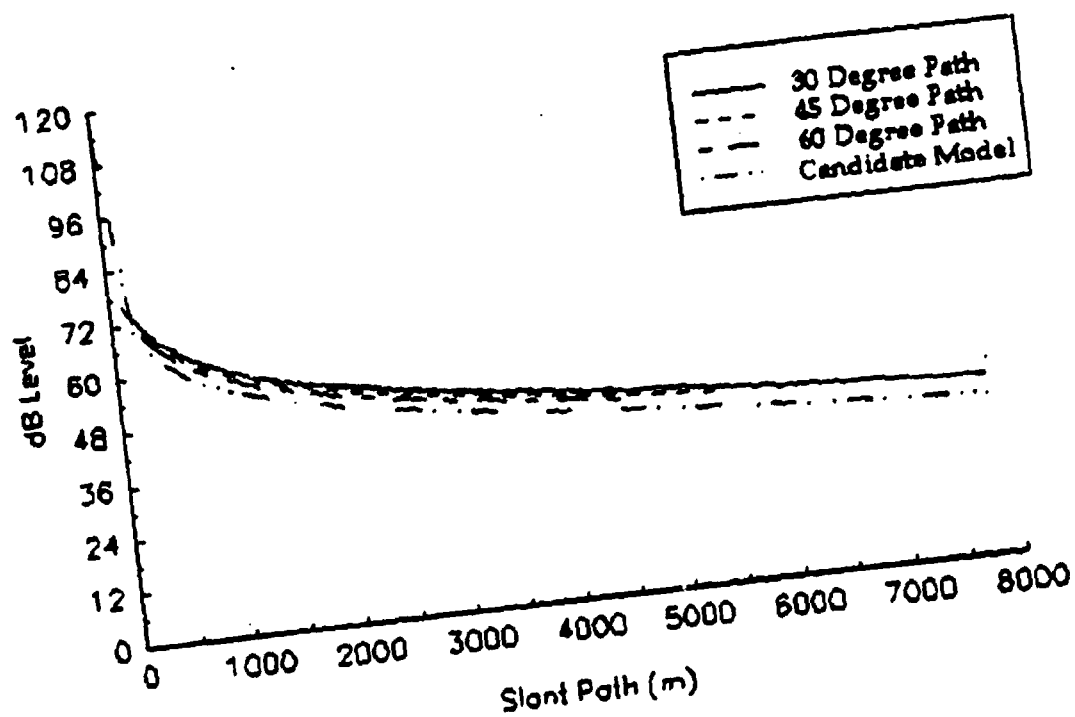
Figure C-7. 50 Hz for mild upward refraction profile.
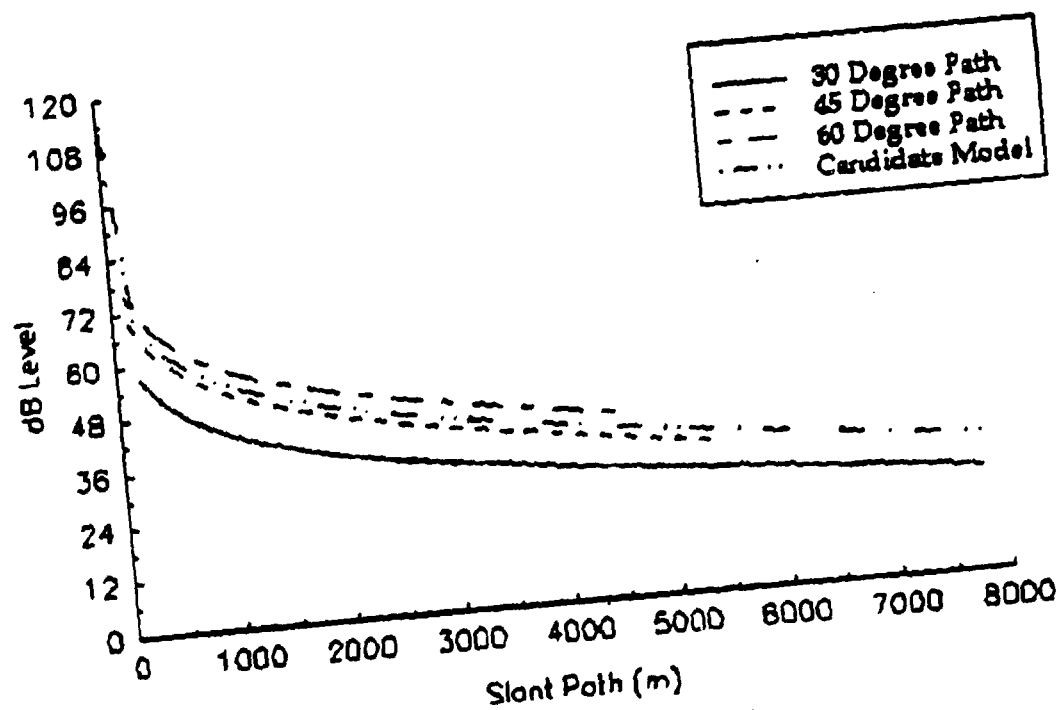
Figure C-8. 150 Hz for mild upward refraction profile.

59
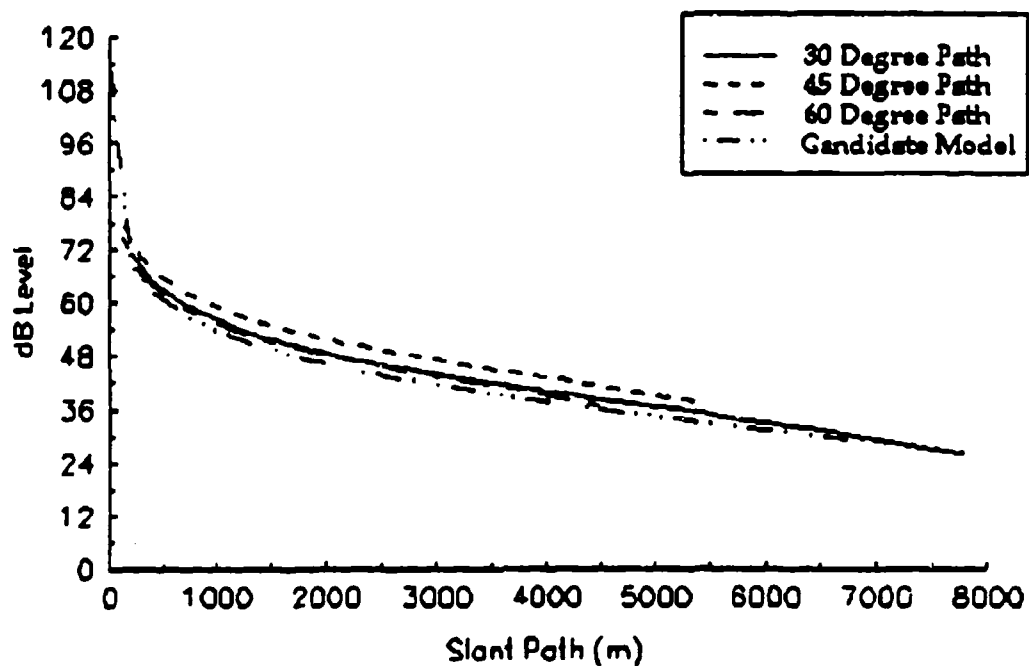
Figure C-9. 250 Hz for mild upward refraction profile.
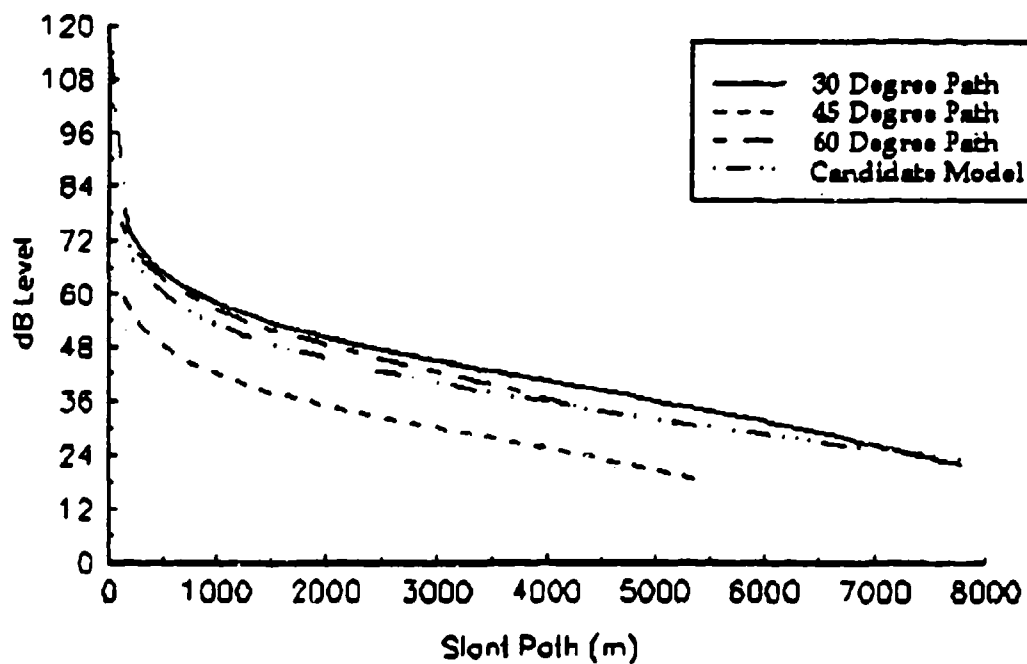
Figure C-10. 350 Hz for mild upward refraction profile.
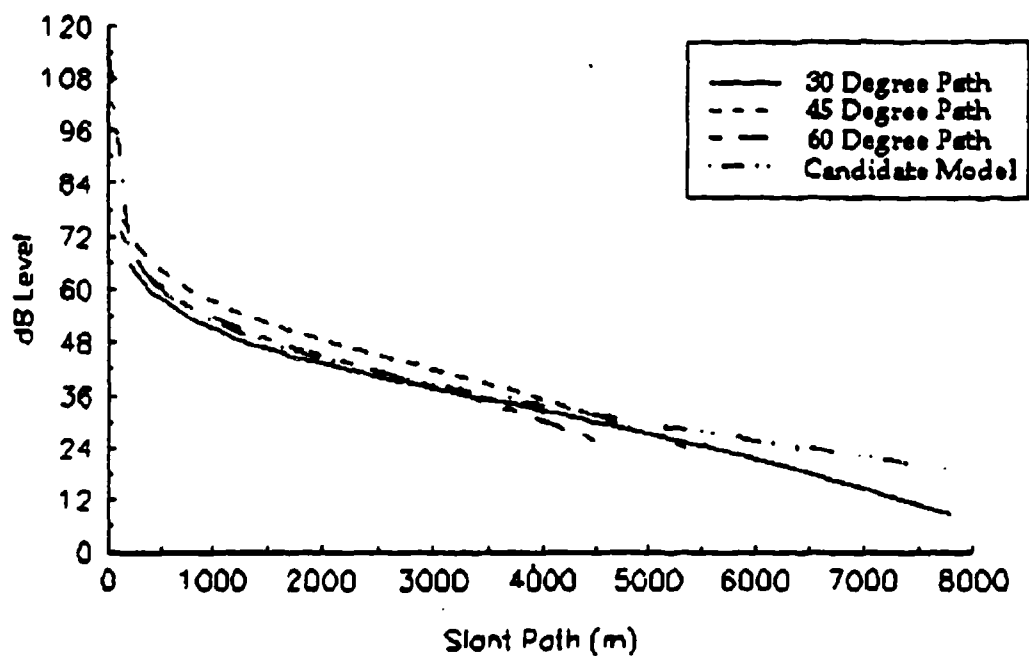
Figure C-11. 450 Hz for mild upward refraction profile.
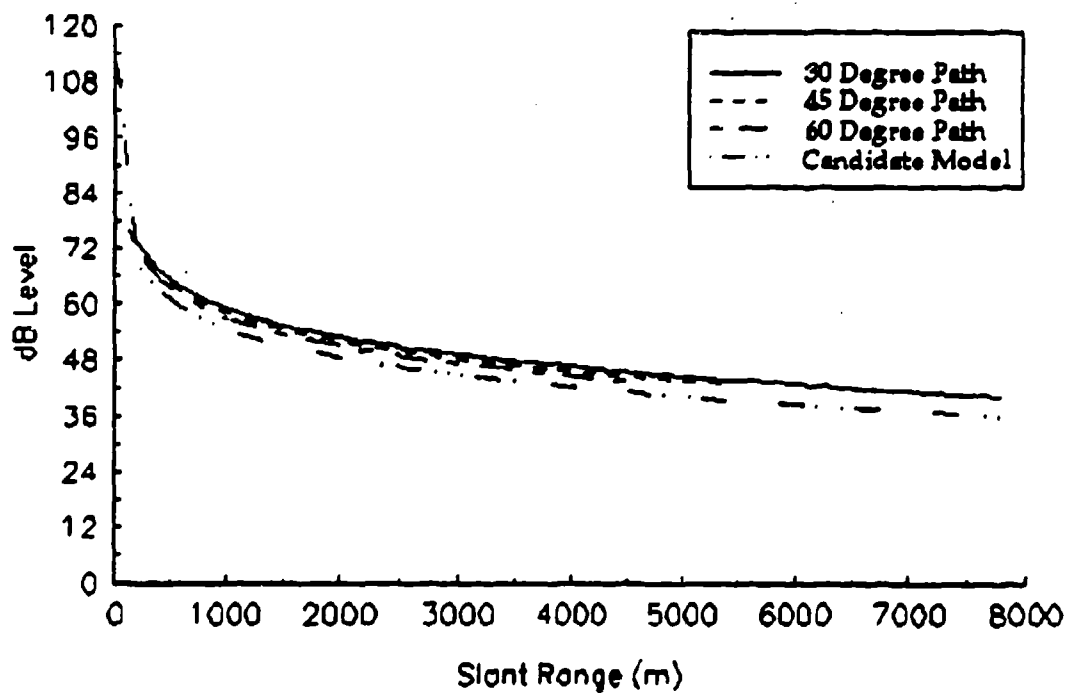
Figure C-12. 50 Hz for strong upward refraction profile.

61
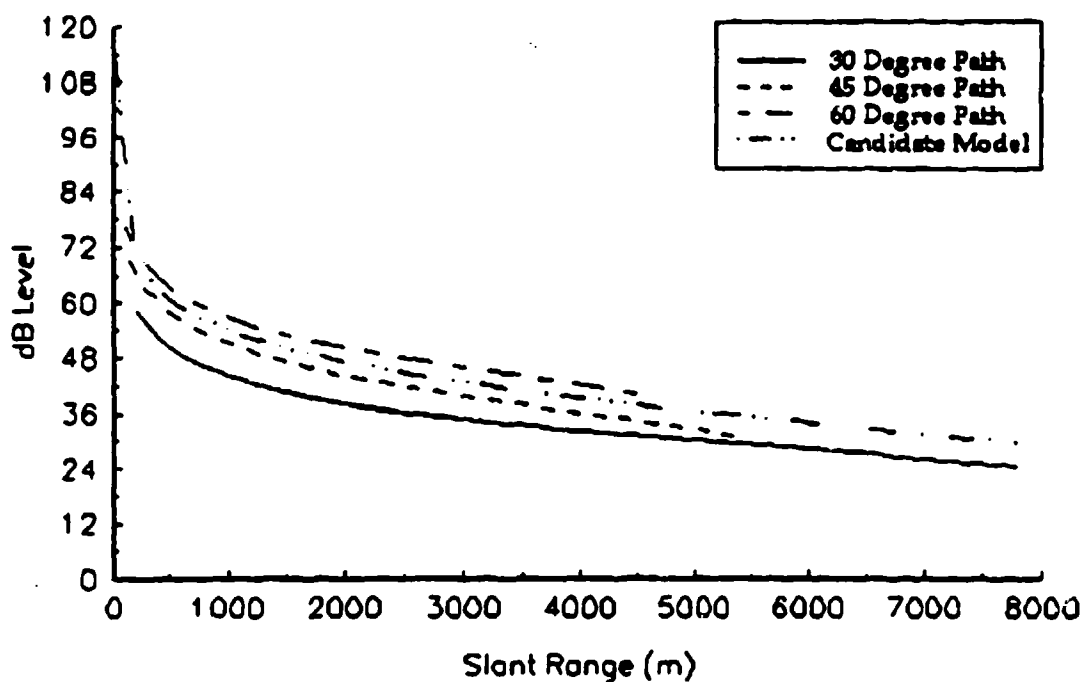
Figure C-13. 150 Hz for strong upward refraction profile.
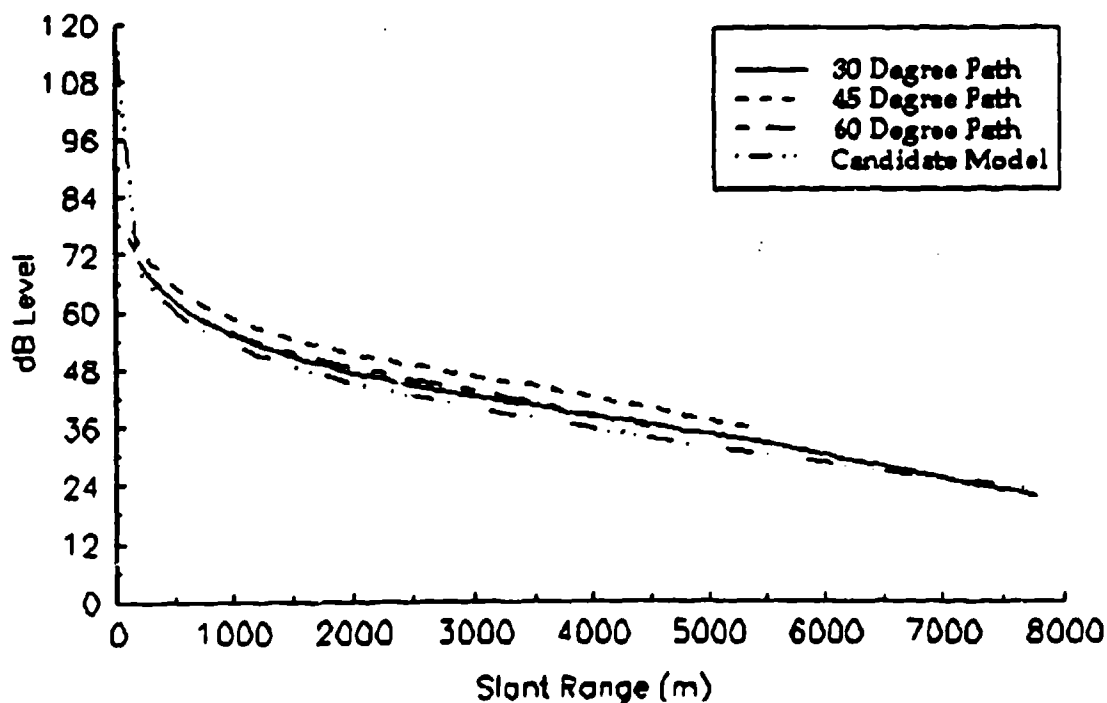
Figure C-14. 250 Hz for strong upward refraction profile.

62
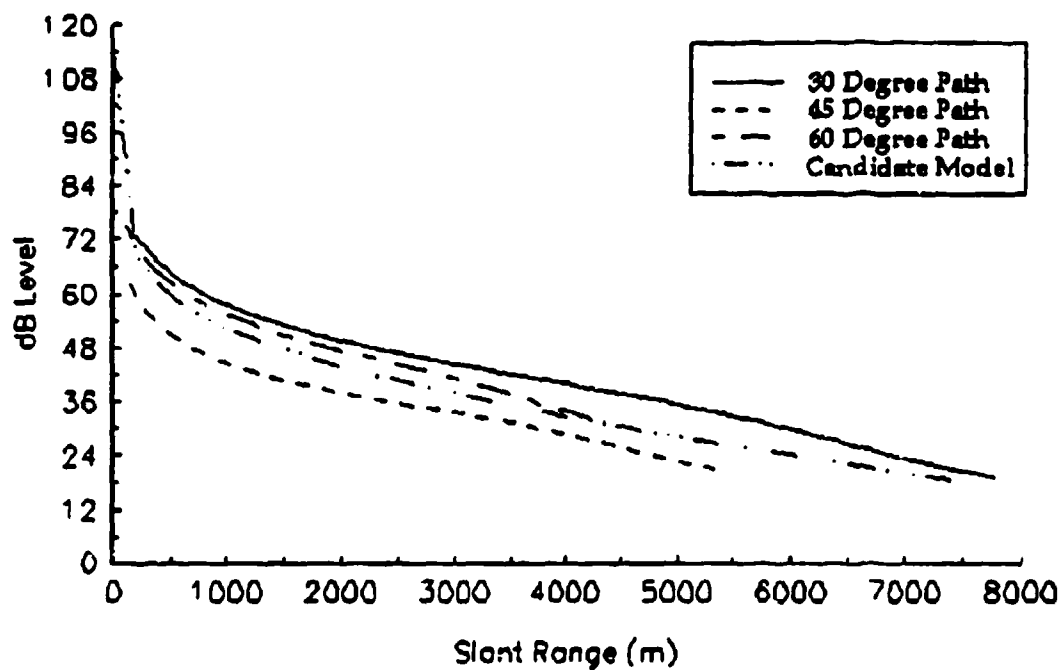
Figure C-15. 350 Hz for strong upward refraction profile.
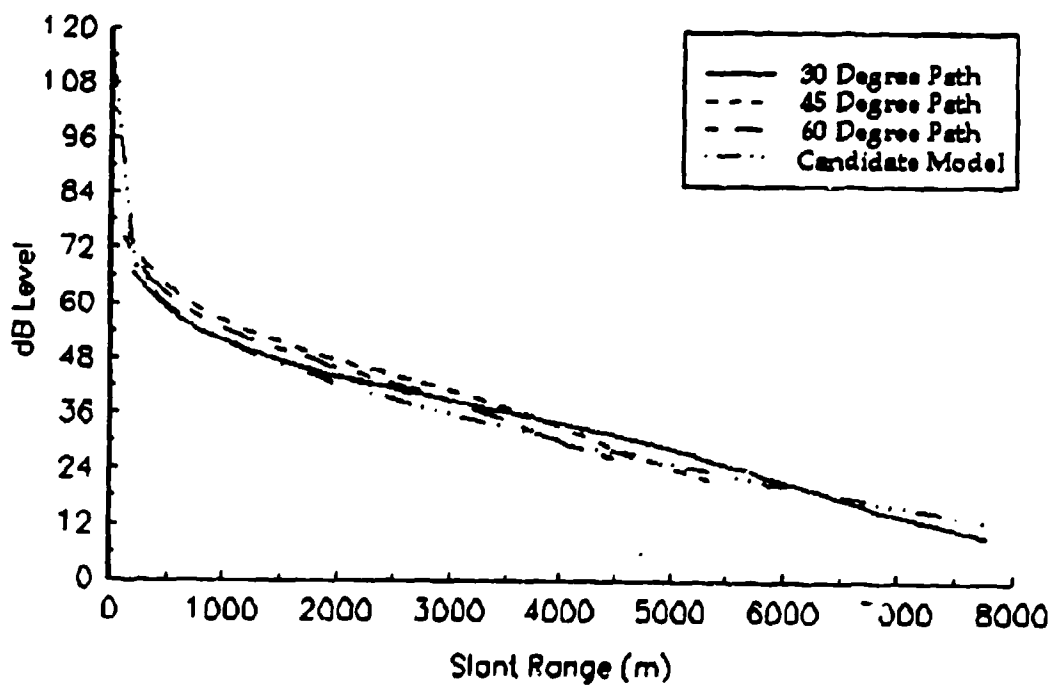
Figure C-16. 450 Hz for strong upward refraction profile.

63
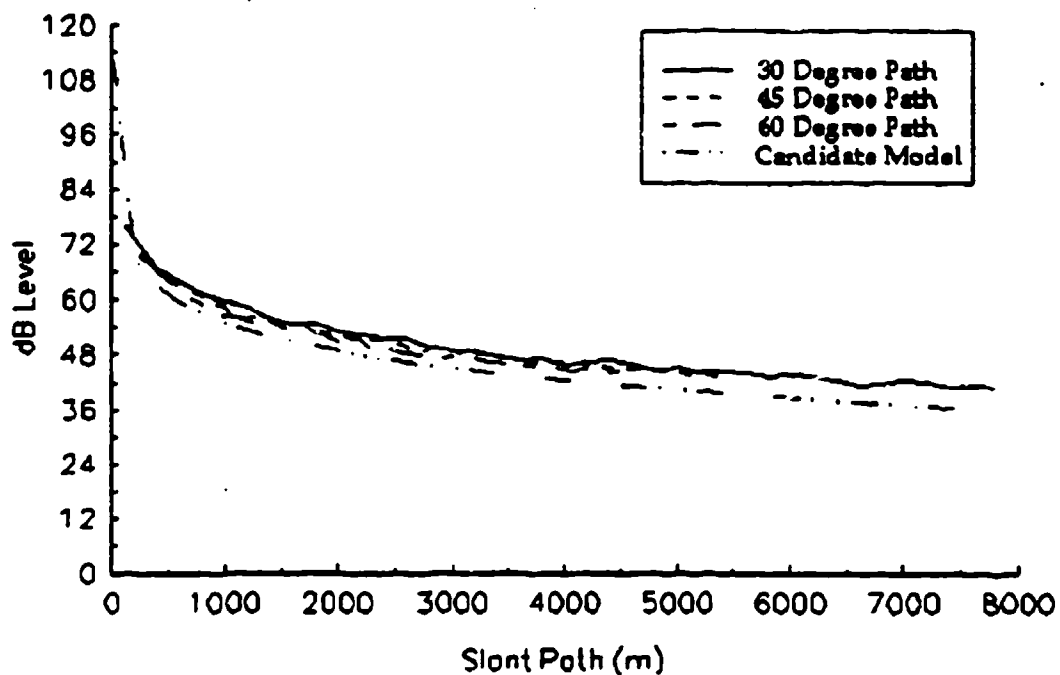
Figure C-17. 50 Hz for downward refraction profile.
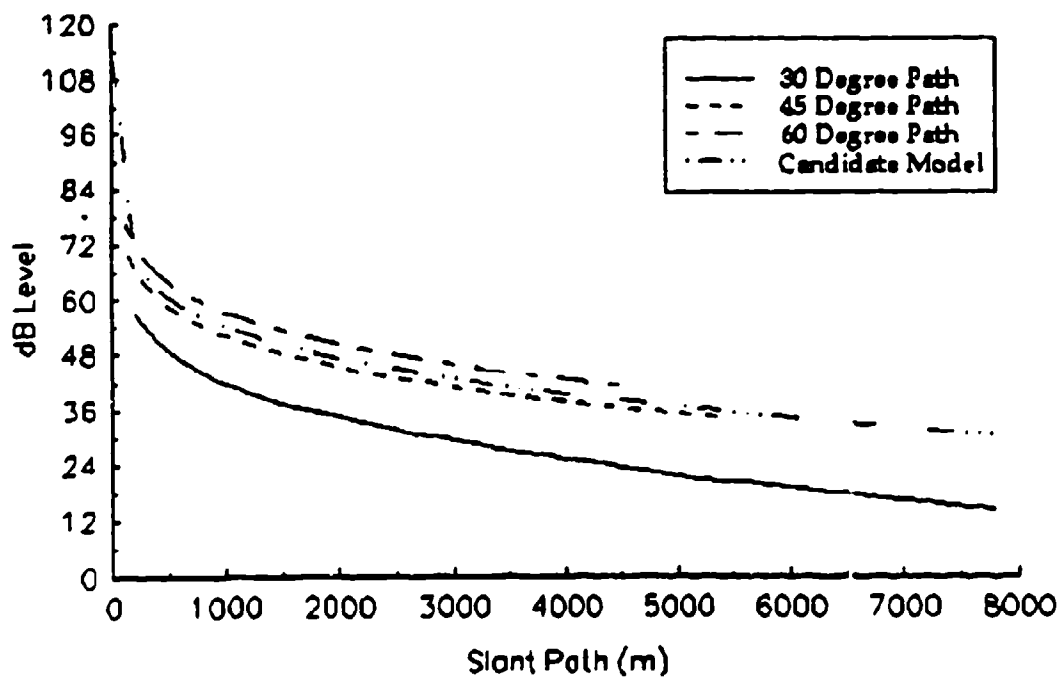
Figure C-18. 150 Hz for downward refraction profile.

64
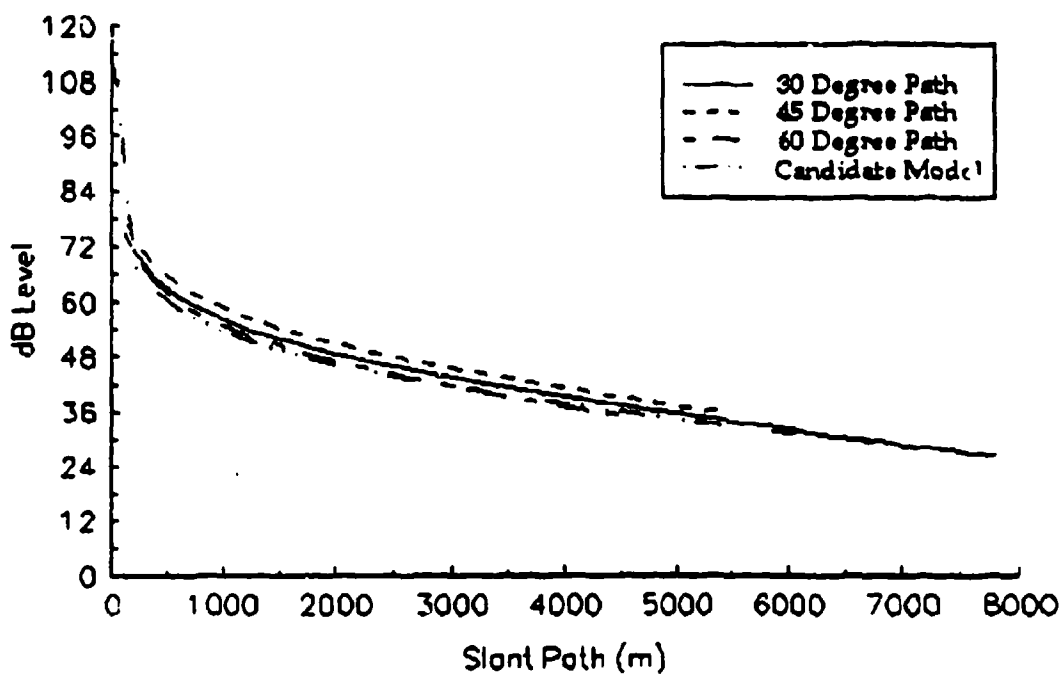
Figure C-19. 250 Hz for downward refraction profile.
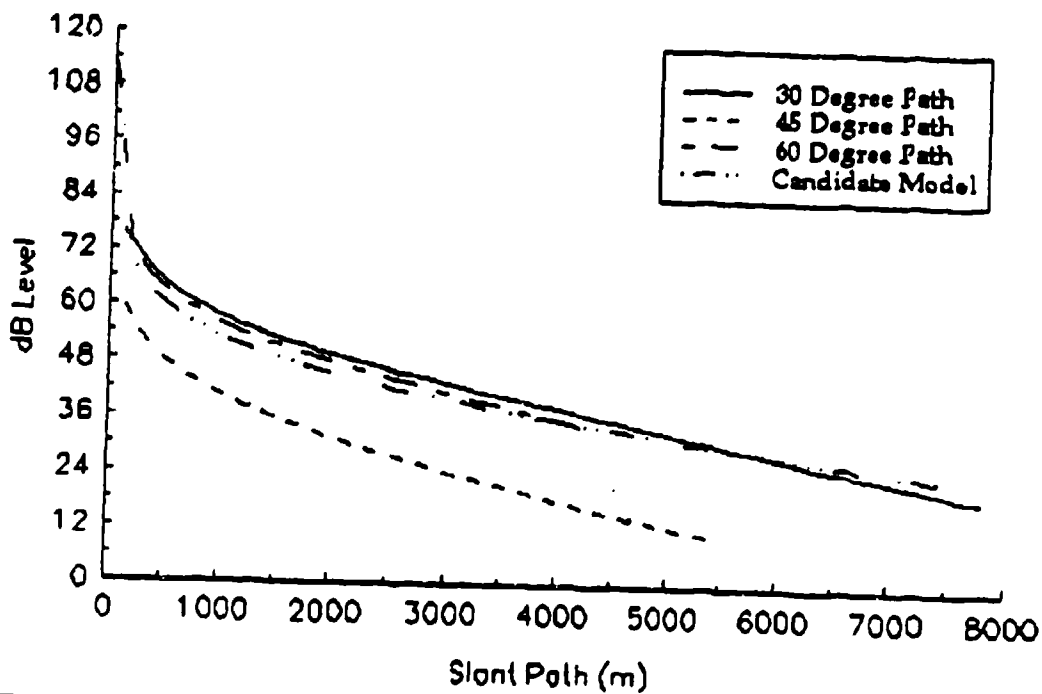
Figure C-20. 350 Hz for downward refraction profile.

65
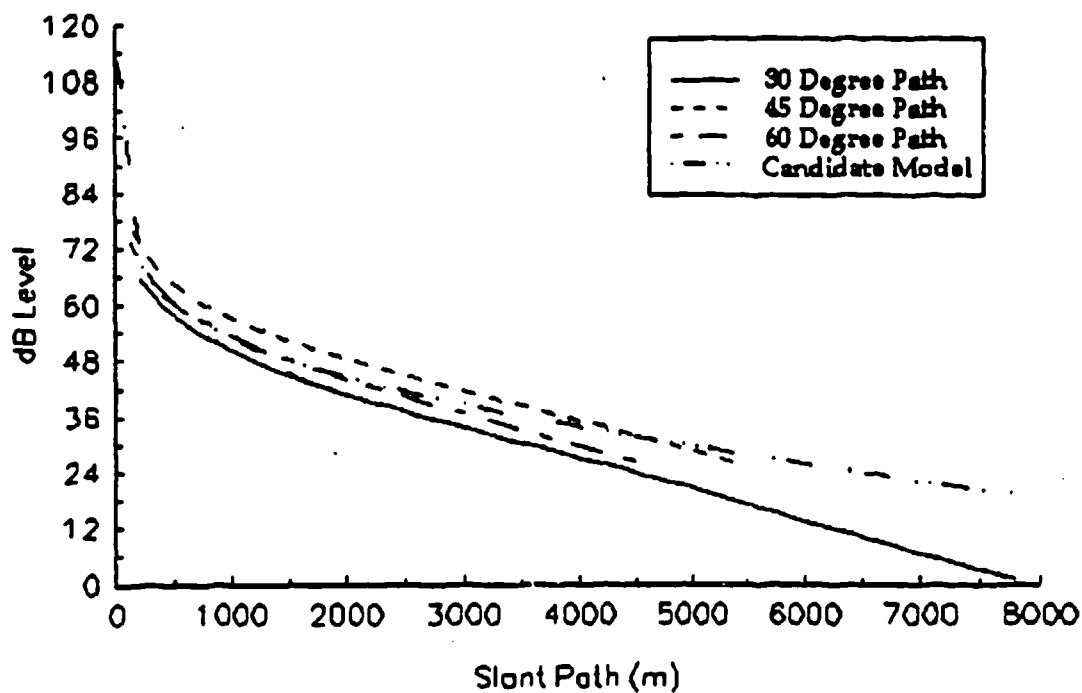
Figure C-21. 450 Hz for downward refraction profile.
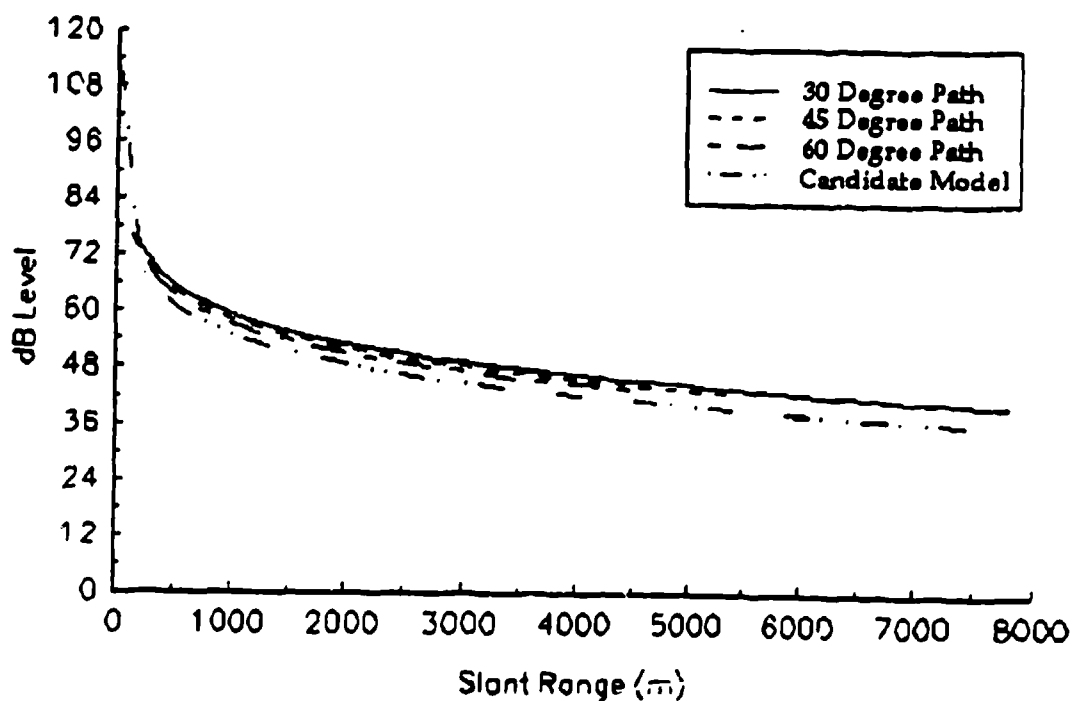
Figure C-22. 50 Hz for shallow inversion profile.

66
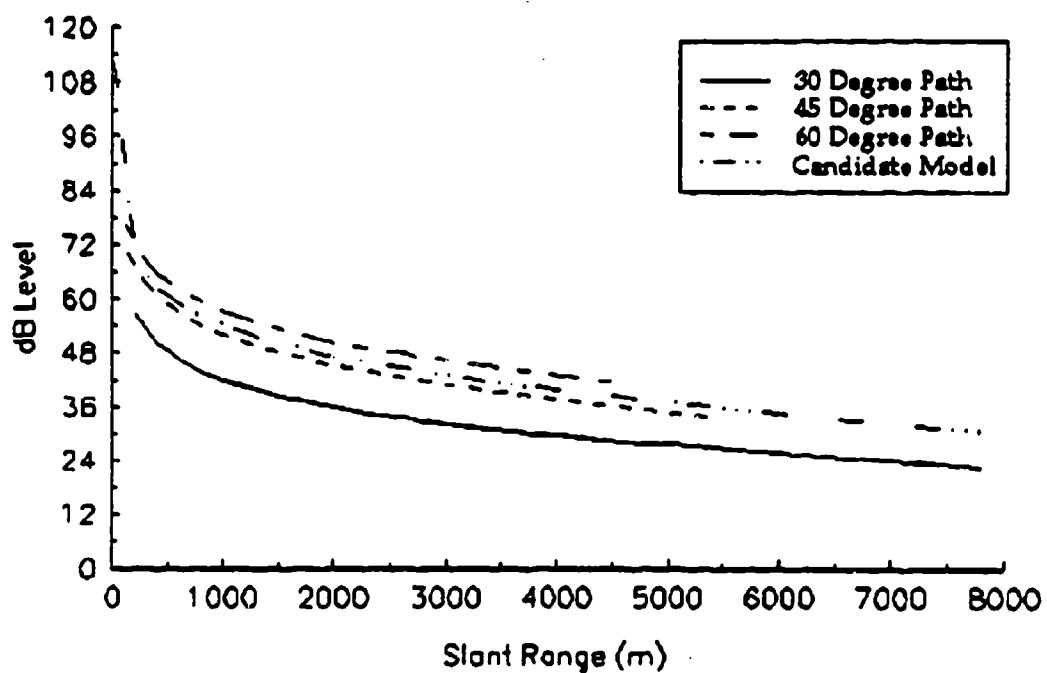
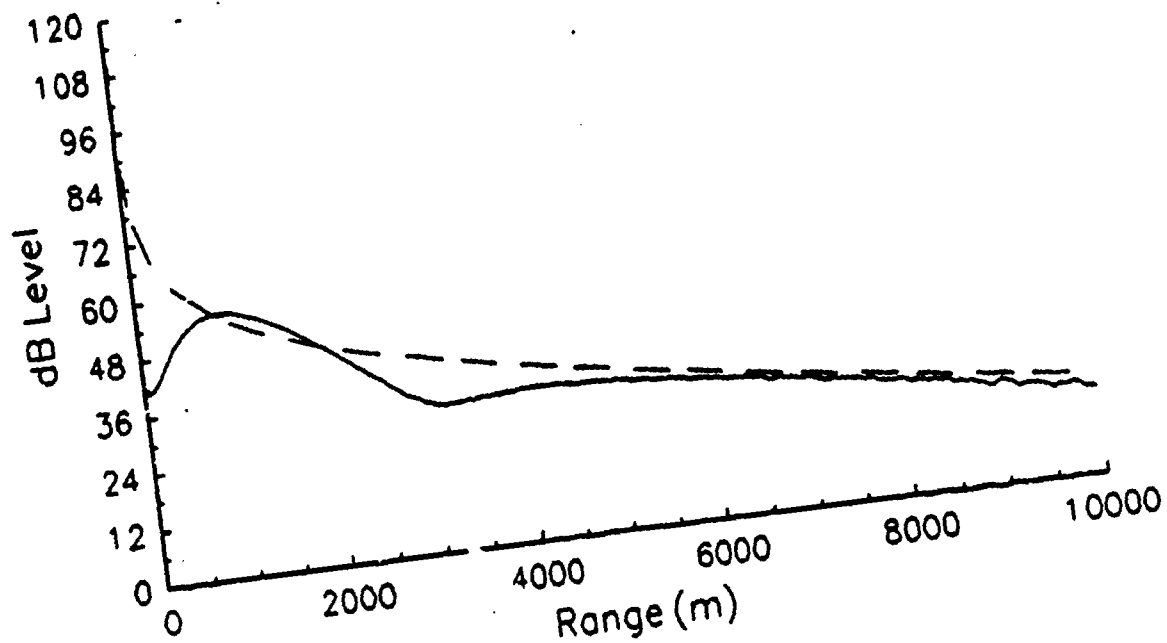**Figure C-23. 150 Hz for shallow inversion profile.**
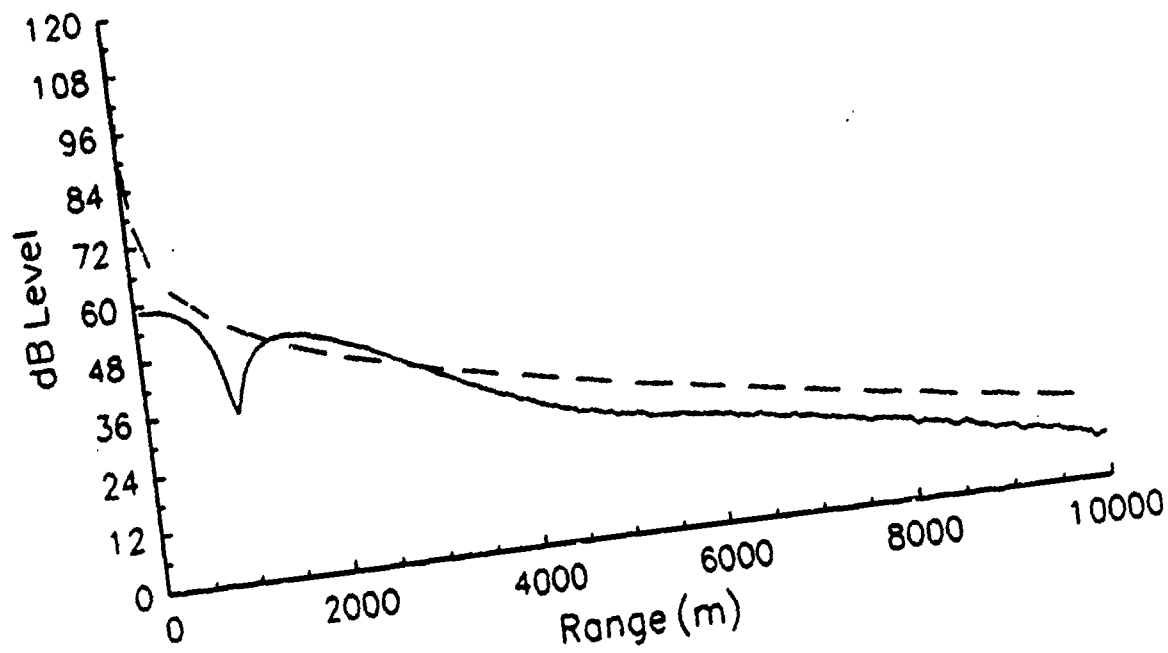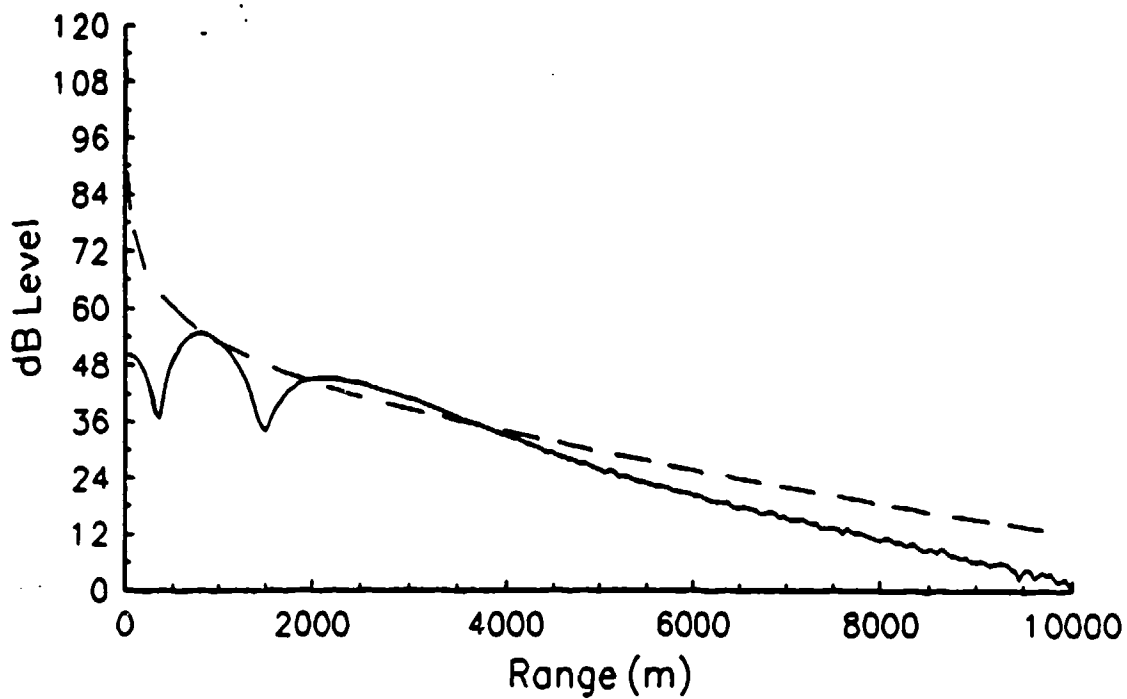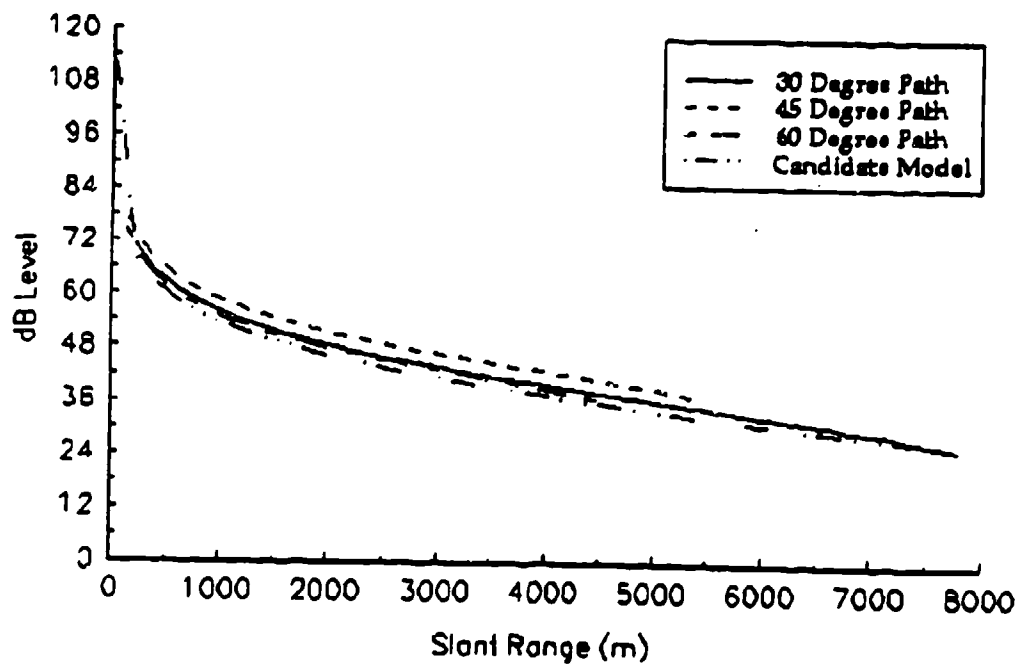

Figure C-24. 250 Hz for shallow inversion profile.

67
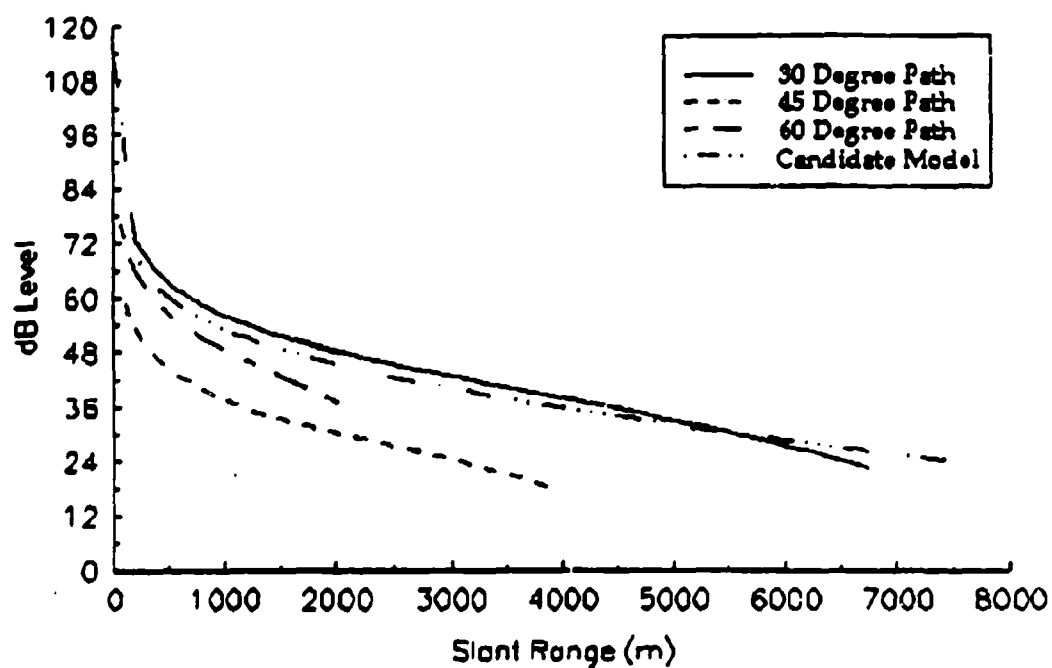
Figure C-25. 350 Hz for shallow inversion profile.
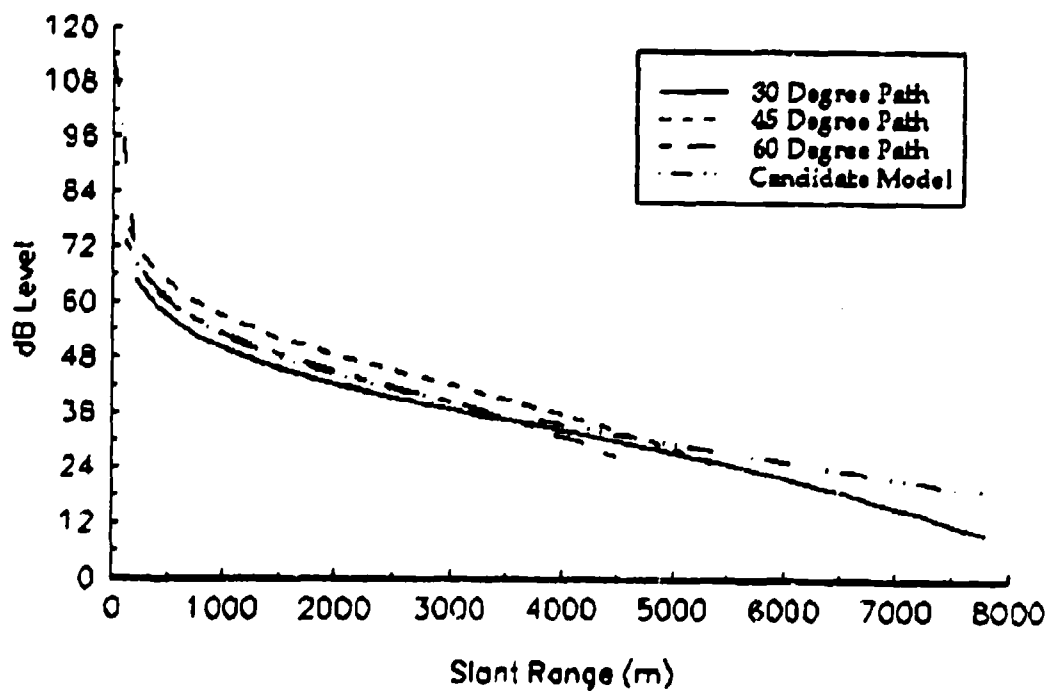
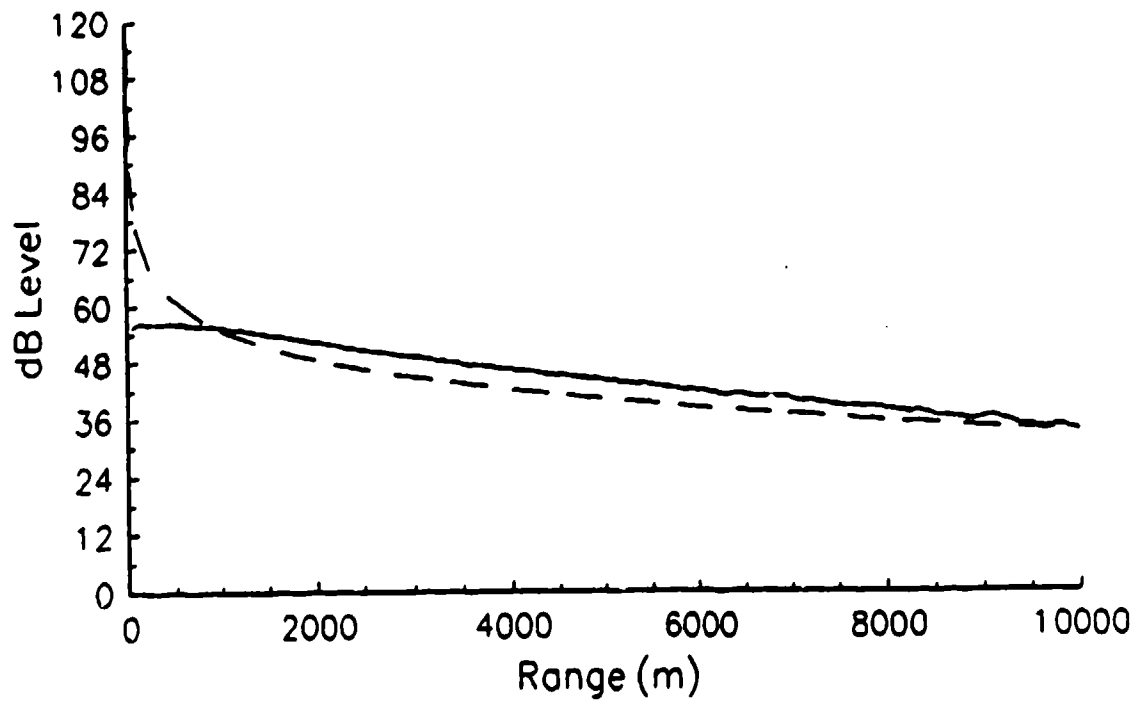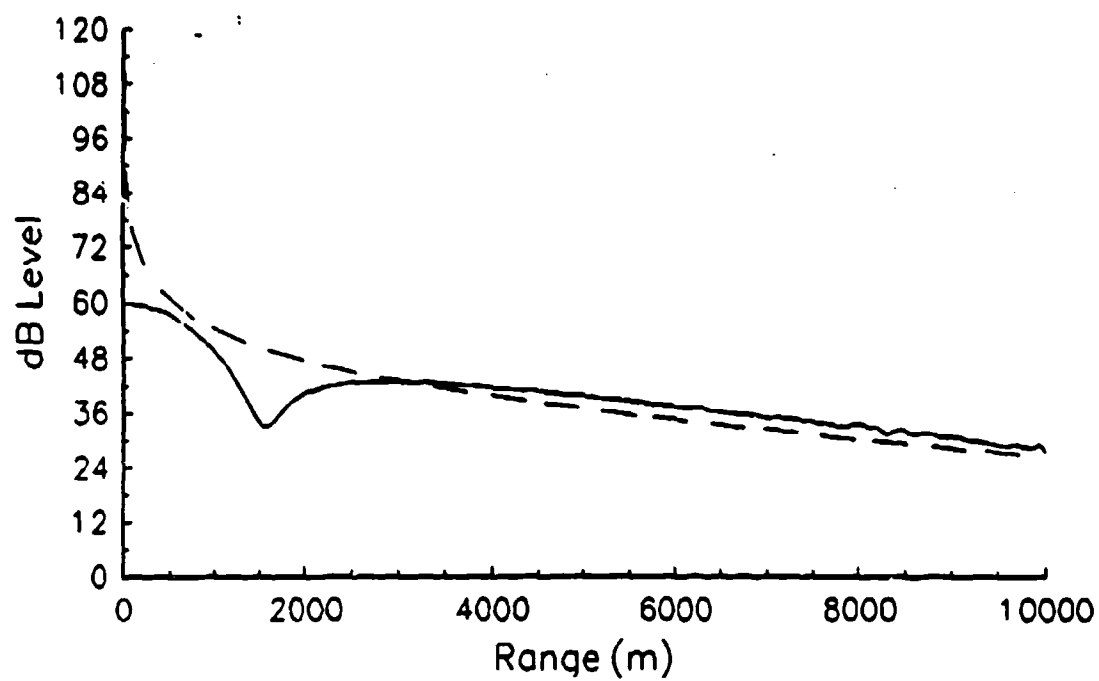**Figure C-26. 450 Hz for shallow inversion profile.**

68
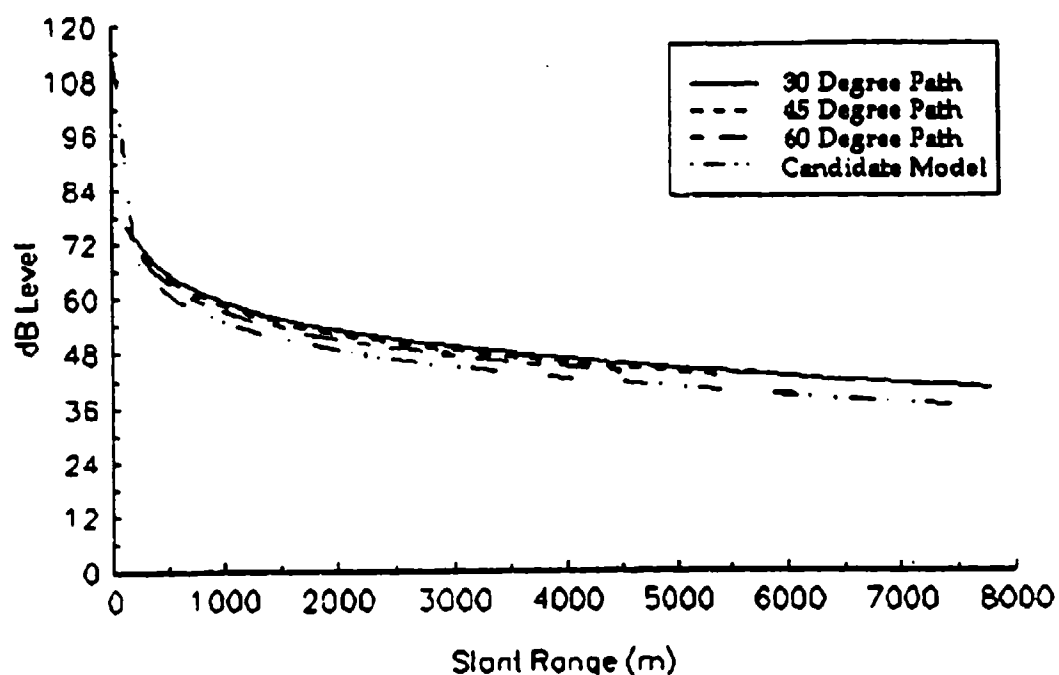
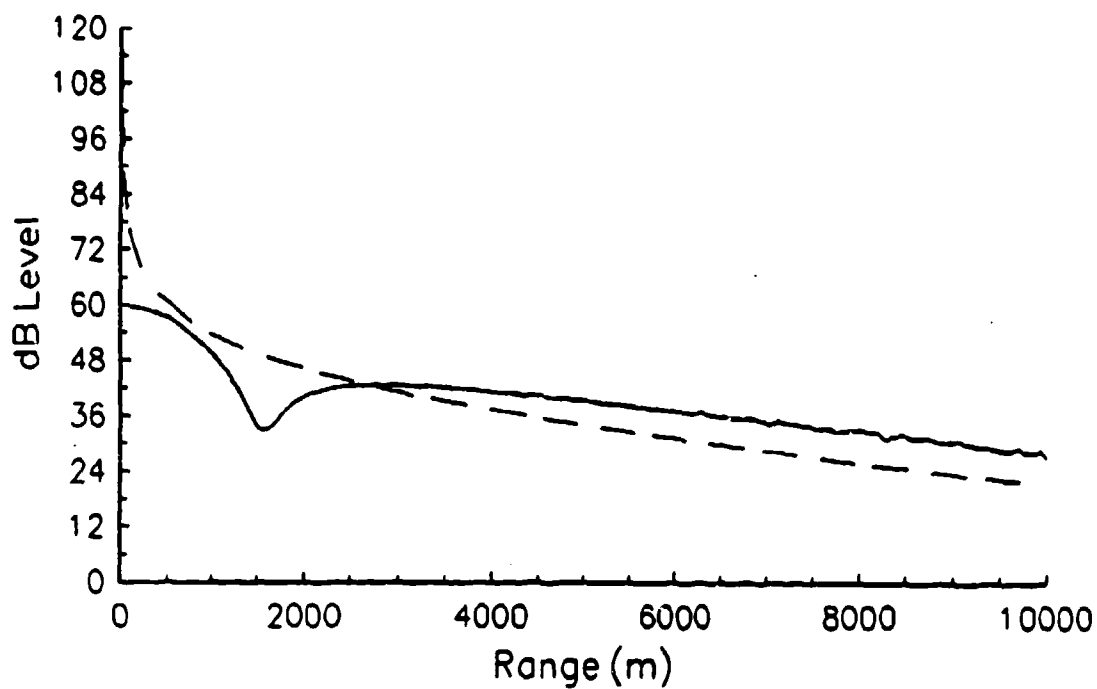**Figure C-27. 50 Hz for deep inversion profile.**
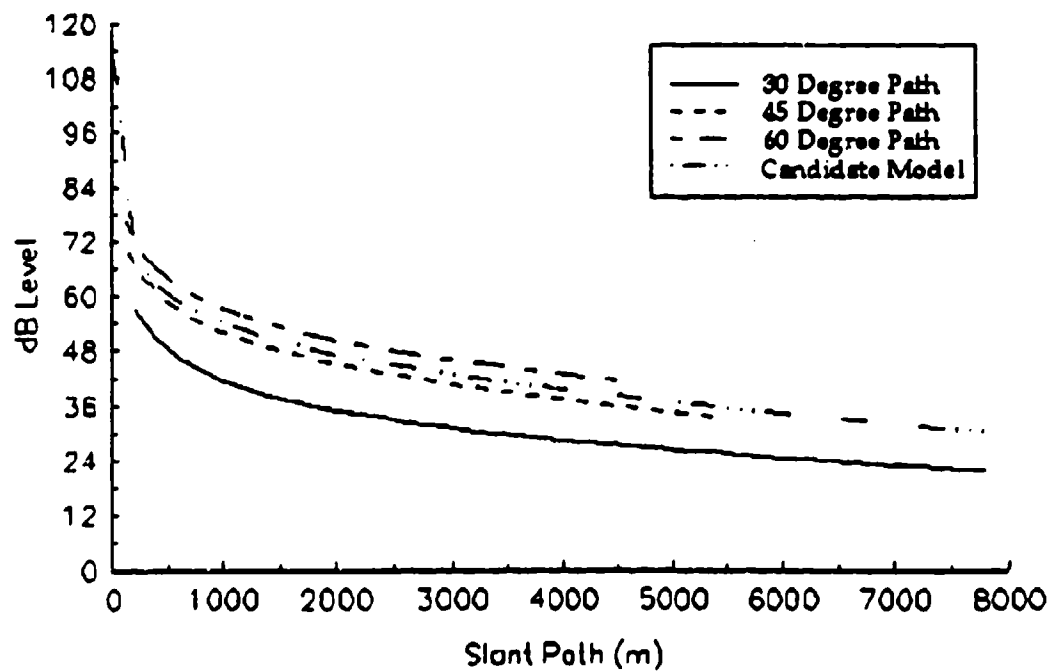
Figure C-28. 150 Hz for deep inversion profile.
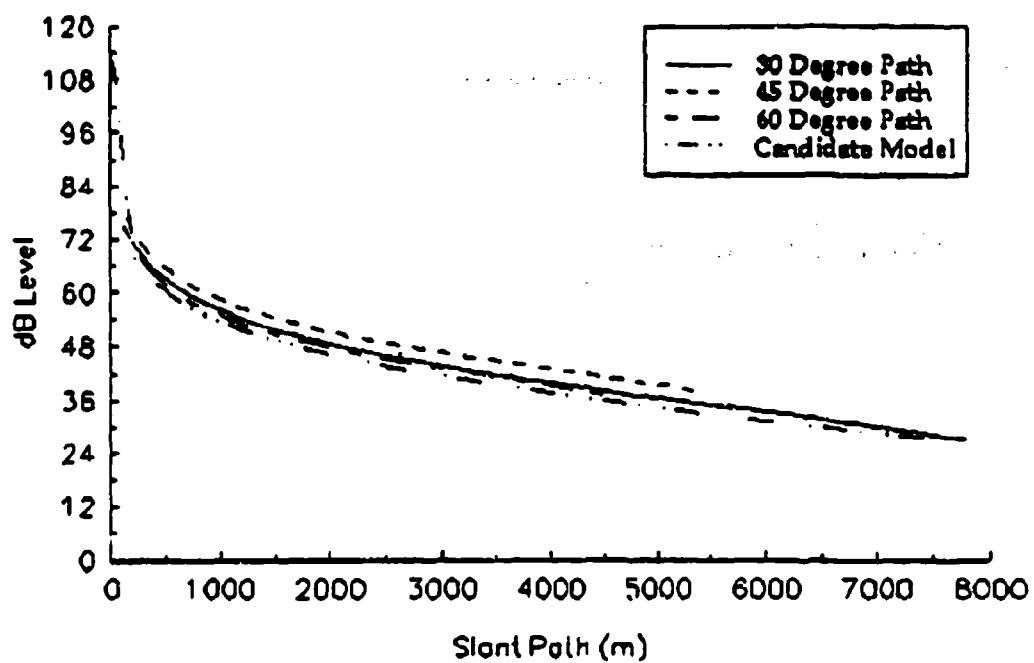
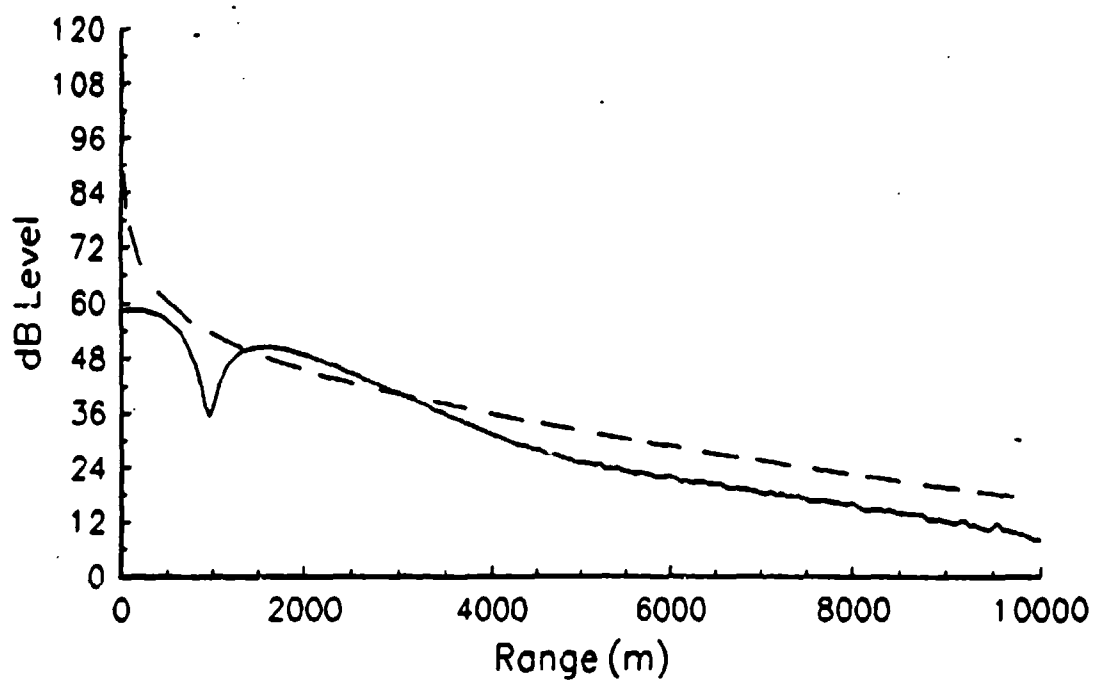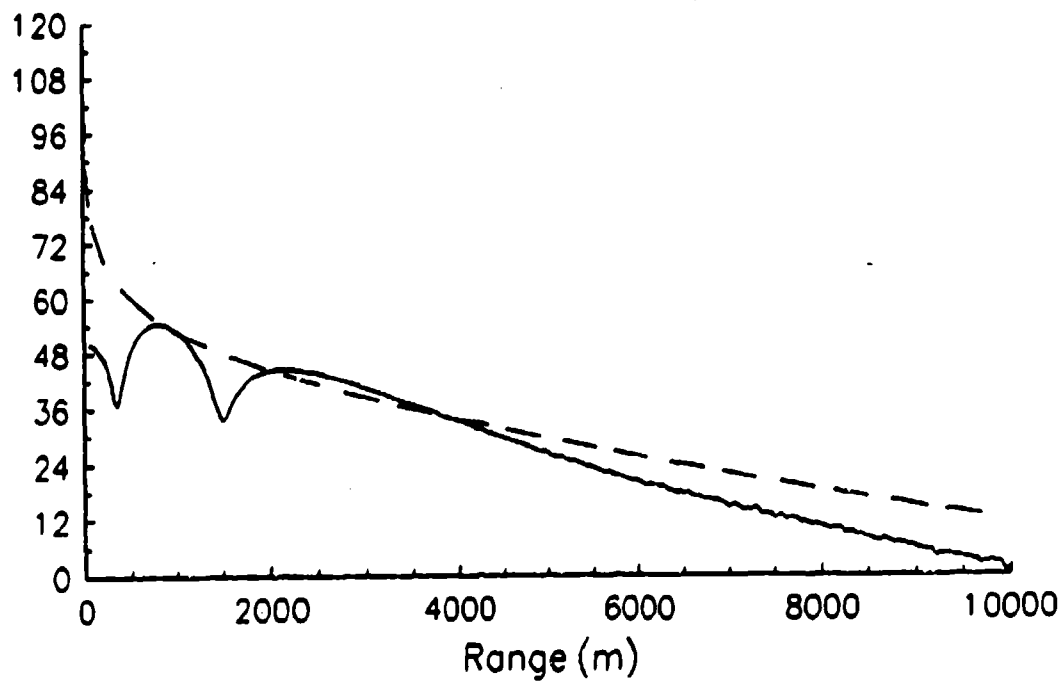**Figure C-29. 250 Hz for deep inversion profile.**
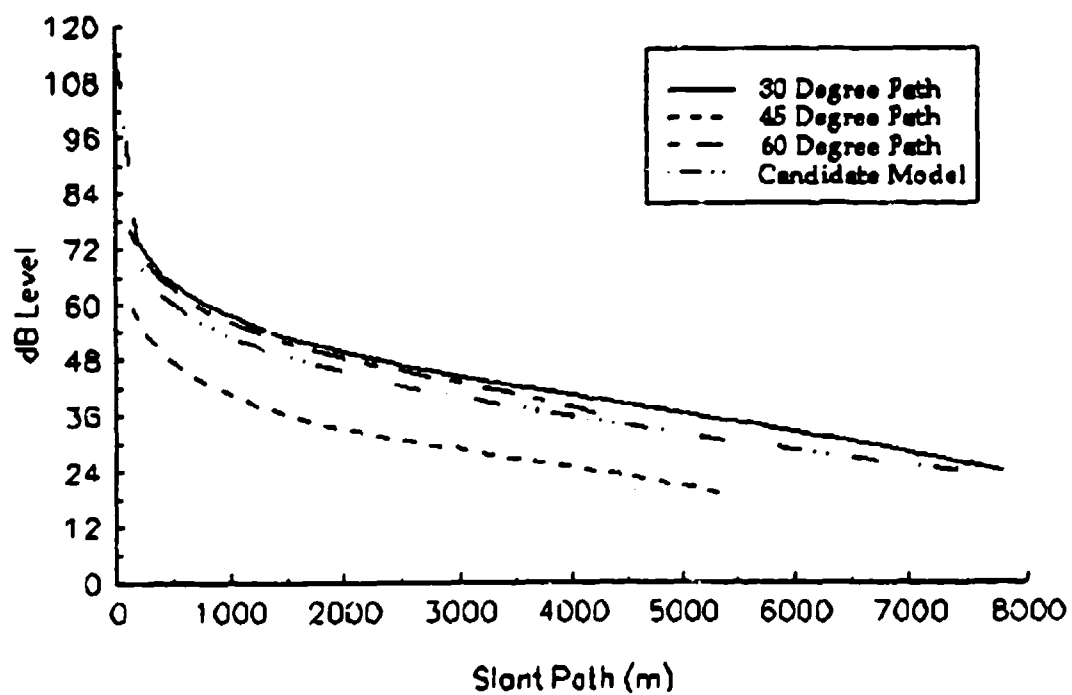
Figure C-30. 350 Hz for deep inversion profile.

70
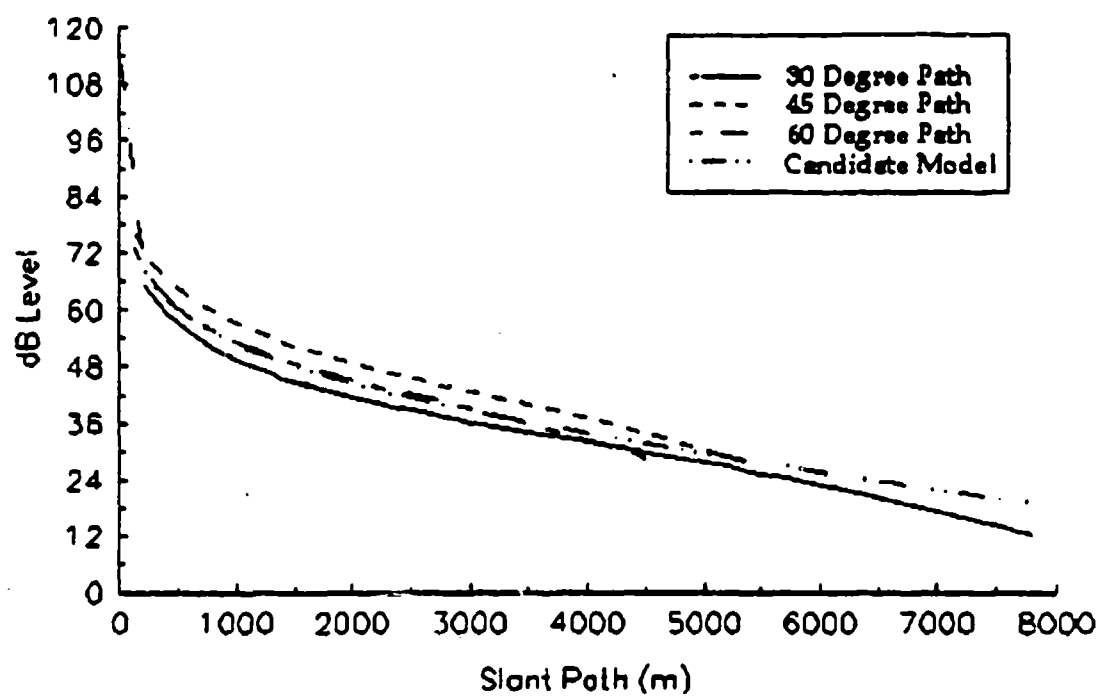
Figure C-31. 450 Hz for deep inversion profile.

Appendix D

Sound Speed Profiles From Cases and Measured Meteorological Profiles
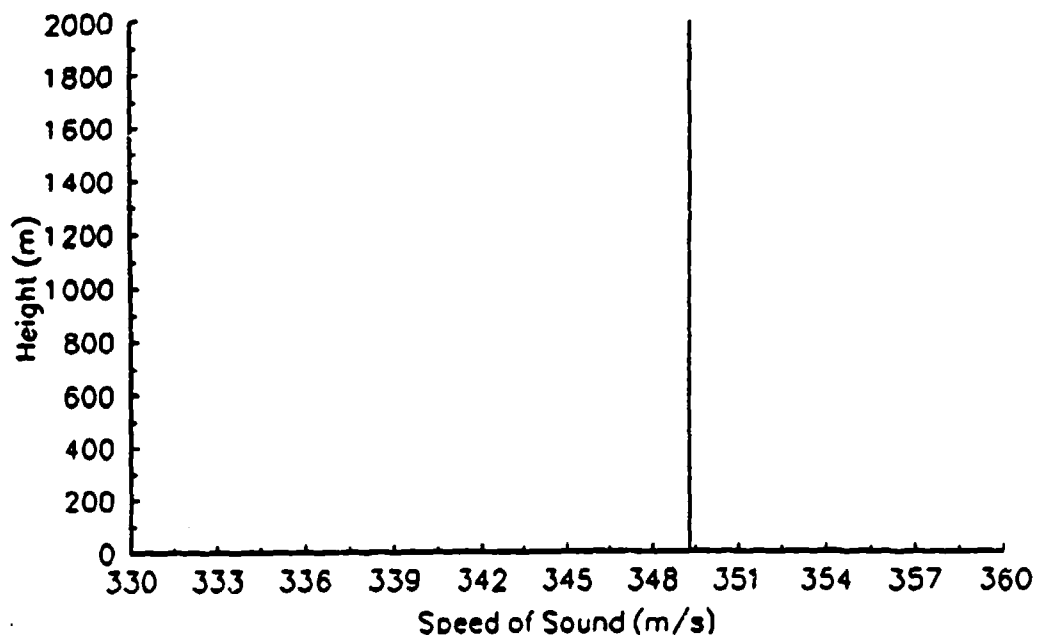
Figure D-1. Sound speed profile for homogeneous profile.
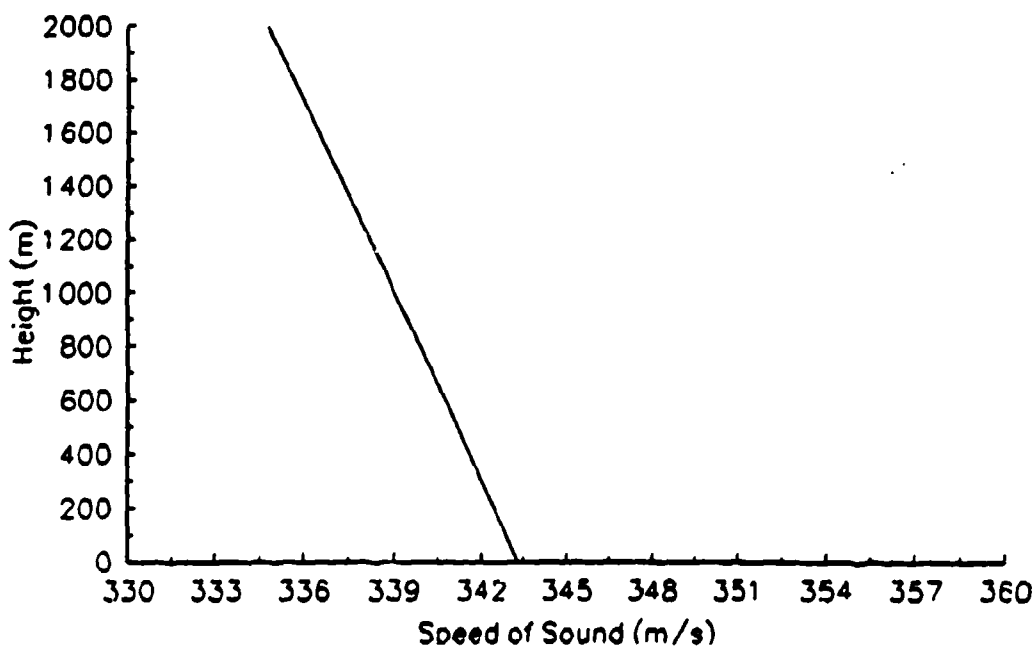
Figure D-2. Sound speed profile for mild upward refraction profile.
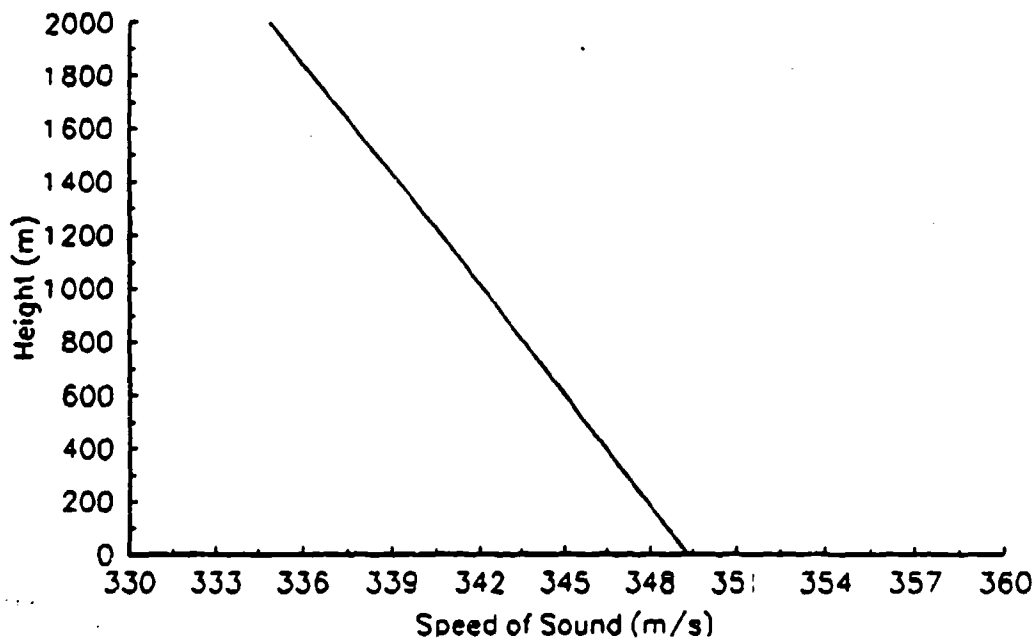
Figure D-3. Sound speed profile for strong upward refraction profile.
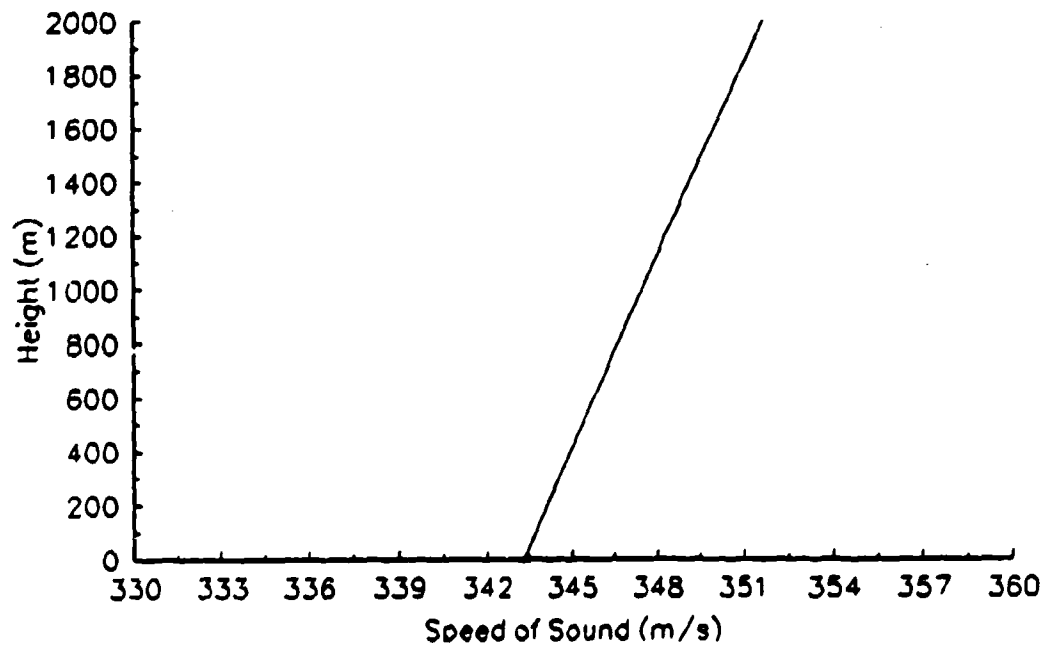
Figure D-4. Sound speed profile for downward refraction profile.

75
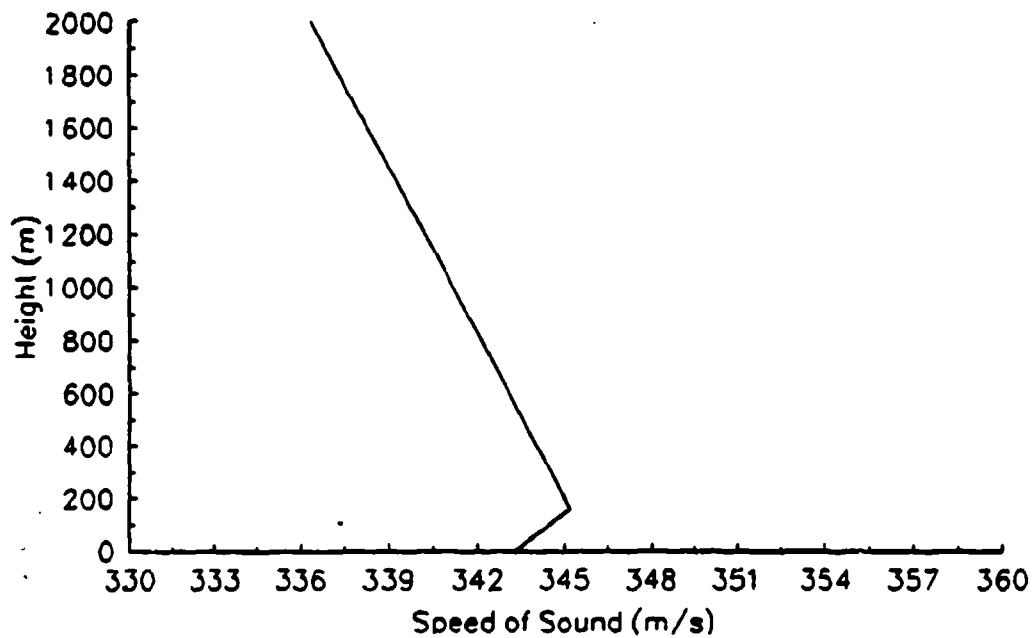
Figure D-5. Sound speed profile for shallow inversion profile.
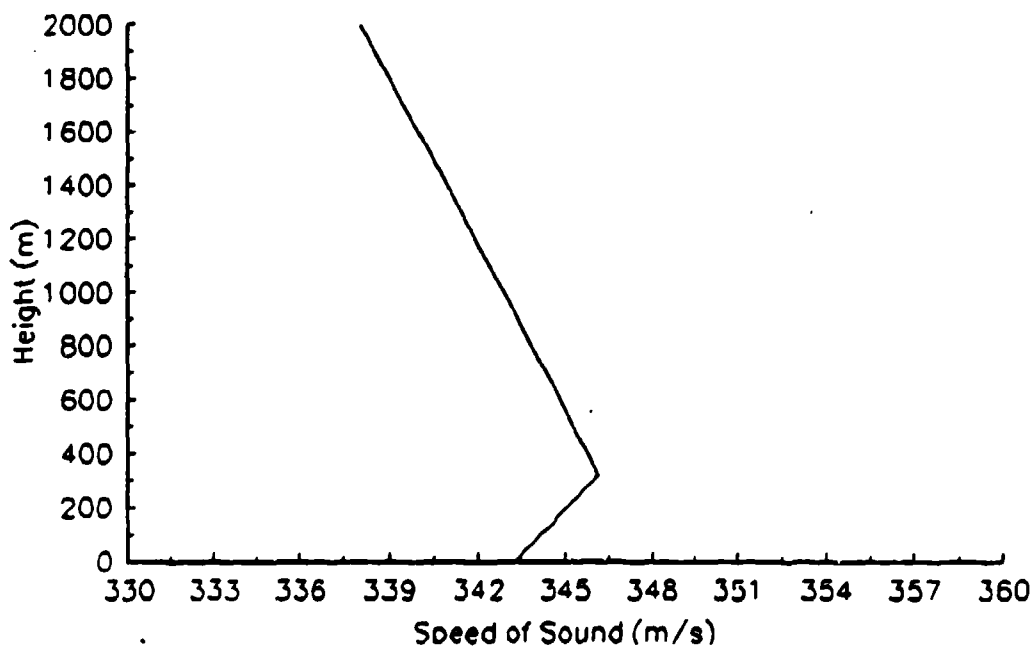
Figure D-6. Sound speed profile for deep inversion profile.

76
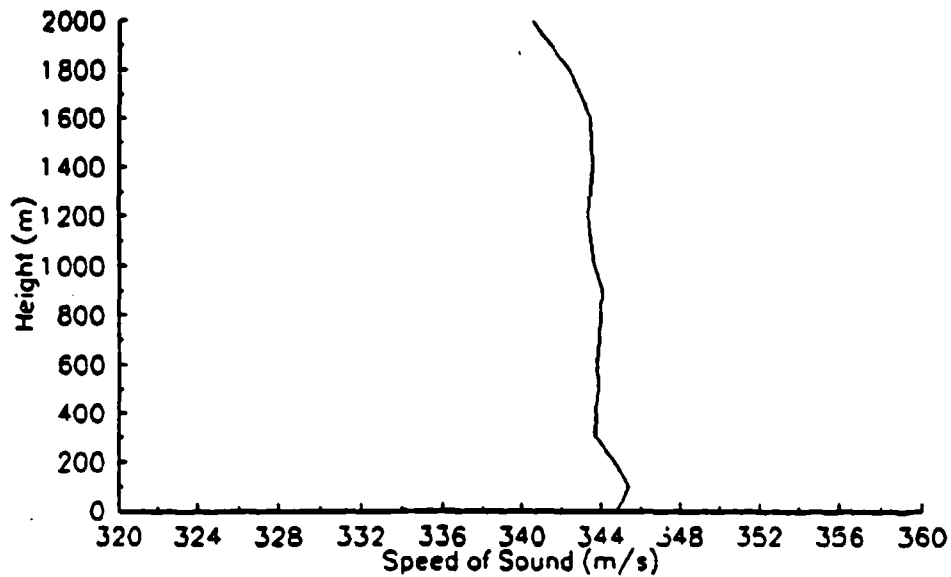
Figure D-7. Sound speed profile calculated from JAPE meteorological data that shows a state close to the homogeneous profile used in the comparison.
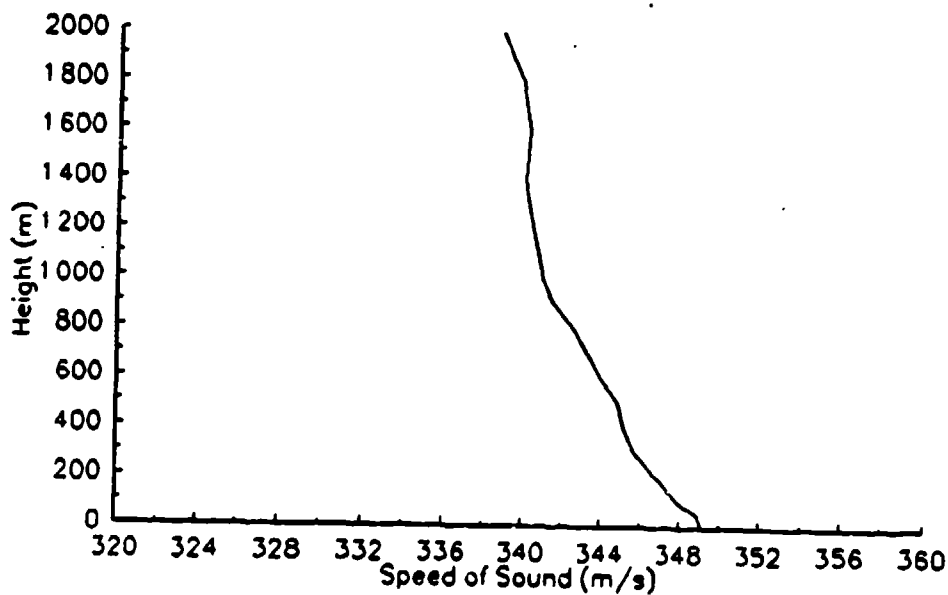
Figure D-8. Sound speed profile calculated from JAPE meteorological data that shows a state close to the mild upward refraction profile used in the comparison.
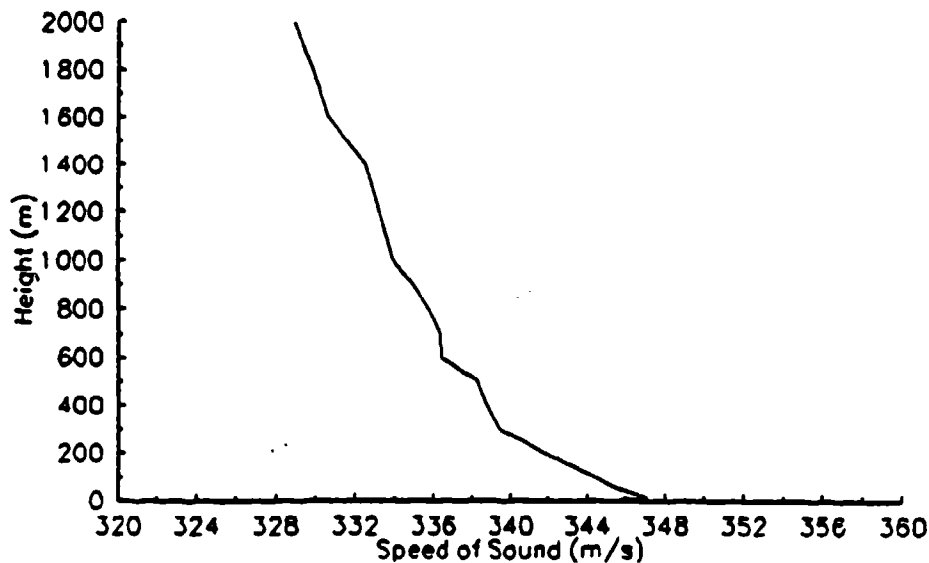
Figure D-9. Sound speed profile calculated from JAPE meteorological data that shows a state close to the strong upward refraction profile used in the comparison.
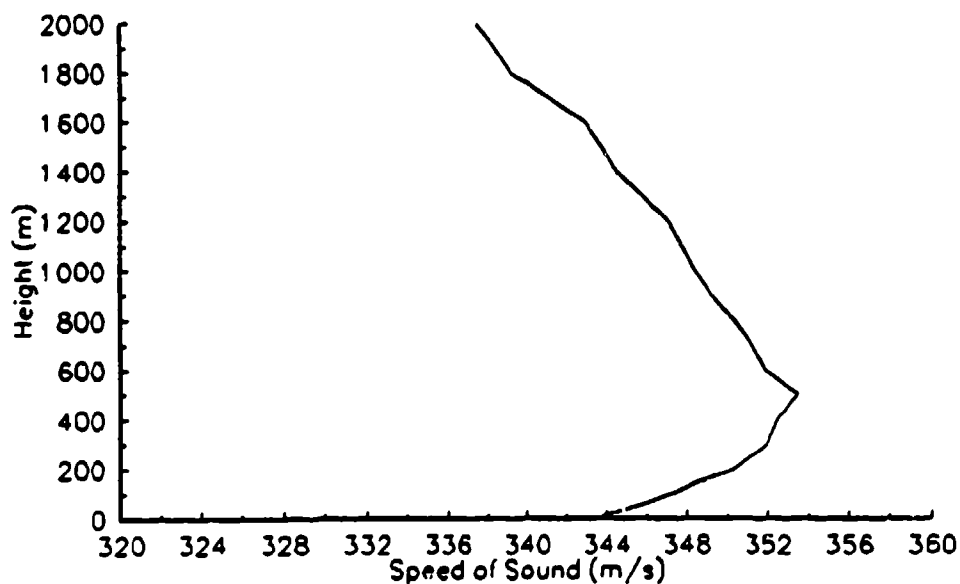
Figure D-10. Sound speed profile calculated from JAPE meteorological data that shows an approximate state to the downward refraction profile used in the comparison.
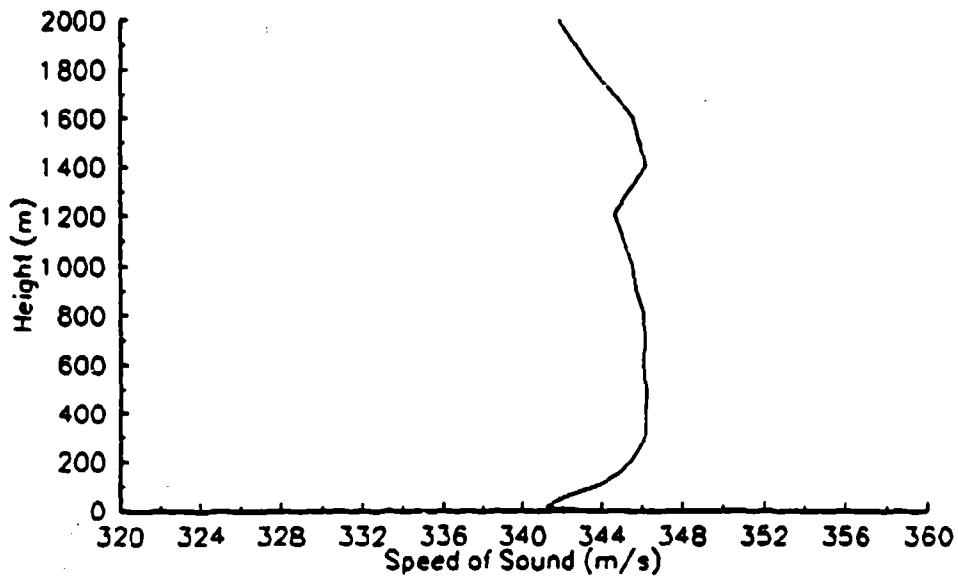
Figure D-11. Sound speed profile calculated from JAPE meteorological data that shows a state close to the shallow inversion profile used in the comparison.
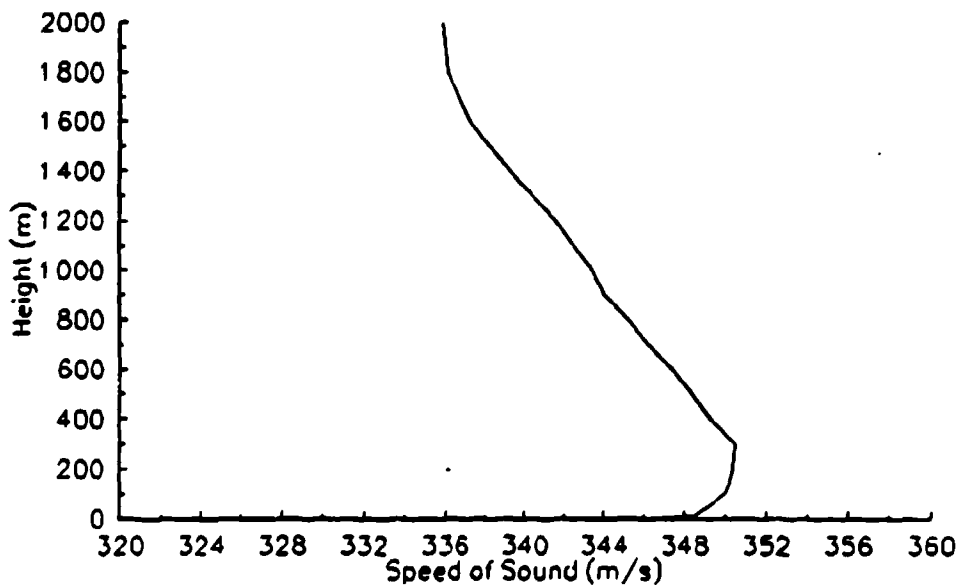
Figure D-12. Sound speed profile calculated from JAPE meteorological data that shows a state close to the deep inversion profile used in the comparison.

Appendix E

Ray Traces to Illustrate How Sound is Propagating for Each Case
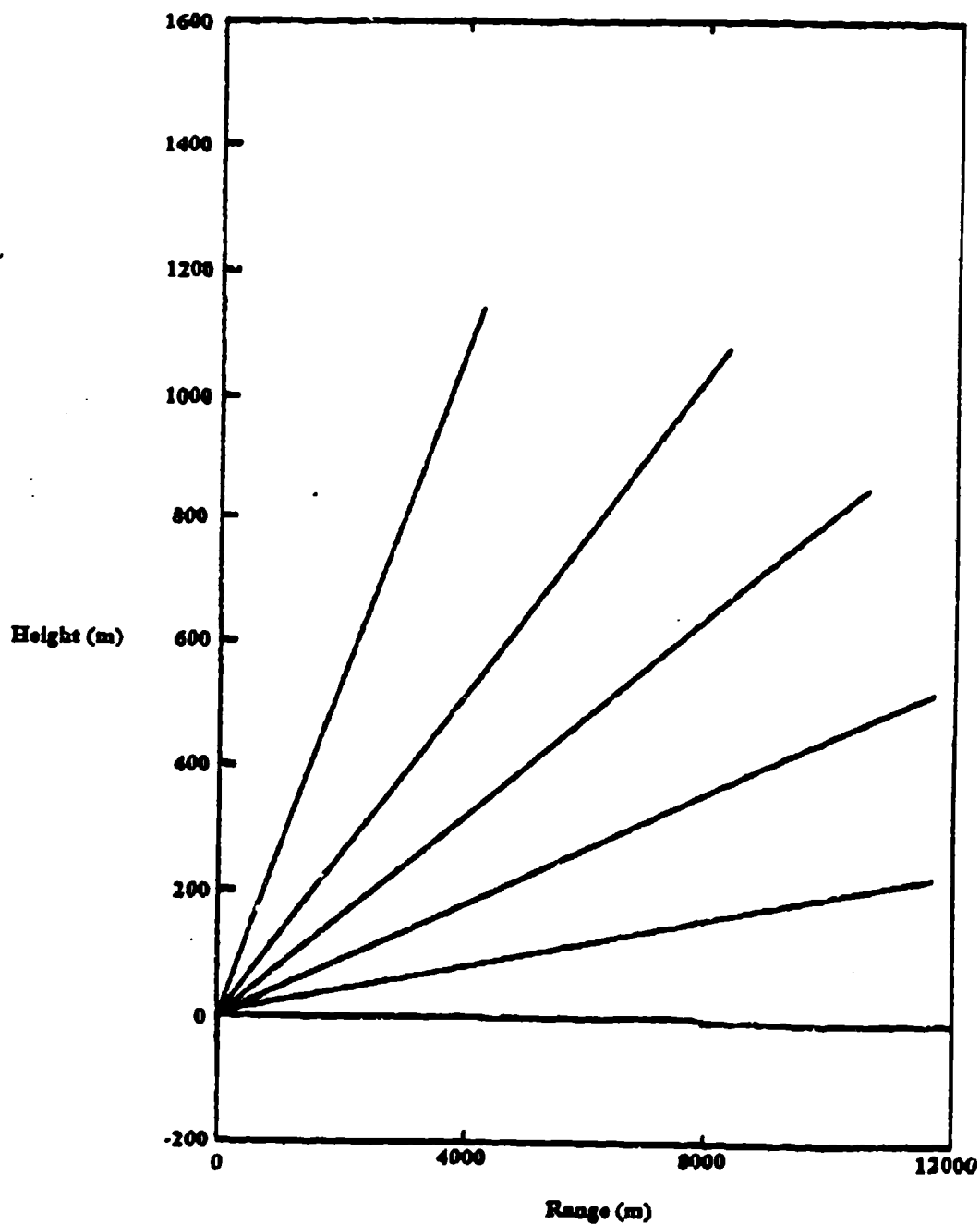
Figure E-1. Traces of acoustic rays for the homogeneous profile. The rays are not bent because the sound speed gradient is zero.
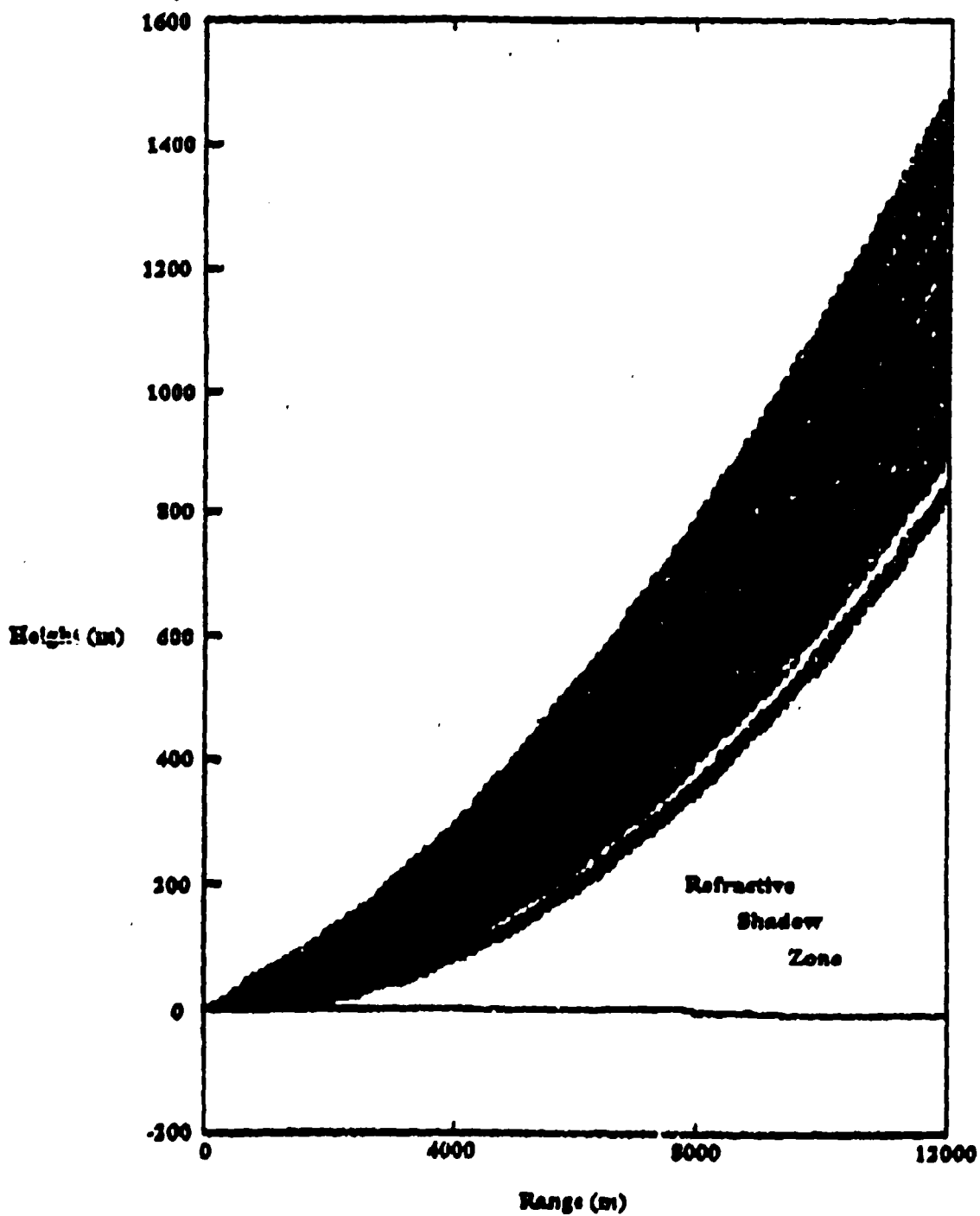
Figure E-2. Traces of acoustic rays for the mild upward refraction profile showing the refractive shadow zone.
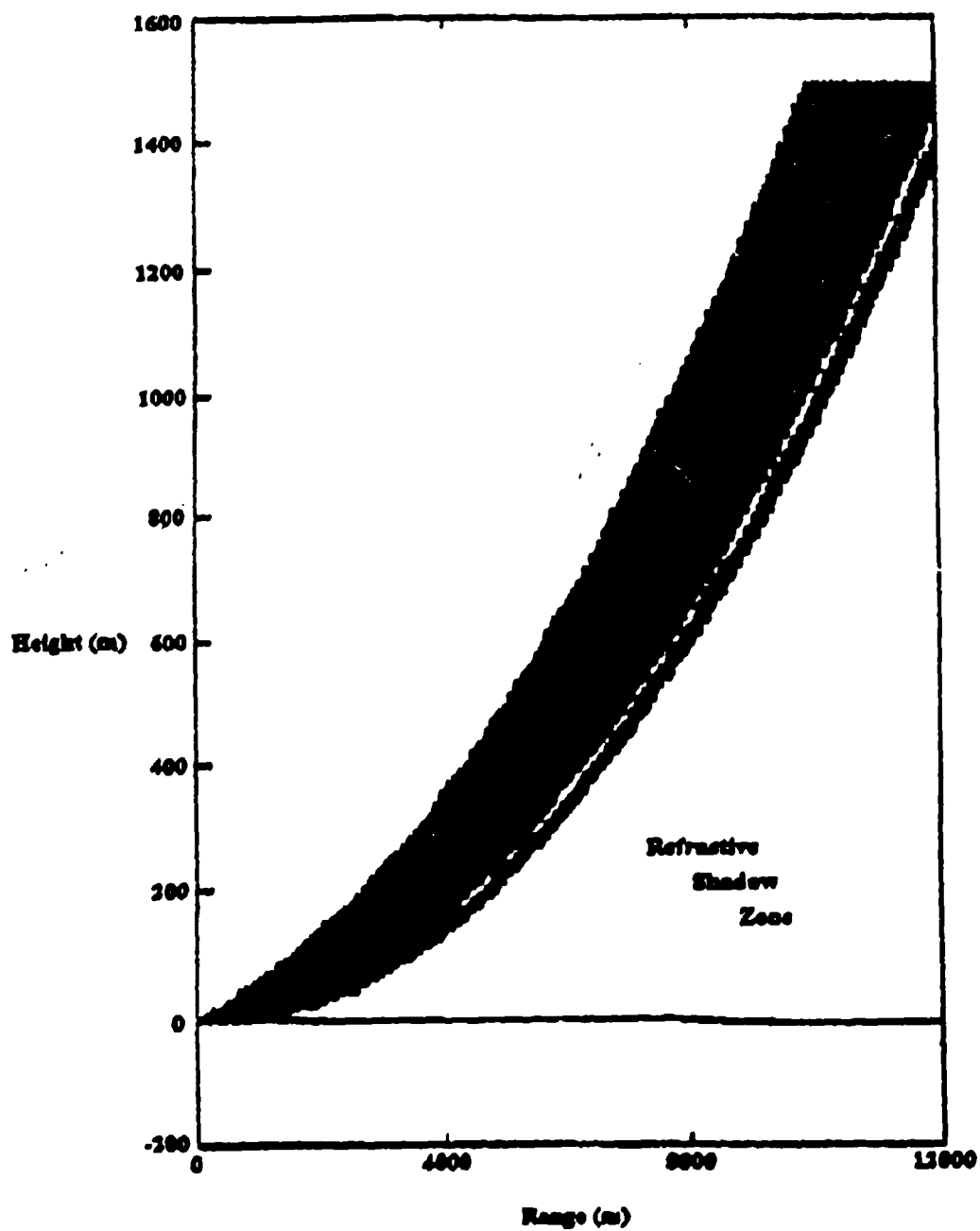
Figure E-3. Traces of acoustic rays for the strong upward refraction profile showing the refractive shadow zone.
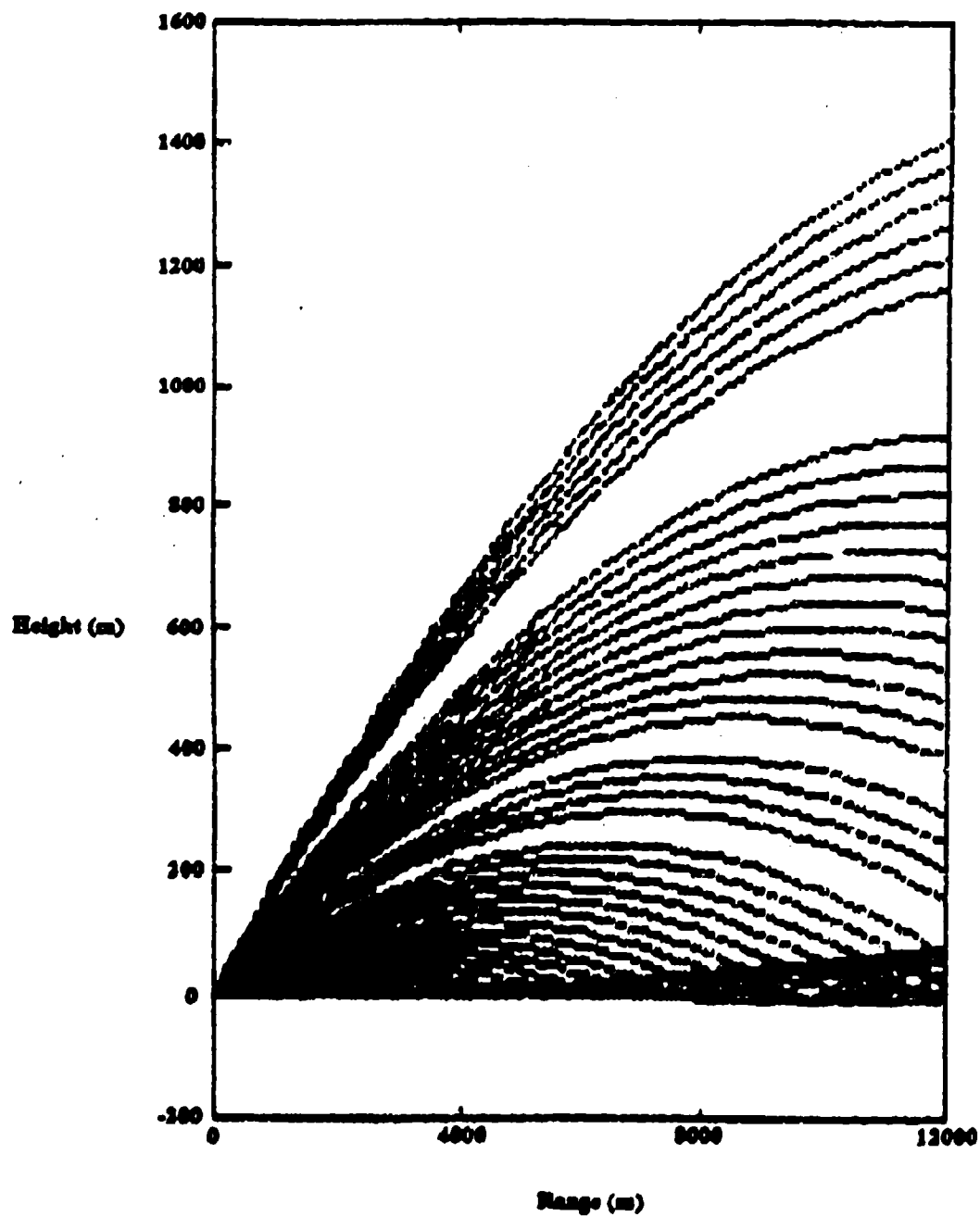
Figure E-4. Traces of acoustic rays for the downward refraction profile.
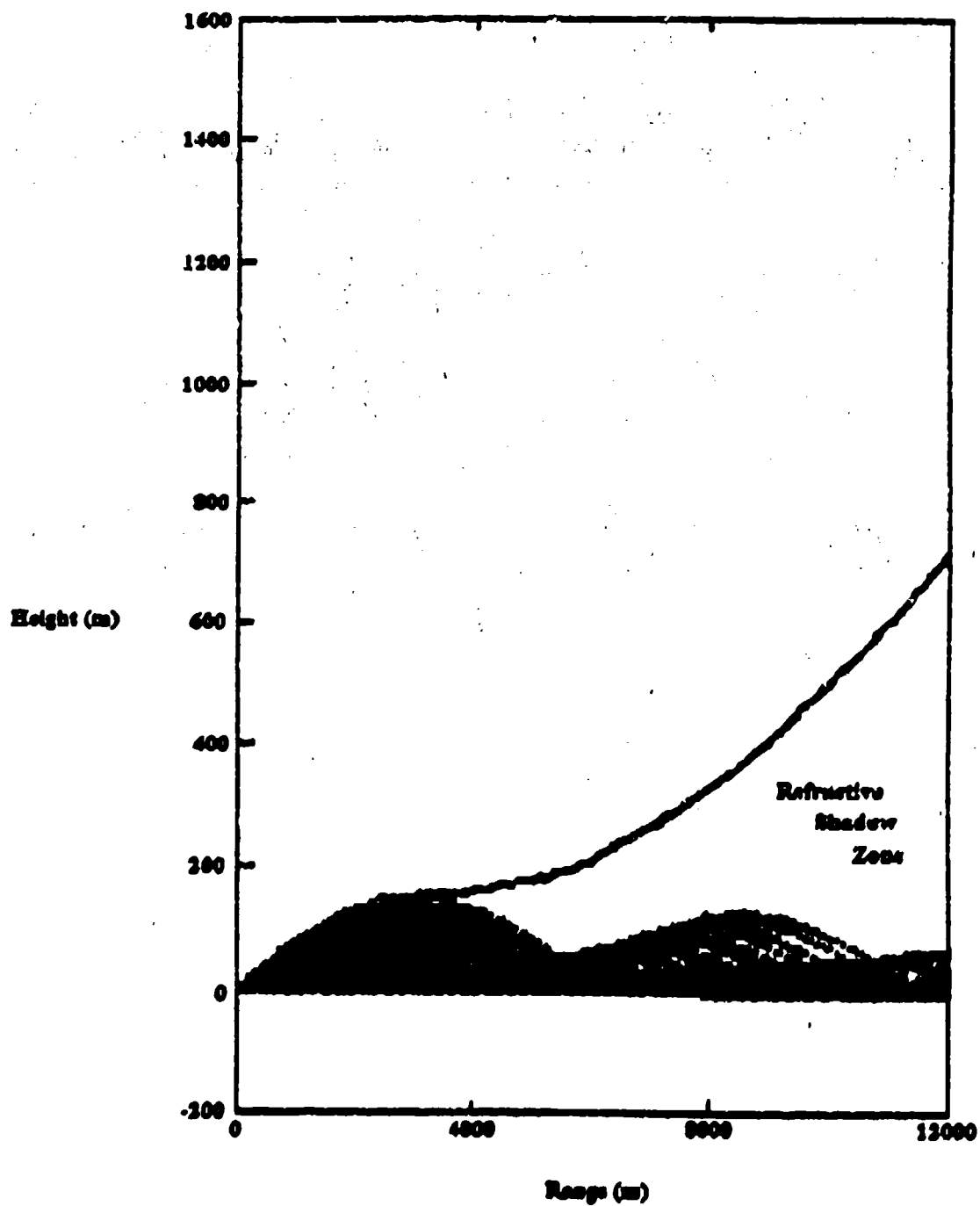
Figure E-5. Traces of acoustic rays for the for the shallow inversion profile showing the sound duct and the refractive shadow zone above the duct.
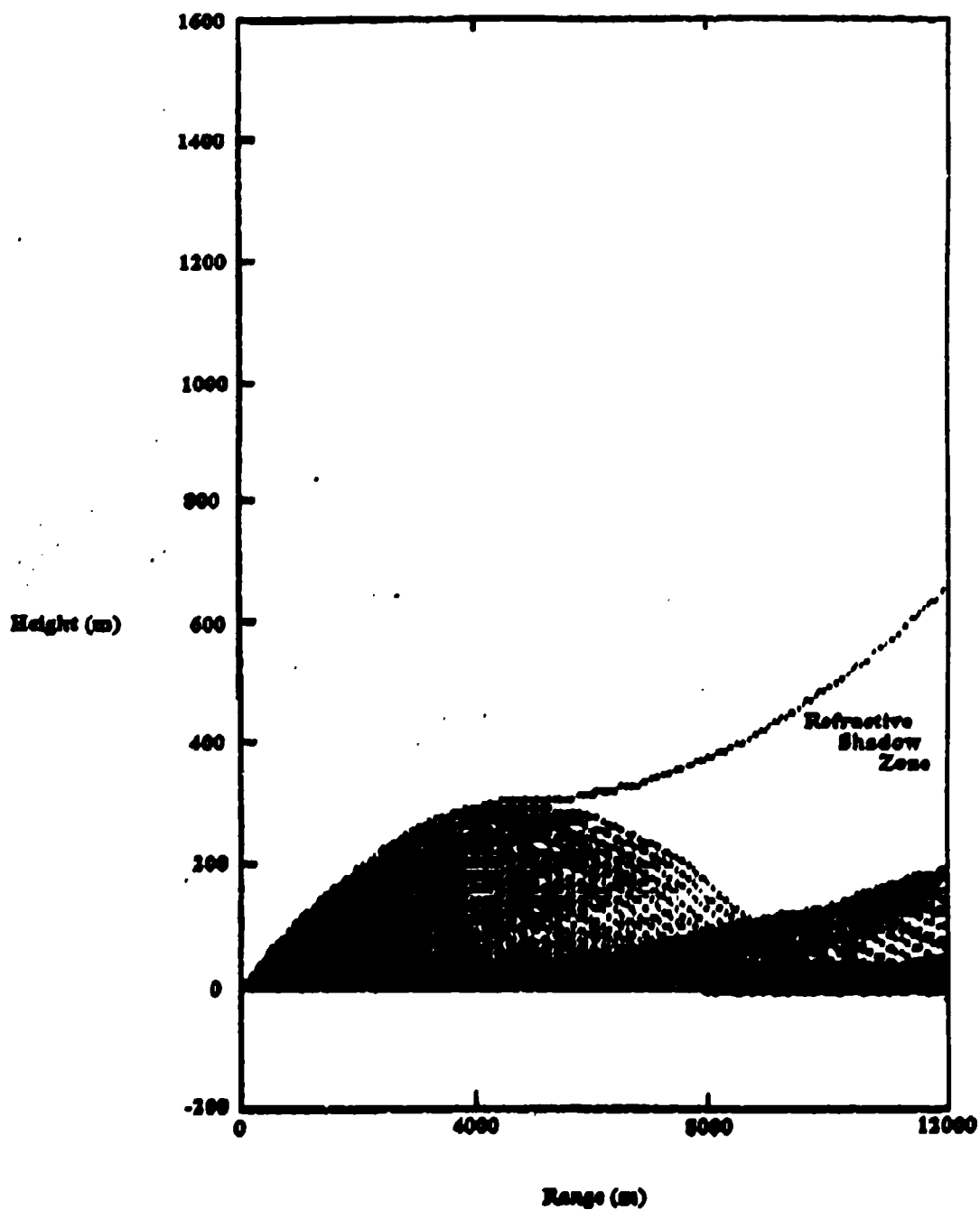
Figure E-6. Traces of acoustic rays for the for the deep inversion profile showing the sound duct and the refractive shadow zone above the duct.

DISTRIBUTION

Copies

Commandant
U.S. Army Chemical School
ATTN: ATZN-CM-CC (Mr. Barnes)   11
Fort McClellan, AL 36205-5020

NASA Marshal Space Flight Center
Deputy Director
Space Science Laboratory
Atmospheric Sciences Division
ATTN: E501 (Dr. Fichtl)   1
Huntsville, AL 35802

NASA/Marshall Space Flight Center
Atmospheric Sciences Division
ATTN: Code ED-41   1
Huntsville, AL 35812

Deputy Commander
U.S. Army Strategic Defense Command
ATTN: CSSD-SL-L (Dr. Lilly)   1
P.O. Box 1500
Huntsville, AL 35807-3801

Deputy Commander
U.S. Army Missile Command
ATTN: AMSMI-RD-AC-AD (Dr. Peterson)   1
Redstone Arsenal, AL 35898-5242

Commander
U.S. Army Missile Command
ATTN: AMSMI-RD-DE-SE (Mr. Lill, Jr.)   1
Redstone Arsenal, AL 35898-5245

Commander
U.S. Army Missile Command
ATTN: AMSMI-RD-AS-SS (Mr. Anderson)   1
Redstone Arsenal, AL 35898-5253

Commander
U.S. Army Missile Command
ATTN: AMSMI-RD-AS-SS (Mr. B. Williams)   1
Redstone Arsenal, AL 35898-5253

Commander
U.S. Army Missile Command
Redstone Scientific Information Center
ATTN: AMSMI-RD-CS-R/Documents   1
Redstone Arsenal, AL 35898-5241

Commander
U.S. Army Aviation Center
ATTN: ATZQ-D-MA (Mr. Heath)   1
Fort Rucker, AL 36362

Commander
U.S. Army Intelligence Center
and Fort Huachuca
ATTN: ATSI-CDC-C (Mr. Colanto)   1
Fort Huachuca, AZ 85613-7000

Northrup Corporation
Electronics Systems Division
ATTN: Dr. Tooley   1
2301 West 120th Street, Box 5032
Hawthorne, CA 90251-5032

Commander
Pacific Missile Test Center
Geophysics Division
ATTN: Code 3250 (Mr. Battalino)   1
Point Mugu, CA 93042-5000

Commander
Code 3331
Naval Weapons Center
ATTN: Dr. Shlanta   1
China Lake, CA 93555

Lockheed Missiles & Space Co., Inc.
Kenneth R. Hardy
ORG/91-01 B/255   1
3251 Hanover Street
Palo Alto, CA 94304-1191

Commander
Naval Ocean Systems Center
ATTN: Code 54 (Dr. Richter)   1
San Diego, CA 92152-5000

Meteorologist in Charge
Kwajalein Missile Range
P.O. Box 67   1
APO San Francisco, CA 96555

U.S. Department of Commerce Center
Mountain Administration
Support Center, Library, R-51
Technical Reports
325 S. Broadway   1
Boulder, CO 80303

Dr. Hans J. Liebe
NTIA/ITS S 3
325 S. Broadway   1
Boulder, CO 80303

NCAR Library Serials
National Center for Atmos Research
P.O. Box 3000   1
Boulder, CO 80307-3000

Headquarters
Department of the Army
ATTN: DAMI-POI   1
Washington, DC 20310-1067

Mil Asst for Env Sci Ofc of
the Undersecretary of Defense
for Rsch & Engr/R&AT/E&LS
Pentagon - Room 3D129   1
Washington, DC 20301-3080

Headquarters
Department of the Army
DEAN-RMD/Dr. Gomez   1
Washington, DC 20314

Director
Division of Atmospheric Science
National Science Foundation
ATTN: Dr. Bierly   1
1800 G. Street, N.W.
Washington, DC 20550

92

Commander
Space & Naval Warfare System Command
ATTN: PMW-145-1G   1
Washington, DC 20362-5100

Director
Naval Research Laboratory
ATTN: Code 4110
(Mr. Ruhnke)   1
Washington, DC 20375-5000

Commandant
U.S. Army Infantry
ATTN: ATSH-CD-CS-OR (Dr. E. Dutoit)   1
Fort Benning, GA 30905-5090

USAFETAC/DNE   1
Scott AFB, IL 62225

Air Weather Service
Technical Library - FL4414   1
Scott AFB, IL 62225-5458

USAFETAC/DNE
ATTN: Mr. Glauber   1
Scott AFB, IL 62225-5008

Headquarters
AWS/DOO   1
Scott AFB, IL 62225-5008

Commander
U.S. Army Combined Arms Combat
ATTN: ATZL-CAW   1
Fort Leavenworth, KS 66027-5300

Commander
U.S. Army Space Institute
ATTN: ATZI-SI   1
Fort Leavenworth, KS 66027-5300

Commander
U.S. Army Space Institute
ATTN: ATZL-SI-D   1
Fort Leavenworth, KS 66027-7300

Commander
Phillips Lab
ATTN: PL/LYP (Mr. Chisholm)   1
Hanscom AFB, MA 01731-5000

Director
Atmospheric Sciences Division
Geophysics Directorate
Phillips Lab
ATTN: Dr. McClatchey   1
Hanscom AFB, MA 01731-5000

Raytheon Company
Dr. Sonnenschein
Equipment Division
528 Boston Post Road   1
Sudbury, MA 01776
Mail Stop 1K9

Director
U.S. Army Materiel Systems Analysis Activity
ATTN: AMXSY-CR (Mr. Marchetti)   1
Aberdeen Proving Ground, MD 21005-5071

Director
U.S. Army Materiel Systems Analysis Activity
ATTN: AMXSY-MP (Mr. Cohen)   1
Aberdeen Proving Ground, MD 21005-5071

Director
U.S. Army Materiel Systems Analysis Activity
ATTN: AMXSY-AT (Mr. Campbell)   1
Aberdeen Proving Ground, MD 21005-5071

Director
U.S. Army Materiel Systems
Analysis Activity
ATTN: AMXSY-CS (Mr. Bradley)   1
Aberdeen Proving Ground, MD 21005-5071

Director
ARL Chemical Biology
Nuclear Effects Division
ATTN: AMSRL-SL-CO   1
Aberdeen Proving Ground, MD 21010-5423

Army Research Laboratory
ATTN: AMSRL-D   1
2800 Powder Mill Road
Adelphi, MD 20783-1145

Army Research Laboratory
ATTN: AMSRL-OP-SD-TP   1
Technical Publishing
2800 Powder Mill Road
Adelphi, MD 20783-1145

Army Research Laboratory
ATTN: AMSRL-OP-CI-SD-TL   1
2800 Powder Mill Road
Adelphi, MD 20783-1145

Army Research laboratory
ATTN: AMSRL-SS-SH   1
(Dr. Sztankay)
2800 Powder Mill Road
Adelphi, MD 20783-1145

U.S. Army Space Technology
and Research Office
ATTN: Ms. Brathwaite   1
5321 Riggs Road
Gaithersburg, MD 20882

National Security Agency
ATTN: W21 (Dr. Longbothum)   1
9800 Savage Road
Fort George G. Meade, MD 20755-6000

OIC-NAVSWC
Technical Library (Code E-232)   1
Silver Springs, MD 20903-5000

Commander
U.S. Army Research office
ATTN: DRXRO-GS (Dr. Flood)   1
P.O. Box 12211
Research Triangle Park, NC 27009

Dr. Jerry Davis
North Carolina State University
Department of Marine, Earth, and
Atmospheric Sciences   1
P.O. Box 8208
Raleigh, NC 27650-8208

Commander
U.S. Army CECRL
ATTN: CECRL-RG (Dr. Boyne)   1
Hanover, NH 03755-1290

Commanding Officer
U.S. Army ARDEC
ATTN: SMCAR-IMI-I, Bldg 59   1
Dover, NJ 07806-5000

Commander
U.S. Army Satellite Comm Agency
ATTN: DRCPM-SC-3   1
Fort Monmouth, NJ 07703-5303

Commander
U.S. Army Communications-Electronics
Center for EW/RSTA
ATTN: AMSEL-EW-MD   1
Fort Monmouth, NJ 07703-5303

Commander
U.S. Army Communications-Electronics
Center for EW/RSTA
ATTN: AMSEL-EW·D   1
Fort Monmouth, NJ 07703-5303

Commander
U.S. Army Communications-Electronics
Center for EW/RSTA
ATTN: AMSEL-RD-EW-SP   1
Fort Monmouth, NJ 07703-5206

Commander
Department of the Air Force
OL/A 2d Weather Squadron (MAC)   1
Holloman AFB, NM 88330-5000

PL/WE   1
Kirtland AFB, NM 87118-6008

Director
U.S. Army TRADOC Analysis Center
ATTN: ATRC-WSS-R   1
White Sands Missile Range, NM 88002-5502

Director
U.S. Army White Sands Missile Range
Technical Library Branch
ATTN: STEWS-IM-IT   3
White Sands Missile Range, NM 88002

Army Research Laboratory
ATTN: AMSRL-BE (Mr. Veazy)   1
Battlefield Environment Directorate
White Sands Missile Range, NM 88002-5501

Army Research Laboratory
ATTN: AMSRL-BE-A (Mr. Rubio)   1
Battlefield Environment Directorate
White Sands Missile Range, NM 88002-5501

Army Research Laboratory
ATTN: AMSRL-BE-M (Dr. Niles)   1
Battlefield Environment Directorate
White Sands Missile Range, NM 88002-5501

Army Research Laboratory
ATTN: AMSRL-BE-W (Dr. Seagraves)   1
Battlefield Environment Directorate
White Sands Missile Range, NM 88002-5501

USAF Rome Laboratory Technical
Library, FL2810   1
Corridor W, STE 262, RL/SUL
26 Electronics Parkway, Bldg 106
Griffiss AFB, NY 13441-4514

AFMC/DOW   1
Wright-Patterson AFB, OH 03340-5000

Commandant
U.S. Army Field Artillery School
ATTN: ATSF-TSM-TA (Mr. Taylor)   1
Fort Sill, OK 73503-5600

Commander
U.S. Army Field Artillery School
ATTN: ATSF-F-FD (Mr. Gullion)   1
Fort Sill, OK 73503-5600

Commander
Naval Air Development Center
ATTN: Al Salik (Code 5012)   1
Warminister, PA 18974

Commander
U.S. Army Dugway Proving Ground
ATTN: STEDP-MT-M (Mr. Bowers)   1
Dugway, UT 84022-5000

Commander
U.S. Army Dugway Proving Ground
ATTN: STEDP-MT-DA-L   1
Dugway, UT 84022-5000

Defense Technical Information Center
ATTN: DTIC-OCP   2
Cameron Station
Alexandria, VA 22314-6145

Commander
U.S. Army OEC
ATTN: CSTE-EFS   1
Park Center IV
4501 Ford Ave
Alexandria, VA 22302-1458

Commanding Officer
U.S. Army Foreign Science & Technology Center
ATTN: CM   1
220 7th Street, NE
Charlottesville, VA 22901-5396

Naval Surface Weapons Center
Code G63   1
Dahlgren, VA 22448-5000

Commander and Director
U.S. Army Corps of Engineers
Engineer Topographics Laboratory
ATTN: ETL-GS-LB   1
Fort Belvoir, VA 22060

U.S. Army Topo Engineering Center
ATTN: CETEC-ZC   1
Fort Belvoir, VA 22060-5546

Commander
USATRADOC
ATTN: ATCD-FA   1
Fort Monroe, VA 23651-5170

TAC/DOWP   1
Langley AFB, VA 23665-5524

Commander
Logistics Center
ATTN: ATCL-CE   1
Fort Lee, VA 23801-6000

Science and Technology
101 Research Drive   1
Hampton, VA 23666-1340

Commander
U.S. Army Nuclear and Chemical Agency
ATTN: MONA-ZB, Bldg 2073   1
Springfield, VA 22150-3198

Record Copy   3

   Total   89